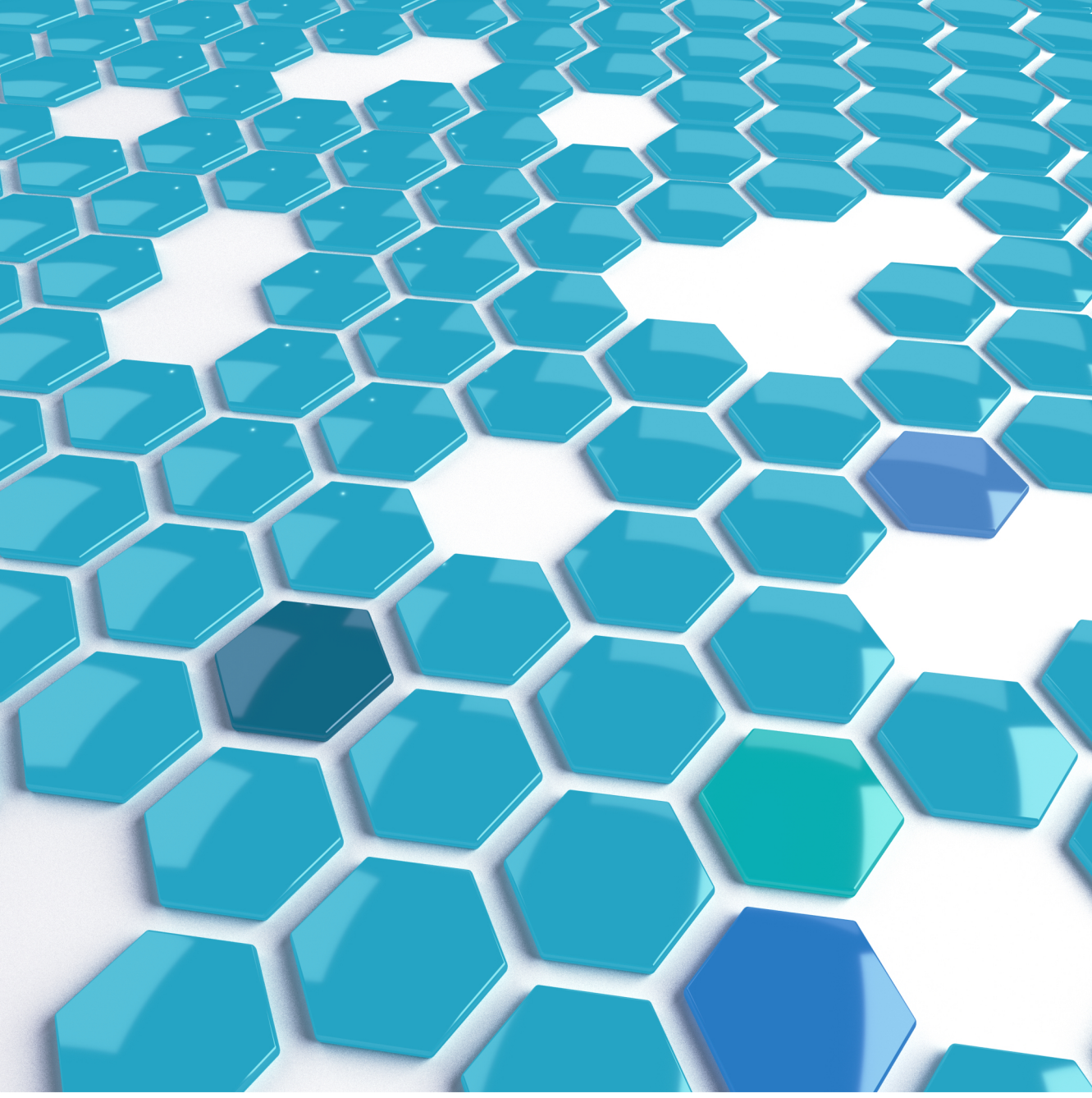

Interaction of Small Molecules with Carbon Nanostructures

Martin Pykal

PALACKÝ
UNIVERSITY
OLOMOUC

Interaction of Small Molecules with Carbon Nanomaterial Surfaces

Martin Pykal

A thesis submited in fulfillment of the requirements
for the degree of
Doctor of Philosophy

Supervisor: doc. RNDr. Petr Jurečka, Ph.D.

DEPARTMENT OF PHYSICAL CHEMISTRY, 2016

Declaration of the author

I declare that this thesis and the work presented in it are my own and has been generated by me as a result of my own original research. I have duly acknowledged all the sources of information which have been used in this thesis.

Olomouc, August 2016

Martin Pykal

"Success consists of going from failure to failure without loss of enthusiasm."

Winston Churchill

Abstract

Computational chemistry is increasingly becoming a needful part of basic research that has in relatively short period already achieved several successes in diverse areas of interest, including nanomaterial science. The strength of these methods lies especially in the atomic resolution that enables to study processes and interactions at their most fundamental level. This thesis focuses on the theoretical description of various small molecules that are in contact with carbon nanostructures and whose mutual interactions are essential in myriad technological processes and applications. Special attention is paid to the liquid-phase exfoliation of graphene, graphene interfaces and the intrinsic reactivity of graphene derivatives. Besides, an overview of computational methods for graphene modeling is provided. Presented data are often result of combination of both experiment and theoretical calculations, whereby the main contribution of this work is in complementing of available experimental data and in additional interpretation of obtained results mainly by using molecular mechanics methods. These techniques were successfully used for study of stabilization mechanism of graphene dispersion in various solvents, where it was suggested that exfoliated graphene may be stabilized in non polar media by addition of lipids that form reverse micelles whose exposed tails prevent aggregation by entropic repulsion. Additionally, it was demonstrated that inclusion of higher electric multipoles of graphene partly influence the aggregation kinetics and thus may be necessary for proper description of non-periodic

graphene sheets in classical molecular simulations. It was also revealed that the variance of contact angle of gas bubbles assembled on graphene-water interface is predominantly determined by nature of the gas, and its mutual interaction. The last part of the dissertation focuses on the reactivity of some graphene derivatives. In the case of graphene oxide initial phase of the oxidation reaction of graphene was studied. The reactive molecular dynamics showed that graphene edges together with folded areas exhibit preferential susceptibility for the oxidation. Finally, present progress in fluorographene chemistry is reviewed.

Acknowledgements

Firstly, I would like to convey my sincere gratitude and appreciation to my advisor Petr Jurečka for his generous help, guidance and friendship. It has been a pleasure working with you.

Next, my sincere thanks also goes to Michal Otyepka who provided me the opportunity to join his research group and for managing such a well-established workplace.

Many thanks are also addressed to all the students, postdocs, senior researchers and staff of the Department of Physical chemistry.

The latest and the greatest thank goes to my family and relatives, especially to my dad, for giving me the endless loving support through my academic journey.

Contents

List of Abbreviations

2D; 3D	two- and three-dimensional
AFM	atomic force microscopy
AIREBO	adaptive intermolecular reactive empirical bond-order
BU	bottom-up
CBS	complete basis set
CC	coupled cluster
CCS	CC singles
CCSD	CC singles, doubles
CCSDT	CC singles, doubles, triples
CCSD(T)	CC singles, doubles, triples perturbatively
CF	fluorographene
CH	graphane
CVD	chemical vapor deposition
DFT	density functional theory
DFT-D	dispersion-corrected DFT
DFT-TS	DFT with Tkatchenko Scheffler correction
DMA	N,N-dimethylacetamide
DNA	deoxyribonucleic acid
DOPC	1,2-dioleoyl-*sn*-glycero-3-phosphocholine
EEM	electronegativity equalization method
FF	force field
GBL	γ-butyrolactone

GGA	generalized gradient approximation
GO	graphene oxide
GW	Green's function with screened Coulomb interaction
HF	Hartree-Fock
HOPG	highly oriented pyrolytic graphite
HSE06	Heyd-Scuseria-Ernzerhof functional
LDA	local density approximation
LJ	Lennard-Jones
LR	long-range
MD	molecular dynamics
MM	molecular mechanics
MPPT; MP	Møller–Plesset perturbation theory
NEXAFS	near edge X-ray absorption fine structure
NMP	N-methyl-pyrrolidone
NMR	nuclear magnetic resonance
OPLS	optimized potentials for liquid simulations
PAH	polyaromatic hydrocarbon
PBC	periodic boundary conditions
PMF	potential of mean force
QM	quantum mechanics
REBO	reactive empirical bond-order
rGO	reduced graphene oxide
SAPT	symmetry-adapted perturbation theory
SCS	spin-component scaled methods
SR	short-range
SWNT	single walled nanotube
TD	top-down
vdW	van der Waals
XPS	X-ray photoelectron spectroscopy
XRD	X-ray diffraction

Motivation

The recent discovery of graphene has sparked enormous interest owing to its unique electrical and optical properties, some of which have not yet been observed. But not only graphene possesses unique character. New class of two-dimensional materials based on graphene are supposed to promote technological progress in both industrial and scientific fields. Unfortunately, despite a great effort, only limited number of graphene-based products have been commercialized to date.

One of the major bottlenecks impeding their further success is certainly the poor production. Generally, there is a need for finding a method, that would be able to provide these materials in large-scales at an affordable price and quality. Several works demonstrated that liquid-phase exfoliation could be a suitable preparation technique that may meet given requirements. This relatively simple and undemanding technique allows to obtain a colloidal dispersion of various lamellar materials purely by solvent treatment. Since the resulting exfoliation efficacy is highly sensitive on the solvent used, proper selection of a suitable exfoliation media is mostly crucial. Nevertheless, the molecular nature of the process of exfoliation and/or aggregation is not known in detail. The first part of this thesis is thus focused on the theoretical description of the mechanism of liquid-phase exfoliation in various solvents using molecular dynamics simulation. In particular, the effect of solvent additives on the total yield is studied. Additionally, the importance of overlooked quadrupolar moments on empirical simulations of graphene and related nanostructures is discussed.

Graphene and its interfacial interactions are of vital importance also in numerous technological processes involving sensing and other electrochemical utilizations. In the second part the gas–graphene interactions are investigated by means of classical molecular dynamics.

Although computational chemistry often offers a powerful tool providing valuable information on the level of individual atoms, knowledge gained through theoretical approaches have to be interpreted wisely with respect to their limitations and restrictions. The following part will target available methods and models currently used for graphene calculations and simulations focusing on their strengths and weaknesses. Moreover, a summary of recent trends in the graphene research from a viewpoint of theoretical chemistry is provided.

The last part of this PhD thesis deals mostly with graphene derivatives, namely with the graphene oxide and fluorographene. Despite their structural similarity, both covalent modifications display fundamentally different behavior, especially in reactivity. Its understanding would be a milestone on the way to controlled synthesis with tailored functionalities. The oxidation mechanism of the former is studied using reactive potential, since the classical approaches in molecular modeling do not allow rearrangement of the chemical bonds. Finally, properties, preparation and existing reactions involving fluorographene are summarized.

1 Graphene

1.1 Graphene and its properties

Without doubt the past decade, at least in chemistry and material sciences, could be described as a graphene era. Everything began in 2004. The group around Andre Geim and Konstantin Novoselov published work where they succeed with isolation of several 2D crystals together with single-layer graphene[1] using the micromechanical cleavage method, despite the predictions from the 1940s that free 2D crystals are generally thermodynamically unstable.[2, 3] Until this achievement graphene was considered mainly as a structural unit of lamellar graphite used for better understanding of this bulk 3D material. Nevertheless, it turned out that in contrast to graphite graphene exhibits dramatically different characteristics that fascinated scientists even long before the finding.[4] Moreover, the essential features are changing profoundly with the number of layers; single, double and few layer graphene exhibit completely different behavior. Currently, also due to unusual properties, graphene holds promise for many oncoming applications (Figure 1).[5]

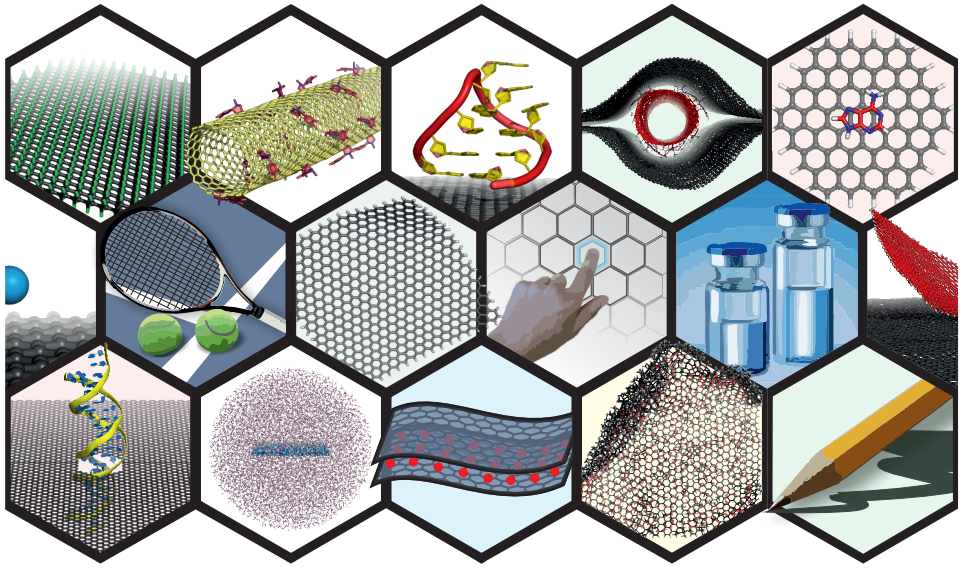

Figure 1: Schematics representing the broad range of graphene utilization ranging from sensing to new nanocomposites.

Graphene[1], an one atom thick carbon allotrope with hexagonal honeycomb-like lattice spreading only into two dimensions (2D), caused literally a revolution in nanoresearch and attracted enormous amount of human and financial resources worldwide primarily because of its remarkable physicochemical properties.[6] Undoped pristine graphene is considered as a semimetal with a zero band gap[6] and from very beginning the unusual electrical properties destined graphene for eventual utilization in future electronics.[5] Nature of this exotic behavior can be found in its structure of connected network of covalently bound sp^2-hybridized carbon atoms enclosed with π-electron clouds from both the top and bottom. The delocalized π-electrons behave like they have no rest mass and the value of intrinsic mobility in high quality crystals could reach up to 100,000 $cm^2\,V^{-1}\,s^{-1}$.[6] But it was shown that graphene's support significantly affect the resulting value and early measurements of suspended graphene on SiO_2 showed ~40,000 $cm^2\,V^{-1}\,s^{-1}$.[7] However, theoretical

limit gives even 200,000 $cm^2\,V^{-1}\,s^{-1}$.[6] It is worth mentioning that most of the electrical properties are generally sensitive to the relative stacking arrangement.[8]

The structure is also tightly bound to the mechanical strength and durability of graphene. Despite the atomic thickness, lightweight (multiplying by mass of carbon one get the value of 0.77 $mg\,m^{-2}$) and structural simplicity, the defect-free crystal lattice exhibits exceptionally high in-plane stiffness and Young modulus about 1 TPa.[9] Additionally, it was demonstrated that the elastic modulus is relatively conserved (~14 % decrease in value) even at a high density of sp^3-hybridized defects.[10] Pioneer measurements of mechanical properties of pristine graphene were performed on graphene monolayer suspended on perforated substrate, where the sheet was subsequently loaded by an AFM (atomic force microscopy) probe. Obtained intrinsic breaking strength of 130 ± 10 GPa was the highest value ever measured for known material.[9] Moreover, acquired experimental data were in good agreement with former theoretical calculations.[11]

Important feature in many technologies is the ability to conduct heat. Especially in integrated circuits the thermal dissipation may be essential for its proper function. Thermal conductivity of free standing graphene was experimentally measured to be ~5,000 $W\,m^{-1}\,K^{-1}$ at room temperature,[12] which is significantly greater than single walled nanotube (SWNT) and graphite—other members of the broad carbon allotrope family—with nearly 3,500 $W\,m^{-1}\,K^{-1}$[13] and 2,000 $W\,m^{-1}\,K^{-1}$,[14] respectively, and also typical semiconductors under the same conditions (e.g., 46 $W\,m^{-1}\,K^{-1}$ for GeAs and 141 $W\,m^{-1}\,K^{-1}$ for Si).[15] And even though the thermal conductivity will drop when the graphene sheet is suspended on a substrate, compared to most other materials, it will remain still high. With this in mind it was recently shown, that graphene coating can enhance thermal conductivity in otherwise poor heat conductors as common plastic materials by two orders of magnitude,[16] which might have many practical implications.

Another prospect for graphene may be in the area of photonics and optoelectronics. Defect free monolayer graphene sheet shows high optical transmittance and absorbs only 2.3 % of incident white light, whereby the reflectance is nearly zero (< 0.1 %). Additionally, this value is practically independent of frequency in the visible range[17] and since the opacity is sensitive to the number of layers, it can be used also for determining the thickness of graphene layers.[18] Some of the successful utilization of graphene's optical properties was shown in recent photonic devices.[19] Bae *et al.* suggested that graphene films could even outperform present conductive transparent electrodes.[20] Main drawback is still a lack of the robust efficient large-scale method of preparation and subsequent operations necessary for the production of high quality samples.

Similarly as other graphite-based composites, graphene is considered as a valuable adsorbing agent for both small (e.g. gas and organic molecules)[21, 22] and large (e.g. DNA, proteins)[23] molecules due to its large surface area that was theoretically determined up to 2,630 $m^2\ g^{-1}$.[24] Furthermore, growing debate is held also about the hydrophobicity and related wettability of graphene that can dramatically influence its sorption properties as well. It was found out that due to the adsorbed contaminants generally present in the air, graphene and other graphitic surfaces might be even slightly hydrophilic.[25] Unclear is also graphene's behavior at the interface. It was suggested that graphene is to a certain extent "transparent" to wetting and do not affect the substrate contact angle for liquid above the monolayer when placed on top of the substrate. Thus the van der Waals (vdW) interactions between graphene and adjacent fluids are negligible.[26] However, the above-mentioned is not applicable for superhydrophilic and superhydrophobic substrates.[27]

1.2 Graphene preparation

For the vast majority of novel materials there is always a need for development of mass-production techniques that will produce high-quality samples for reasonable price for forthcoming industrial applications and successful commercialization of graphene.

Generally, the fabrication of graphene may be categorized into two traditional directions: top-down (TD) and bottom-up (BU) approaches. The former exploits the structure of lamellar graphite consisting of many graphene sheets that are held together by weak non-covalent interactions. Subsequent disrupting of these weak interactions lead to individual graphene sheets. Accordingly, first attempts were based on the mechanical reducing of graphite layers using the AFM probe.[28] By taking this approach one was able to prepare quite rough samples of thinner graphite still comprising of hundreds of layers. Therefore, the real graphene was first prepared by the previously mentioned mechanical cleavage method used by Nobel laureates, where the individual sheets of graphene was gradually peeled of from highly oriented pyrolytic graphite (HOPG) by adhesive tape. Although it is relatively straightforward procedure providing high-quality 2D crystals, it suffers from low yield and limited size of samples reaching a maximum of tens of μm.[1] Price of a flake of given dimensions cost more than $ 1,000 and if one rely solely on this approach graphene would be one of the most expensive material per gram on Earth.[29] Further proposed methods as intercalative expansion of graphite[30] or chemical reduction of graphene oxide[31] did not provide either the required thickness or quality.

Another relatively large group of TD methods is liquid-phase exfoliation of graphite employing deep knowledge already gained from nanotube preparation.[32] Graphite powder fragments are ultrasonicated in a variety of organic solvents and dissipated into colloidal dispersion of

high-quality (low defect ratio) graphene with a certain amount of monolayers.[33–35] Despite the fact that resulting graphene flakes are only ~1 μm in length, this technique benefits from its simplicity and rather cheap instrumentation allowing for its large-scale production. Suitable exfoliation solvents, that are sufficient to overcome the interaction forces acting between individual graphene layers, are characterized by their surface energy approaching that of graphene, which is around 68 $\mathrm{mJ\,m^{-2}}$.[36] Tentative solvent selection might be done also according to Hildebrand and Hansen solubility parameters. Stable dispersions were prepared using N-methyl-pyrrolidone (NMP), γ-butyrolactone (GBL), N,N-dimethylacetamide (DMA)[35], perfluorinated aromatic molecules[33] as hexafluorobenzene ($\mathrm{C_6F_6}$), octafluorotoulene ($\mathrm{C_6F_5CF_3}$), and several low boiling points solvents[37], etc. However, searching for additional solvents remains still challenging. It is worth noting that colloids are inherently thermodynamically unstable owing to their high interfacial free energy and exfoliated graphene sheets tend to re-stack and thus need to be stabilized against aggregation. Stabilization may be achieved by additives (for instance by specific surfactants or polymers) that prevent the agglomeration of graphene dispersion through non-covalent interactions. Their role will be discussed in more detail afterwards in *Results* section.

Industrial practice focused mainly on the BU procedures that include more sophisticated chemical processes as epitaxy or deposition of thin films commonly utilized in semiconductor industry. One of the most promising direction for large-scale production might be the bottom-up growth of epitaxial graphene by high temperature annealing of SiC.[38, 39] Silicon atoms starts to desorb from the surface of SiC wafer after exposure to high temperatures creating a carbon-rich layer that will rearrange into few-layer graphene. However, the mechanism of the growth mechanism requires deeper understanding.[40] Another possibility of fabricating large-area of relatively high-quality graphene is chemical vapor deposition (CVD) using

hydrocarbon precursors.[41] Usually, methane is brought on heated catalytic copper foil, causing a formation of small graphene islands and their subsequent coalescence. Nevertheless, further processing requires harsh chemicals to etch away the Cu foil and transport of the detached graphene to a silica or polymer substrate. Although the prepared graphene sheets dimensions are reaching several dozen centimeters and approaches to application requirements,[20] the presence of grain boundaries, planar defects formed by combining of separate carbon grains, degrade the resulting mechanical and electronic properties.[42]

1.3 Graphene derivatives

The applicability of graphene is narrowing in particular cases owing to a zero band gap and relatively low reactivity and dispersibility. Thus the potential areas of graphene's application (for instance the band gap modulation or increasing of the gas storage capacity) can be remarkably enhanced by non-covalent and covalent modification.[43] Especially chemically modified graphene derivatives such as graphane (CH), fluorographene (CF) or graphene oxide (GO), etc., are subject of vigorous research. The two latter mentioned graphene analogues will be discussed in more detail with respect to the presented thesis.

Graphene Oxide

GO is basically a graphene-like sheet randomly covered by oxygen containing groups forming sp_3-hybridized domains within the layers. However, this change of hybridization naturally bears disruption of the planarity. The topology of GO is not clearly defined and strongly depends (together with resulting properties) on oxidation degree and preparation method, which can also incorporate additional impurities.[44, 45] Moreover, monitoring of the structural evolution during graphene oxidation

process is highly challenging. Several models differing in presence of various oxygen containing groups have been proposed over the years.[46] With respect to recent observation it is generally considered that epoxy and hydroxyl groups are located on the basal plane, whereby carboxyl, ketone, peroxide and quinone may occur at the edges.[47, 48] Introduction of these oxygenated functional groups significantly increases the hydrophilicity of GO. Hence, it can be readily dispersed in water and other organic solvents to form stable colloids. This simple solution treatment facilitates the further manipulation into various processes and technologies, when it might be basically deposited on any substrate or mixed with certain polymers to improve resulting properties.[49]

Interestingly, in contrast to pristine zero band gap graphene, GO is fluorescent over a broad range of wavelengths making it attractive for optical applications.[50] Furthermore, because of the graphene reluctance to react chemically, GO is often used as a substrate for further graphene derivatization.[51] On the other hand GO is generally a poor electrical conductor. Nevertheless, the hexagonal graphene lattice might be partly recovered together with the conductivity by chemical or thermal reduction of the GO. This technique is also currently most common and simultaneously most economic large-scale preparation method of graphene. Although reduction processes remove major part of the oxygen groups, particular methods differ in residual oxygen of reduced graphene oxide (rGO) resulting in different properties.[52, 53]

GO is synthesized using several synthetic routes, when graphite is treated with strong oxidizing agents producing graphite oxide, which is subsequently exfoliated. Graphite oxide was prepared already in 1859 by B. C. Brodie, who dealt with chemistry of graphite.[54] Nevertheless, this method was very time consuming and consisted of multiple steps, therefore it was gradually improved and simplified.[55, 56] A few decades later in 1958, Hummers reported an alternative oxidation procedure providing higher degree of oxidation.[57] Nowadays, Hummers method is widely

used technique for GO fabrication, often with numerous modifications.[58]

Fluorographene

Fluorographene, also known as graphene fluoride, was first synthesized independently on several places at the same time in 2010; individual original studies were published in the same journal issue separated by only a few pages.[59, 60] CF is a 2D graphene analog and similarly as its parental material consists of hexagonal carbon rings forming a planar lattice. However, the main skeleton is locally warped due to covalently bonded fluorine that is attached to each carbon atom (so its chemical formula is written as $(CF)_n$). Thus carbons in fluorographene are in sp^3 hybridization, unlike the sp^2-configuration in graphene. Furthermore, it results in losing of free π-electrons and more importantly in alteration of basic characteristics (Figure 2). In terms of electronic properties, CF is an insulator with a band gap reaching value as high as 8.3 eV[61] according recent quantum chemical calculations that explicitly include electron-electron correlation (at the GW-HSE06 level). The Young modulus has been measured to be one third of that for graphene.[59] By far the most interesting part is the reactivity of this material.[62]

It was initially assumed that CF will be a chemically inert material like other perfluorinated hydrocarbons and this hypothesis was further supported by its high thermal stability.[59] It was shown that CF is thermally stable up to 300 °C and decomposes into volatile low-molecular-weight compounds at temperatures above 500 °C.[63, 64] However, current studies have suggested that CF might be a subject of diverse substitution reactions. It has been shown that by reaction with KI one is able to convert CF back into graphene. The mechanism of the reaction involves transitional formation of unstable $C—I$ bond, which proceeds in spontaneous graphene and I_2 release.[60] Furthermore, CF reacts with variety of reagents, for instance with $NaSH$, $NaOH$, CCl_2, $NaNH_2$, N_2H_4 even at

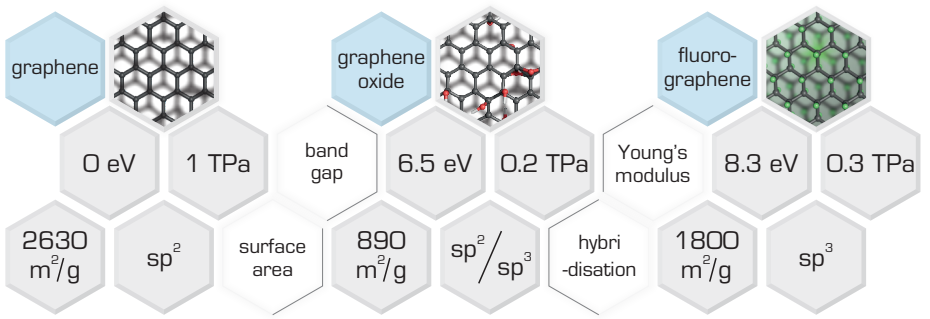

Figure 2: Comparison of basic characteristics of graphene[5], graphene oxide[69, 70] and fluorographene[59].

room temperatures.[65–67] One reason for the increased reactivity could be found in so called "semi-ionic" character of the $C-F$ bond in CF, that is rather an intermediate between ionic and covalent bond owing to the hyper-conjugation between $C-C$ and $C-F$ bonds.[68]

Fabrication of CF is commonly done using three leading methods. First approach involves mechanical and chemical (liquid-phase) exfoliation of fluorographite.[60, 71] Appropriate solvents for chemical etching of fluorographite are for instance sulfolane, tetrahydrofuran, NMP, etc. Basic principles of these methods as well as its pros and cons have been described in detail in the previous section. Fluorographene can be prepared also by reaction of graphene with XeF_2 or F_2. The C/F ratio of resulting products can be controlled by the choice of experimental conditions.[72] Moreover, by exposing only one side of the sample (leaving CVD graphene on copper foil) one is able to prepare single-side fluorinated graphene with dominant stoichiometry of C_4F.[64] The last popular method is fluorination of GO using HF or F_2.[73] Here one encounter on an ill-defined structure of the precursor resulting rather in highly-fluorinated GO. However, there are known experiments with well-defined composition.[74]

2 Theory and Methods

2.1 Intermolecular interactions

As the name implies, intermolecular interactions are found between the neighboring particles that are not linked by covalent bonds (therefore they are also known as non-bonded or non-covalent interactions). Although the particular interactions seem to be weak (compared to intramolecular interactions that keep a whole molecule together), their collective contribution is often significant and are of great importance in diverse research fields such as protein folding, nanotechnology, sensing and many others. Moreover, they are governing basic physical properties of a material (viscosity, surface tension, etc.). A lot of these interactions also indirectly affect the way how the system reacts by determining relative position of reactants.

In general, non-bonded interactions can be attractive or repulsive and are further classified into two main categories: long-range (LR) and short-range (SR) interactions. The LR terms, which include mostly electrostatic, induction and dispersion interaction, have often an inverse power dependence on the distance, r^{-n}, while the SR potential, typical for repulsion, may be described by means of exponentially decaying potentials, $e^{-\alpha r}$.

Electrostatic (Coulombic) energy

Electrostatic interactions originate from the electric charge distributions of atoms and molecules and are governed by the Coulomb law. For instance, the interaction between stationary point charges, Q_1 and Q_2, of two molecules separated at the distance r is given by

$$U_{\text{coul}}(r) = \frac{Q_1 Q_2}{4\pi\epsilon_0 r} \tag{1}$$

where ϵ_0 is the vacuum permittivity (in a dielectric medium the vacuum permittivity is replaced by relative permittivity, ϵ, lowering the final potential experienced by molecules). This particular Coulombic interaction is extremely long-ranged, decaying very slowly with the distance (see Table 1). Generally, the distance-dependence of m-pole and n-pole (assuming non-rotating molecules) can be expressed as

$$U_{m+n}(r) \propto \pm\frac{1}{r^{(m+n+1)}}, \tag{2}$$

where m and n are the multipole orders and r is the separation distance of two multipoles.

For a given charge distribution one may describe the resulting electrostatic potential by means of a multipole expansion

$$U_{\text{coul}}(\boldsymbol{r}) = \frac{1}{4\pi\epsilon_0}\left(\frac{q}{r} + \frac{\boldsymbol{r}\cdot\boldsymbol{p}}{r^3} + \frac{1}{2}\sum_{ij} Q_{ij}\frac{x_i x_j}{r^5} + \dots\right). \tag{3}$$

Here, $x_{i,j}$ are the Cartesian components of vector $\boldsymbol{r}$, q is the monopole moment, $\boldsymbol{p}$ is the dipole moment, and Q_{ij} is the quadrupole moment. The above-mentioned expression is only valid when the intermolecular distance is larger than the dimensions of the interacting molecules. Both the electrostatic potential and electric field are then dominated by the first non-vanishing term, whereby monopole is dominant term for ions, whereas

Table 1: Main characteristics of intermolecular interactions.

	Interaction	Pair-additive	Sign	Distance dependence	Typical magnitude [kcal mol^{-1}]
	Covalent bond		$-$		35–250
LR	*Electrostatics*	✓	$\pm$		
	ion-ion			r^{-1}	< 100
	ion-dipole			r^{-2}	10–100
	dipole-dipole			r^{-3}	1–6
	dipole-quadrupole			r^{-4}	
	quadrupole-quadrupole			r^{-5}	
	induction	✗	$-$		
	ion-induced dipole			r^{-4}	0.8–3.5
	dipole-induced dipole			r^{-6}	0.5–2
	dispersion	approx.	$-$	r^{-6}	0.01–10
SR	*repulsion*	approx.	$+$	e^{-r}	
	charge trasnfer	✗	$-$		

for neutral molecules higher-order terms are gaining in importance. In empirical force field methods the expansion is often truncated after the monopole moment (and in many cases graphene is modeled even as uncharged species). However, the quadrupole contribution may be very important in some cases including the nanostructures.

Electrostatics is also a dominant contribution of a special type of attractive dipole-dipole interaction that has a profound impact in diverse fields is the hydrogen bond. The hydrogen bond may form between molecules that have an H atom covalently bonded to a highly electronegative atom with lone pair such as N, O, F or C. The partially positive hydrogen is then attracted to the electronegative atom, which is charged partially negative. In some cases systems with delocalized electrons can act as proton acceptor as well.[75]

Induction energy

Permanent multipoles can induce a dipole in neighboring polarizable molecules. These permanent multipole moments (electric monopole, dipole, quadrupole, etc.) generate an electric field around that manages electronic distribution of nearby molecule producing therein a small dipole moment. This induced multipole is then attracted together with the adjacent permanent multipole; thus induction energy is always stabilizing. The interaction potential at an interatomic separation r, when an ion, Q_1, can induce a dipole in a non-polar molecule is

$$U_{\mathrm{ind}}(r) = -\frac{{Q_1}^2 \alpha_2}{2r^4(4\pi\epsilon_0)^2}, \tag{4}$$

where α_2 is the polarizability of the second molecule.

Charge transfer is also often considered as a component of the induction interaction (according to the SAPT, symmetry-adapted perturbation theory[76]), nevertheless this effect is difficult to precisely differentiate from the others.

It should be noted that induction term is not usually explicitly included in classical empirical force fields. Moreover, this contribution is not pair additive that makes it even more complicated. Neglecting of induction (polarization) effects is one of the most serious drawback of common pairwise additive classical force fields when modeling graphene and its derivatives.

Dispersion energy

Dispersion interactions are dominating primarily in non-polar molecules and closed shell atoms. However, they are present in polar molecules as well, but it represents only a small part of the total interaction energy. This ubiquitous attractive interaction (known also as London dispersion) arises due to the continuous electron motion that leads to asymmetrical charge

distribution of the particle forming time variable dipoles (and higher multipoles), which in turn induce another momentary multipole in neighboring atoms or molecules. These correlated instantaneous multipoles may subsequently interact among themselves. The dispersion interaction potential U_{disp} can be expressed as

$$U_{\mathrm{disp}}(r) = -\left\{ \frac{C_6}{r^6} + \frac{C_8}{r^8} + \frac{C_{10}}{r^{10}} + \dots \right\}, \tag{5}$$

where C_n are dispersion coefficients and r is the interatomic or intermolecular distance. Here, the first term in the expansion represents the instantaneous dipole-dipole interaction that is typically the leading one. Following coefficients account for higher order dispersion terms (namely for dipole–quadrupole and quadrupole–quadrupole interaction). Nevertheless, these terms are often neglected in molecular simulations when calculating dispersion energies (since they do not contribute significantly to the total dispersion energy). A simple approximation is then given by London equation[77]

$$U_{\mathrm{disp}}(r) = -\frac{C_6}{r^6} = -\frac{3}{2}\frac{I_1 I_2}{(I_1 + I_2)}\left(\frac{\alpha_1 \alpha_2}{r^6}\right), \tag{6}$$

where α_1 and α_2 are the dipole polarizabilities of interacting atoms or molecules, I_1 and I_2 are ionization potentials of relevant particles. Considering that the polarizability of an atom is affected by its chemical environment, dispersion exhibits non-additive behavior. Most molecular models are pairwise additive and do not explicitly cover these many-body effects, whose contribution might be essential in some cases.[78, 79] However, they are effectively included in two-body interactions.

Repulsion energy

This repulsive term has purely quantum mechanical origin that results from the Pauli's exclusion principle and is dominant at very small interatomic separation of neighboring closed-shell atoms. At such a distance electron densities of interacting atoms begin to overlap, which leads to deformation of wave functions. In other words, two electrons (or any fermions in general) cannot acquire simultaneously the same state; cannot occupy the same region of space, i.e. they have to differ in at least one principal quantum number.

Although repulsion is usually modeled also due to time saving reasons as inverse function of distance, $1/r^n$ (where n is frequently equal to 12), as stated before an exponential form, e^{-r}, is more suitable for proper description of the repulsion potential.

2.2 Computational chemistry

While it is challenging to perform experimental studies on nanoscale systems at the atomistic level, the atomic scale is the "native" scale of computational chemistry. Moreover, computational methods are increasingly being used to complement experimental research in many areas of chemistry and nanotechnology. Modeling of graphene and its derivatives can be achieved using either electronic structure methods based on quantum mechanics, which explicitly account for the electronic structure of the studied molecular systems, or with molecular mechanics methods (also known as empirical force fields) that simplify molecular systems by representing them as collections of covalently bound van der Waals spheres.

2.2.1 Electronic structure methods

Quantum mechanical models and approaches allow study matter at its most fundamental level. The electronic structure (and all properties of the

studied chemical system) is determined by solving the Schrödinger equation that can be written in the form

$$\hat{H}\Psi = E\Psi. \tag{7}$$

The core of the equation is the wavefunction, Ψ, describing the quantum state of a particle, E represents the system energy and $\hat{H}$ is an operator of the total energy (the Hamiltonian operator). The later implies a sum of five contributions to the total energy: the kinetic energy of electrons and nuclei, and the potential energy of nucleus-nucleus, electron-nucleus and electron-electron interaction:

$$\hat{H} = \hat{T}_{\mathrm{e}} + \hat{T}_{\mathrm{n}} + \hat{V}_{\mathrm{nn}} + \hat{V}_{\mathrm{en}} + \hat{V}_{\mathrm{ee}}. \tag{8}$$

Exact solution to the Schrödinger equation can be found only for systems containing at most two interacting particles, i.e. hydrogen atom, He^{+}, etc. The vast majority of many-particle equations are not analytically solvable; thus the quantum chemistry deals exclusively with an approximate solution to Schrödinger's equation when are introducing variety of simplifications. The basic approximation is the Born-Oppenheimer approximation that enables to separate the nuclear and electronic motion leading to molecular wavefunction in terms of electron and nuclear position. Further approximations are introduced depending on the level of theory.

Hartree-Fock

Common approach of wavefunction based methods is the Hartree-Fock (HF) method, that is due to its low computational demands also used as a starting point of more sophisticated methods, so called post-HF methods. The many-electron system and thus the molecular wavefunction is

in this theory approximated as a product of one-electron functions (spin-orbitals), where the particular one-electron orbitals are found by expanding in a fixed basis set (usually a set of atom centered gaussians). The interaction with the other electrons is accounted for only through an effective potential–average field generated by the other electrons. To satisfy the Pauli exclusion principle and thus the postulate of antisymmetry, the wavefunction must be written in the form of a Slater determinant. This notation ensures also the requirement that the fermions are indistinguishable from each other. The orbital energy for a given system can be obtained by variational principle, which says that any tentative wavefunction will always provide a higher energy than the energy for the exact solution. In a complete basis set (CBS) approximation this will give the upper limit of the energy, the HF-limit energy.

Møller-Plesset perturbation theory

The most serious drawback of the HF theory is that it neglects the correlation effects between electrons of opposite spin. Therefore, it is necessary to use post-HF methods to correct the missing electronic correlation. The Møller–Plesset perturbation theory (MPPT or simply MP) is a useful method for treating the correlation effects.[80] Although the second-order Møller–Plesset perturbation method (MP2) accounts for a large fraction of the electronic correlation, it is considerably more computationally demanding than the classical HF method and especially tends to overestimate the dispersion interactions of weakly bonded complexes.[81] However, several methods derived from MP2 offer better accuracy. For instance the spin-component scaled MP2 methods (SCS-MP2[82] and SCS(MI)-MP2 [83]) are able to predict binding energies significantly more accurately than MP2 without additional computational cost.

Coupled cluster methods

The coupled cluster (CC) theory provides high accuracy computation technique for atomic and molecular electronic structure, based on the exponential expansion of the exact many-electron wavefunction (generating excited Slater's determinants). Unfortunately, due to its computational complexity this method is only applicable for small systems. In practice, the full expansion of the cluster operator is inapplicable, therefore the expansion is often truncated at some level of excitation to include the single (CCS), double (CCSD), triple excitations (CCSDT), etc. Moreover, this method might be further combined with the perturbation theory; for instance CCSD(T) stands for full CC treatment of single and double excitations whereas triples are handled perturbatively. Calculations performed at the CCSD(T)/CBS level of theory provide benchmark results of interaction energies of non-covalent complexes.[84, 85]

Density functional theory

Electronic energy and other characteristics of the system in the ground state may be unambiguously determined also as a function of the electron density of the molecule. Generally, this group of methods offers results comparable (or better) to MP2 with similar (or less) computational expenses as HF. Additionally, unlike the HF method, the density functional theory (DFT) approach covers large fraction of the electronic correlation by means of an exchange-correlation functional. However, exact form of the exchange-correlation functional is not known and thus its assessment is the most challenging step. Classical DFT methods based on the local density approximation (LDA), the generalized gradient approximation (GGA) or hybrid functionals do not account for non-local electron correlation effects,

which are essential for the proper description of vdW forces[86–88]. Currently, several strategies have been developed to describe dispersion interactions within the framework of DFT (DFT-D[89, 90], DFT-D2[91], DFT-D3[79], DFT-TS[92], etc.). An alternative strategy resulted in the development of non-local density functionals that account directly for dispersive correlation effects.[93]

2.2.2 Empirical methods

Whereas advanced quantum chemical methods provide highly accurate descriptions of systems comprising a few tens of atoms, molecular mechanics (MM) can be used to perform calculations on systems comprising thousands of atoms such as nucleic acids, proteins and nanostructures. Of course, this advantage is counterbalanced by many simplifications and limitations (e.g. the inability to describe charge transport involved in many of graphene's intermolecular interactions, explicit polarization, and the charge redistribution caused by wrinkling of a graphene surface) resulting from the omission of the electronic degrees of freedom; molecular mechanics only accounts for the motion of nuclei. In molecular mechanics, the system is considered to be an ensemble of beads and springs that are held together by simple harmonic forces. The core of the molecular mechanics calculation is a force field (abbr. as FF; also known as an empirical potential) consisting of a set of equations and some associated parameters that are used to describe the system's energetics. The resulting energy U_{ff} is calculated as the sum of several terms, whose form and number is determined by the method's degree of simplification

$$U_{\mathrm{ff}} = U_{\mathrm{bond}} + U_{\mathrm{ang}} + U_{\mathrm{tors}} + U_{\mathrm{vdW}} + U_{\mathrm{elec}} + (U_{\mathrm{pol}}) + (U_{\mathrm{other\ terms}}), \quad (9)$$

here, U_{bond}, U_{ang} and U_{tors} represent the contributions to the total energy from bonding terms (bond stretching, angle bending and torsion angle twisting), while U_{vdW} and U_{elec} represent the non-bonding van der Waals

and electrostatic terms, respectively. Further optional terms for polarization, U_{pol}, and other additional energy terms (for instance dispersive many-body terms) are included in brackets. Non-covalent interactions are accounted for using simple expressions for the electrostatic (Eqation 1) and vdW forces (encompassing together repulsion and London dispersion); one of the most widely used intermolecular potential in molecular simulations is the Lennard-Jones (LJ or 12-6) potential

$$U_{\mathrm{vdW}} = 4\epsilon \left[\left(\frac{\sigma}{r}\right)^{12} - \left(\frac{\sigma}{r}\right)^{6} \right] = \frac{A}{r^{12}} - \frac{B}{r^{6}}. \tag{10}$$

Here, ϵ and σ are the Lennard-Jones parameters, r is the interatomic distance. The first listed LJ parameter, ϵ, specifies the well depth, which determines how strongly two particles interact; σ represents the distance at which the potential between the two particles is zero (for clarity see Figure 3). Despite its weaknesses (especially in the repulsion part as discussed above), this crude approximation is sufficient for many applications. However, some alternative potentials (Buckingham, exp-6, Hill etc.) are trying to eliminate this deficiency, but the computational demands will increase up to 4 times compared to the original LJ function.[94]

As stated above, major part of FFs does not explicitly include the polarizability. Force fields are parameterized against experimental data and thus include these many-body effects implicitly and should be more accurately referred to as an effective potential. In some force fields this problem is partly solved by adding an explicit term for electronic polarization. The contribution of polarization may be especially important in the case of nanomaterials and it can be accounted for in several ways. A frequently used and technically simple option is the classical Drude model[95] (the so-called "charge on spring" model), where an additional particle is attached to the atom. The particle has its own charge and, along with its attached atom, generates an induced dipole moment that depends on the external field. A similar way of including polarizability is the rigid rod

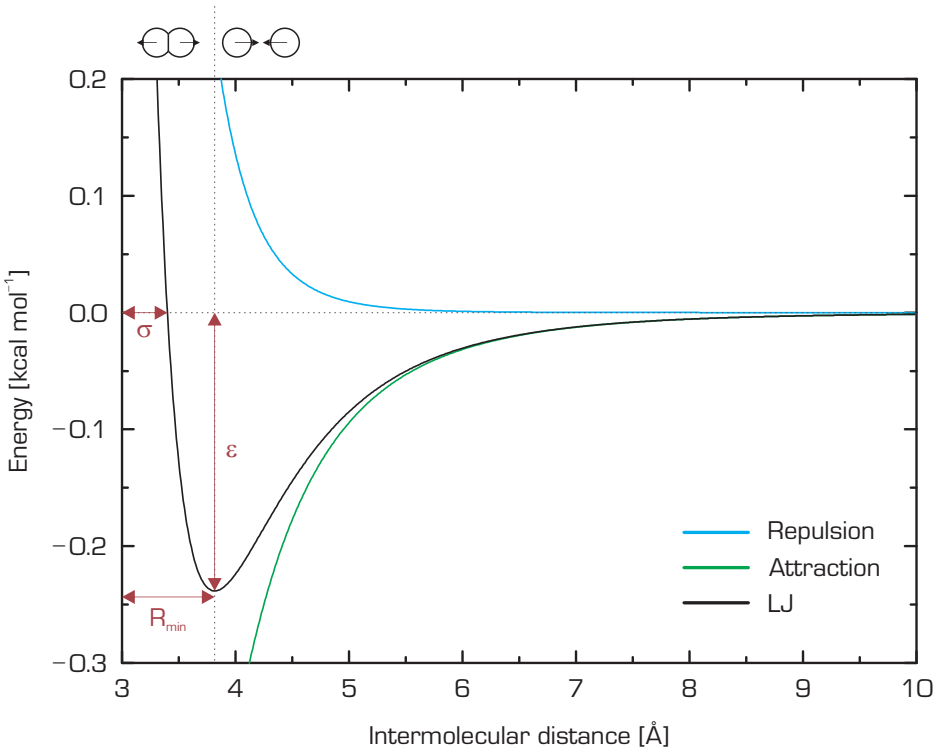

Figure 3: The Lennard-Jones potential for argon dimer with two LJ parameters, ϵ and σ.

model.[96] Like the Drude model, this approach involves attaching a virtual interaction site to the atom, but the assigned charge is kept at a fixed distance and is only permitted to rotate. For instance the GRAPPA force field, which was specifically designed for simulations of water-graphitic interfaces, uses the rigid rod model.[97] A third way of including polarization is to assign atomic polarizabilities to the atoms and then calculate the resulting induced dipoles, whose orientation is determined by the external field felt at each atomic site in the molecule.

Current empirical force fields

Numerous force fields for various kinds of structures have been developed over the past few decades.[98–101] Force fields are often very specialized and designed to target quite narrow groups of molecules. The greatest number of empirical calculations are performed on biological systems and thus efforts to develop and refine force fields have largely focused on proteins, nucleic acids and so on. While the transferability of parameters from one molecule to another is one of the principal assumptions of molecular mechanics models, their validity is far from clear, when transferring parameters from biomolecules to nanomaterials. Fortunately, several modified force field parameters have been developed specifically for simulating graphene. Nevertheless, their rigorous form is not known so far. Likewise, the suitability of current parameters has not been thoroughly tested yet. Table 2 compares the non-bonded parameters for aromatic carbon atoms from the three most widely used bio-molecular force fields to those from several modified potentials that were developed for modeling carbon allotropes and which have been used by various groups. Since in most cases the carbon atoms in graphene are treated as uncharged Lennard-Jones spheres, the molecular mechanics descriptions of the interactions between graphene and other molecules are governed exclusively by these non-bonded vdW parameters. Clearly, the listed force fields differ quite significantly with respect to these parameters, so it is important to choose a force field carefully if planning to use molecular mechanics to study graphene or its derivatives.

Reactive potentials

Classical force fields do not allow bond cleavage and formation because they model bonds with harmonic potentials. This is sufficient for the study of various non-covalent modifications of graphene and other materials.

Table 2: Non-bonded parameters for aromatic carbon atoms from different force fields used in molecular dynamics simulations of graphene and graphene derivatives.

Force field	σ **[Å]**	ϵ **[kcal mol^{-1}]**	**Ref.**
Parm 99	3.39967	0.0860	[101]
OPLS	3.55000	0.0700	[99]
CHARMM27	3.55005	0.0700	[98]
Ulbricht *et al.*	3.78108	0.0608	[102]
Girifalco *et al.*	3.41214	0.0551	[103]
Cheng and Steele	3.39967	0.0557	[104]
COMPASS[a]	3.48787	0.0680	[105]

[a] Uses 9-6 LJ potential.

However, a model capable of describing bond cleavage/formation is required for the study of any process involving chemical change such as chemisorption or chemical reactions. In such cases it is necessary to use methods that explicitly account for the system's electronic structure. Unfortunately, such methods can only be applied to relatively small model systems. Empirical reactive force fields such as AIREBO[106], REBO[107] and ReaxFF[108] were developed to enable the study of large reacting molecular systems. These force fields use the standard force field approximations but also include terms for bond formation and dissociation (see Equation 9).

The most commonly used reactive potential is ReaxFF, which is a bond-order dependent potential (whereby bond-orders are updated in every iteration) that was successfully used to describe the bond formation and bond breaking in hydrocarbon systems[108, 109], high-energy materials[110], as well as for combustion chemistry[111], fuel cells[112], hydrogen storage[113], etc. (usually, individual potentials are solely parameterized for particular chemical systems). Unlike the classical FF methods, in ReaxFF is each element described only with one atom type, where the bond order/bond length relation ensures the smooth transition from non-covalent

to covalent (either single, double or triple bond) interactions, which reflect the chemical environment. Polarization effects are accounted for through an atomic charge EEM calculation scheme (electronegativity equalization method)[114] that is geometry dependent. For comparison, the total energy is given by following expression

$$\begin{aligned} U_{\mathrm{ff}} = U_{\mathrm{bond}} + U_{\mathrm{lp}} + U_{\mathrm{over}} + U_{\mathrm{under}} + U_{\mathrm{ang}} + U_{\mathrm{pen}} + U_{\mathrm{coa}} \\ + U_{\mathrm{C2}} + U_{\mathrm{tors}} + U_{\mathrm{conj}} + U_{\mathrm{H\text{-}bond}} + U_{\mathrm{vdW}} + U_{\mathrm{elec}}. \end{aligned} \tag{11}$$

The bonded terms accounting for bond stretching, angle bending and torsion angle twisting are analogical to classical FF approach. In addition, new terms are implemented for lone pair energy, U_{lp}, over-coordination penalty, U_{over}, under-coordination term, U_{under}, stabilizing under-coordinated atoms; penalty for allene-type molecules, U_{pen}, angle conjugation, U_{coa}, $\mathrm{C}{=}\mathrm{C}$ correction, U_{C2}, torsion conjugation, U_{conj}, and finally hydrogen bond term, $U_{\mathrm{H\text{-}bond}}$. As is evident, the form is very complex and contains dozens of parameters (93 parameters were included in the original FF dealing with hydrocarbon systems)[108] of which only some have a physical meaning. Several parameters and therms have been added solely for the purpose to reproduce quantum-mechanical (QM) data. The complicated and unpredictable parameterization represents the main drawback of this approach, as was encountered in study dealing with thermal decomposition of fluorographene producing experimentally undetected products (see above).[115] However, reactive mechanics, given appropriate parameterization, may become very powerful tool indeed in order to explain unusual chemical behavior of some graphene derivatives even at relatively low computational cost.

3 Lipid Enhanced Exfoliation for Production of Graphene Nanosheets[1]

Novel lecithin assisted exfoliation method of production of graphene nanosheets was suggested. However, information was missing about the mechanism of graphene stabilization in non-polar environment in the presence of lipids. Hence, we used molecular dynamics (MD) simulations with a classical force field to study the exfoliation process and the subsequent aggregation of graphene in lecithin-chloroform solution. The theoretical calculations suggested that stability of the obtained colloid may originate from the formation of lecithin reverse hemimicelles and micelles, which prevent aggregation of the exfoliated graphene flakes by entropic repulsion of the exposed lipid hydrophobic chains.

Liquid-phase exfoliation of graphite is a widely used technique that allows preparation of high-quality graphene flakes in large-scales just by solvent treatment, whereby the exfoliated pristine graphene can be used in myriad of applications ranging from nanoelectronics to mechanical reinforcement of materials.[116, 117] Number of conventional solvents have

[1]Published as: Pykal M., Šafářová K., Machalová Šišková K., Jurečka P., Bourlinos A. B., Zbořil R., Otyepka M., J. Phys. Chem. C, 2013, 117 (22), p. 11800–11803.

been suggested in the literature.[33–35] The overall yield of graphene solubilization is typically a few percents; the portion of monolayers in the resulting colloid could be improved by post-processing up to 7–12 %.[35] Searching for new suitable exfoliation media is thus a continuous task. Recently, it has been shown, that relevant solvents should have surface energies matching the surface energy of graphene.[32, 36] However, not every solvent with surface energy close to that of graphene is an efficient exfoliant. Arguably, more relevant are the Hansen solubility parameters derived from polar, non-polar and H-bonding cohesive interactions of organic materials.[36, 118] Here, the rule "like dissolves like" is applicable in a similar manner.

Interestingly, solvent exfoliation may be further assisted by the presence of additives dissolved in the liquid-phase, such as certain surfactants or polymers,[119, 120] which may increase the exfoliation yield and help to split the thick graphite plates into the thinnest possible flakes (< 5 nm). Typical examples of effective additives include long alkyl-chain surfactants having a hydrophobic tail and a polar head group.[121, 122] Here, it was

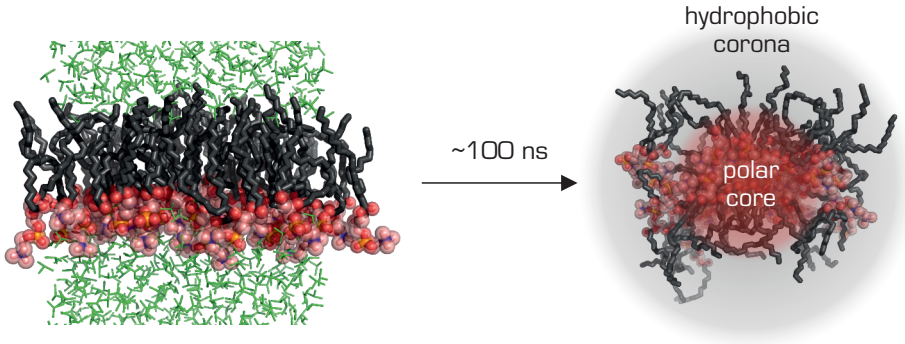

Figure 4: Representation of a reverse DOPC micelle formed in a chloroform solution (after about 100 ns); and its structure layout.

shown that the exfoliation efficacy could be significantly enhanced by addition of lipids, namely lecithin. Nevertheless, the mechanism lying behind the efficiency improvement was rather unclear. Lecithin is a natural occurring phospholipid with two pending hydrophobic alkyl chains and a polar head group in its structure. The choice of lecithin becomes even more attractive when considering the fact that phospholipids are a major component of all cell membranes. Thus, lecithin-graphene hybrids could display good biocompatibility and low toxicity in (bio)applications.[123, 124]

In order to elucidate how the presence of lecithin can enhance the exfoliation process we carried out MD simulations on $+0.5$ μs time scale. The MD represents a powerful computational method that is now frequently used as an integral part of basic research apparatus. Natural lecithin is a complex system mostly composed of phosphocholines, and therefore we simplified lecithin in our simulations by DOPC (1,2-dioleoyl-*sn*-glycero-3-phosphocholine) that is commonly used for membrane models. The MD simulations of DOPC solutions in chloroform showed that DOPC forms reverse micelles spontaneously on a 100 ns time scale (Figure 4), which was in agreement with prior experimental observations for similar solvents.[125] The core of reverse micelles contains polar DOPC heads and the hydrophobic tails are exposed to chloroform. We further analyzed the interaction of DOPC with graphene surface in chloroform. Two different starting geometries were built: one with hydrophobic tails oriented toward the graphene (Figure 5A), and the other one with polar heads oriented toward the graphene (Figure 5B). In both simulations, the reverse micelles were formed on the graphene surface and remained attached to the graphene sheet, leaving a large part of the hydrophobic tails exposed to solvent and free to sample their conformational space. As we will discuss below, this may play an important role in stabilizing the graphene flakes in the exfoliated state by preventing their aggregation.

Let one assume that some reverse micelles are present in solution and

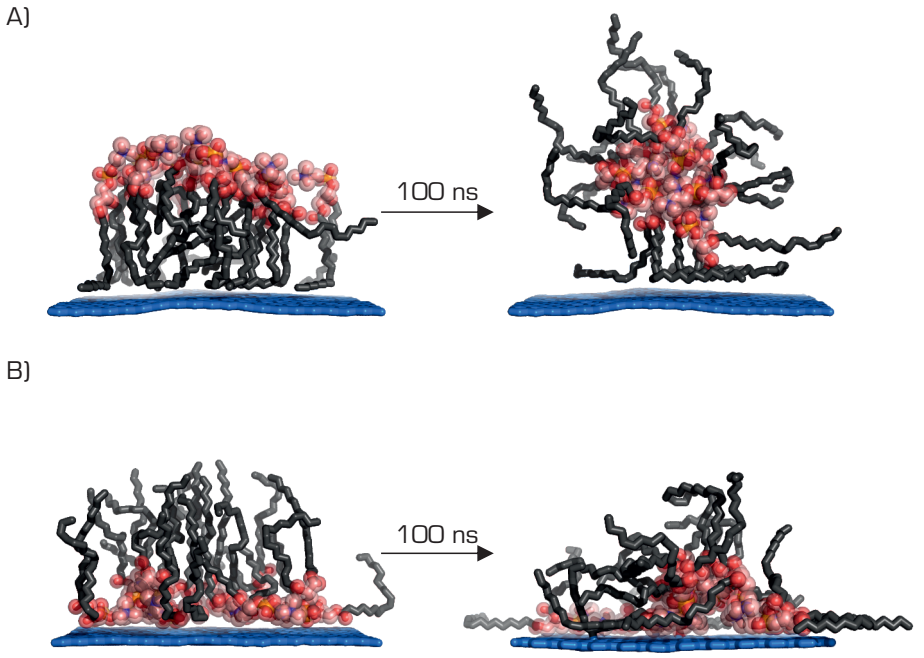

Figure 5: Simulations demonstrating formation of reverse DOPC (lecithin model) micelle (A) and hemimicelle (B) on graphene surface in chloroform. Chloroform molecules are omitted for clarity.

some are attached (and/or formed) on the surface of the freshly exfoliated graphene nanosheets. When approaching each other, the micelles repel due to the volume restriction effect (the system has tendency to increase its entropy), which prevents their aggregation.[126] The volume restriction effect originates from the restriction of the conformational space of exposed hydrophobic tails upon contact with other micelles. A similar effect should also be expected between the micelles and the exfoliated graphene sheets, as well as between the hemimicelles present on the graphene sheets and other graphene sheets (Figure 6). According to kinetic theory of graphene

aggregation, the resulting increase of the association barrier may significantly stabilize the dispersion.[127] Thus, the presence of the lecithin reverse micelles in solution and on the graphene surface may prevent self-aggregation of the exfoliated graphene by creating association barriers of

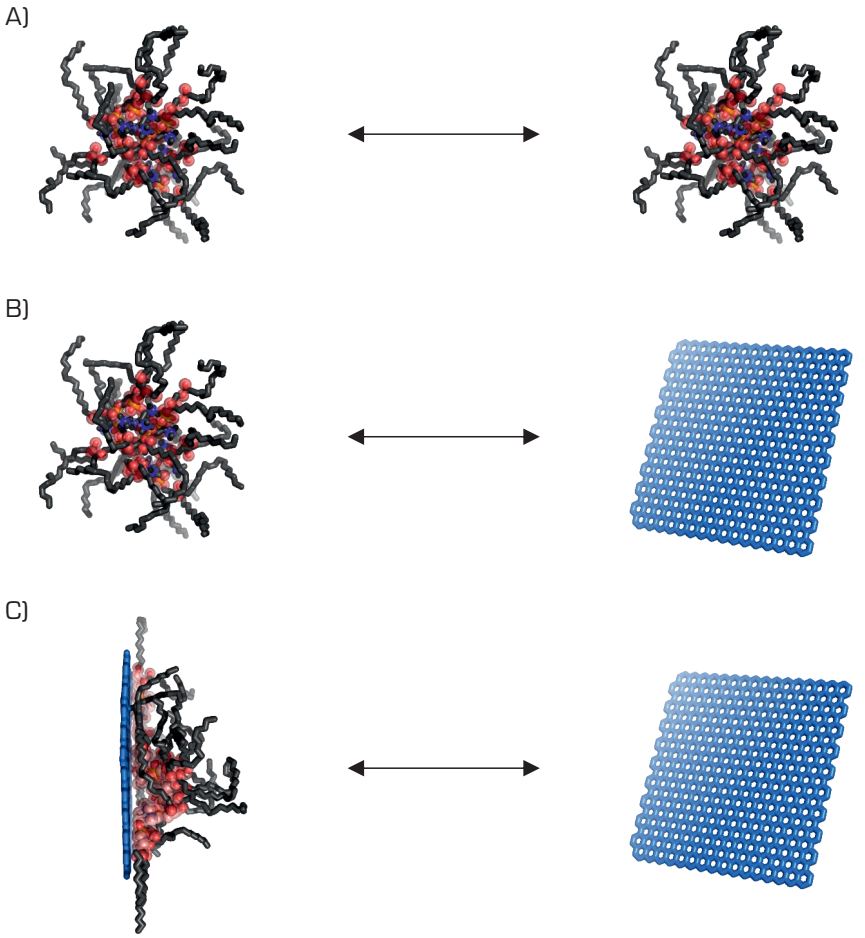

Figure 6: Schematics of steric repulsion between individual micelles (A), between the micelles and the exfoliated graphenes (B), and between attached hemimicelles and the graphenes (C).

entropic origin. It should be noted that lecithin might also play a role in the exfoliation process itself, for instance by stabilizing the exfoliation intermediates during ultrasound agitation, and thermodynamic stabilization of the exfoliated flakes cannot be ruled out as well. Thus, the above-described hypothesis may not be the only contribution to the lecithin effect on the exfoliation efficiency.

In this work we have proposed stabilization mechanism of the presented one-step method of graphene preparation by liquid-phase exfoliation in the lecithin–chloroform solution. Molecular dynamics simulations suggested that the higher stability of exfoliated graphene nanosheets under the presence of lecithin may be due to the formation of reverse micelles and their eventual attachment to graphene. The micelles repel each other by volume restriction effects that prevent aggregation of colloidal graphene.

4 Electric Quadrupole Moment of Graphene and its Effect on Intermolecular Interactions[2]

By their very nature, some effects cannot be covered by classical empirical potentials. It is mainly due to a number of simplifications implemented in the model (general potential functions). In specific cases this omission may lead to serious errors. One such example is the neglect of electronic multipole moments. It was shown, that the explicit quadrupole moment could affect the resulting barrier heights and the associated kinetics of graphene aggregation and thus may partly explain the experimentally observed exfoliation-efficiency difference between benzene and hexafluorobenzene. Equally, the quadrupole should be generally considered when simulating warped graphene sheet.

Importance of the liquid-phase exfoliation as low-cost alternative for mass-production of graphene was already pointed out in previous chapters together with the theory employing the similarity rule based on surface tension values and Hansen parameters of known convenient solvents. [36] However, as mentioned, this practice is not applicable for all solvents. From this perspective, benzene (C_6H_6) and hexafluorobenzene (C_6F_6) seem to be an interesting pair of molecules. Despite the relatively similar Hansen solubility parameters (see Table 3), the experimental data showed that while

[2]Published as: Kocman M., Pykal M., Jurečka P., Phys Chem. Chem. Phys., 2014, 16, p. 3144–3152.

the first is a very poor exfoliation media, C_6F_6 displayed a reasonable good efficacy.[33] One of the possible explanation may be in their differing quadrupole moment sign (but of similar magnitude). To test this hypothesis we decided to carry out molecular dynamics simulations with and without explicit quadrupole moments. Unfortunately, classical empirical potentials are not able to cover higher-order multipole interactions by their definition. Moreover, carbon atoms in simulations featuring graphene are typically treated as uncharged LJ spheres, thus any electrostatics interactions are not considered. It was shown that this simple approximation is reasonable when using large or periodic graphene models, where the electric multipoles will sum to zero. However, it may gain particular importance on edges, near structural defects and in case of small or corrugated graphene flakes. Here, the graphene's quadrupole moment was employing using virtual sites placed above and below each carbon atom located in the graphene lattice. The magnitude and distances were chosen to reproduce the experimentally observed value $-3.03 \pm 0.1 \times 10^{-40}$ C m^2/carbon, that was measured for graphite.[128]

To study the process of graphene exfoliation in benzene and hexafluorobenzene we used the potential of mean force (PMF) technique that may provide a valuable insight into the thermodynamics of this process. It

Table 3: Comparison of Hansen solubility parameters, surface tension and molar volume of benzene and hexafluorobenzene.

	Benzene	**Hexafluorobenzene**	**Graphene**
Dispersion (δ_D) [MPa$^{1/2}$]	18.4	16.9	18[b]
Polar (δ_P) [MPa$^{1/2}$]	0.0	0.0	10[b]
H-bonding (δ_H) [MPa$^{1/2}$]	2.0	0.0	7[b]
Surface tension [mJ m^{-2}]	28.2[a]	21.6[a]	68[b]
Molar volume [ml mol^{-1}]	89.4	115.4	–

[a] at 298.15 K; [125].
[b] [36].

should be noted that the liquid-phase exfoliation mechanism is still not fully understood. In addition, numerous exfoliation pathways could be considered. To model the exfoliation in benzene and C_6F_6 we pulled various graphene flakes from the periodic system by one of the peripheral carbons (as shown on Figure 7A), whereby the resulting PMF was obtained from a series of umbrella sampling simulations.[129] In simulations without explicit quadrupole moment the difference between those solvents was

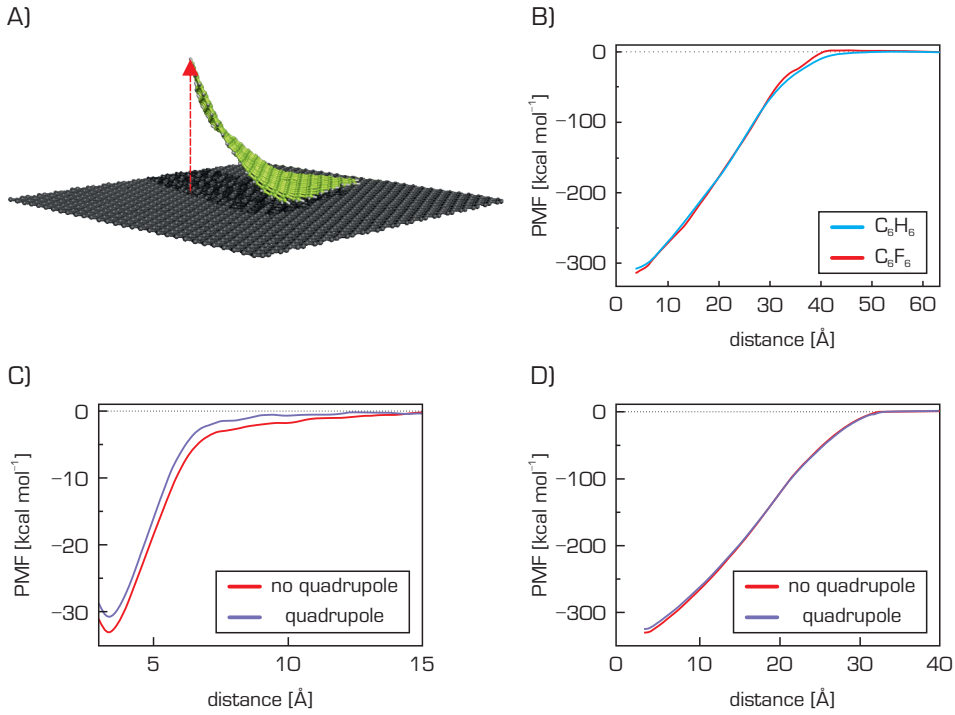

Figure 7: Schematics showing the peeling process with the considered exfoliation pathway (A); the potential of mean force (PMF) calculated for graphene pulled apart the periodic graphene system without quadrupole moment in benzene and hexafluorobenzene (B); circumcoronene (with and without the explicit quadrupole) (C) and C_{478} (again with and without the included quadrupole) in hexafluorobenzene (D).

nearly negligible (Figure 7B), which would result in similar exfoliation efficiency that was in contradiction with experiment. Apparently, the exfoliated state was predicted to be thermodynamically unstable to the given aggregated state, which was in agreement with former MD simulations of graphene in other organic solvents.[127] The energy required to detach the graphene layer recalculated to a single carbon atom in C_6F_6 was about 0.61 kcal mol^{-1} for the circumcoronene (C_{54}) and 0.69 kcal mol^{-1} for the larger graphene containing 478 carbon atoms. When quadrupoles were included in graphene structures, the energy dropped by 0.04 kcal mol^{-1} per carbon atom (from 0.61 to 0.57 kcal mol^{-1}) for circumcoronene (Figure 7C) and by 0.01 kcal mol^{-1} per carbon atom (from 0.69 to 0.68 kcal mol^{-1}) for C_{478} (Figure 7D). From this follows that contribution of the quadrupole is rather small and becomes less important with the increasing size of the peeled graphene.

Further attention was drawn to the stability of graphene colloids. Interactions among graphene-like molecules in benzene and C_6F_6 were studied by calculating PMF of two rigid parallel circumcoronene molecules. One of the circumcoronenes was not carrying any additional virtual sites to mimic the "endless planar" support, whereas the other was simulated using explicit quadrupole moment (it represented the peeled/aggregating flake, where it can be assumed that the quadrupole will be non-zero due to the bended or corrugated graphene structure). Results were compared hereafter with classical FF simulations (without any higher-order multipole contributions). Obtained values of exfoliation energies were in agreement with preceding simulations. Nevertheless, inclusion of quadrupole moments altered markedly the barrier heights (and thereby the kinetics) of resulting PMF curves (Figure 8). When omitting quadrupoles, the barriers were very similar. However, when quadrupoles were included, the association barrier increased by 4.2 kcal mol^{-1} in C_6F_6, while in benzene it decreased by 2.7 kcal mol^{-1} (it gave the resulting value of almost 7 kcal mol^{-1}). The height of the association barrier is of particular importance for kinetic

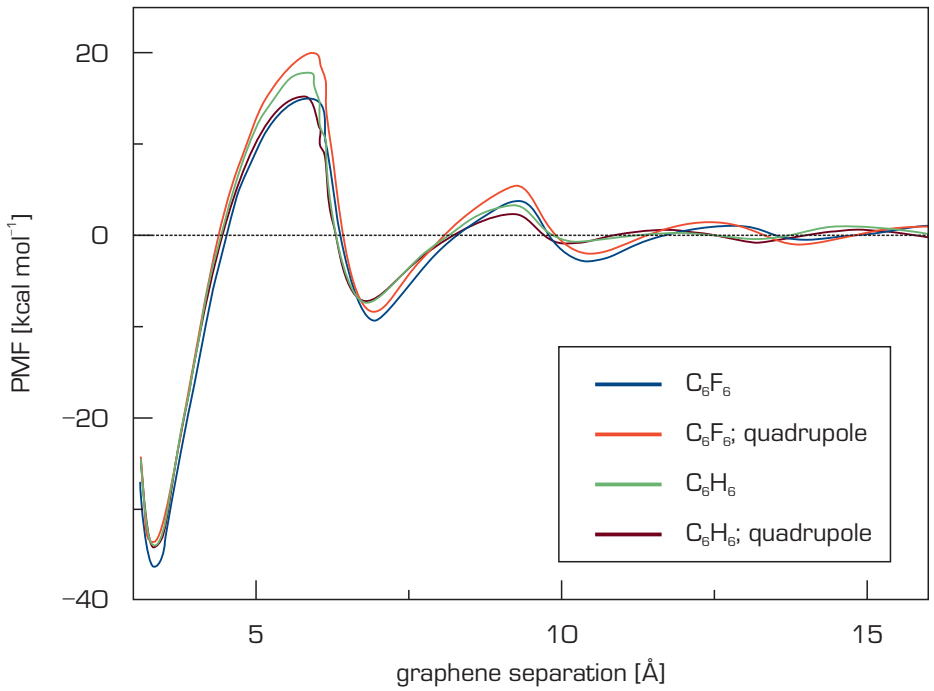

Figure 8: PMF of graphene separation modeled by circumcoronenes in given solvents with and without the inclusion of quadrupoles.

theory of graphene aggregation; increase of this barrier may substantially decrease the aggregation rate in C_6F_6 and stabilize the colloidal dispersion of graphene, which could partly explain the experimental observations.

In conclusion, we investigated the effect of electronic quadrupole moment of graphene on intermolecular interactions. The inclusion of quadrupoles was tested in MD simulations of graphene exfoliation/aggregation in benzene and hexafluorobenzene, which reported contrasting exfoliation efficacy despite their relative similarity. Although the thermodynamics of these processes was not significantly affected considering quadrupoles, it had substantial impact on the association barrier heights, which may kinetically stabilize exfoliated states in C_6F_6 compared to benzene and thus

partially explain the better exfoliation capability of C_6F_6. It indicates that the quadrupolar interactions should be taken into account in molecular simulations concerning exfoliation/aggregation of graphene.

5 Interaction of the Helium, Hydrogen, Air, Argon, and Nitrogen Bubbles with Graphite Surface in Water[3]

*The interaction of interfacial nanobubbles on solids immersed in water may be crucial in numerous industrial processes. The gas-graphite (or optionally the gas-graphene) interaction is in particular relevant for ink-jet printing, spray coating, gas storage, fuel cells or sensing. Moreover, the formation of bubbles on the solid-liquid interface may significantly impact the resulting wettability of the surface. Here, the interaction of gasses (*Ar, He, H_2, N_2 *and air) with graphite immersed in water media was studied both experimentally and theoretically using first principles methods and molecular dynamics simulations. It was shown that there is a relationship between contact angle and gas-graphite/gas-gas interaction ratio.*

The interaction of gasses and liquids with carbon structures is important in many application fields ranging from sensing and electrochemistry to non-covalent functionalization of graphene.[43, 130–133] Air bubbles may have also a serious impact on impinging processes on graphite.[134] In addition, the super-hydrophobic character of the surfaces is in many cases promoted by the interaction of gas bubbles with the substrate.[135,

[3]Submitted as: Bartali R., Micheli V., Gottardi G., Lazar P., Pykal M., Otyepka M., Ladani N., ACS Appl. Mater. Interfaces, 2016

136] Considering the importance of the liquid-gas-solid interface, in this work we explored the interaction of various gas bubbles (Ar, He, H_2, N_2 and air) with the freshly cleaved HOPG graphite surface in water. Firstly, brief experimental overview will be provided, followed by the results from molecular dynamics, that were used to complement the final experimental findings.

The morphology and surface chemistry of cleaved HOPG were evaluated using AFM and X-ray photoelectron spectroscopy (XPS) techniques. Generally, a smooth surface with only small portion of contaminants was observed. Subsequent experiments done in order to study the wetting behavior and the work of adhesion of different liquids on the exfoliated HOPG graphite showed a total surface tension of 52.8 mJ m^{-2}. This value was in agreement with prior measurements.[137] Furthermore, it was estimated that the dispersive component is responsible for more as 95 % of the surface energy (whereby the polar component encompass only small portion of 4.2 % interactions mainly through the oxygen contaminants), which explained the stronger interaction with non-polar liquids as diiodomethane and paraffin oil and weaker interaction with water. It indicates that dispersion is dominant attractive interaction of graphite, which is consistent with theoretical calculations for graphene.[22] Subsequently, the interaction of gasses with graphite in the aqueous media was explored using the captive bubble method. It was estimated that the surface tension with water for all of measured gasses is ~72.8 mJ m^{-2} and the expected decrease of surface tension caused by the internal pressure would be less than 0.4 %. The contact angle measurements showed that HOPG graphite exhibits a gasphilic (contact angle $< 90\,°$) behavior for helium and hydrogen, while a gasphobic (contact angle $> 90\,°$) behavior for air, argon and nitrogen was observed. Similarly, the dispersion is expected to be the governing interaction with gasses as well. The correlation between polarizability (that has fundamental effect on dispersion interactions, see Equation 6) and contact angle was demonstrated. Gasses with low polarizability showed attractive

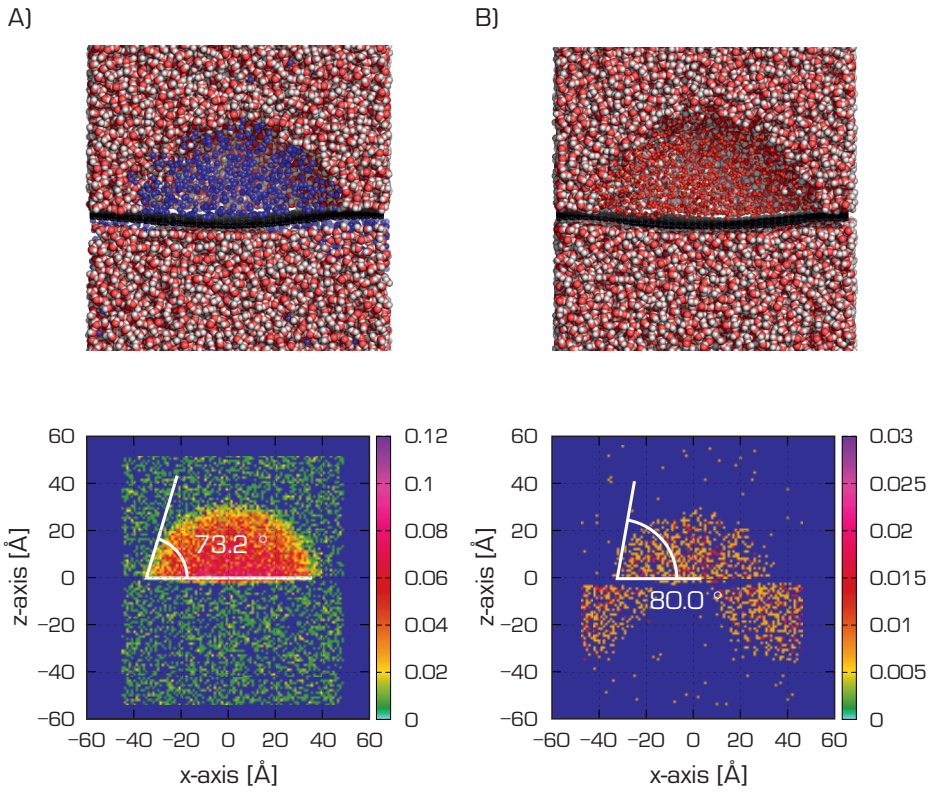

Figure 9: Contact angles of helium (A) and argon (B) calculated on the basis of MD; resulting values were averaged over the production run.

interaction with graphite and conversely. In other words, the higher the gas-gas interaction, the less gas adhesion on surface was shown. For more details, please see *Attachment*.

Even if the HOPG surface was well-controlled the bubble contact angle may be affected, for instance by small amount of airborne contaminants (when exposed to ambient conditions), as reported previously for water[25] or by the roughness of the cleaved surface. Hence, to understand better the interaction of the gas with a pristine surface we carried out MD

simulations in order to estimate the average contact angle of the water-gas-graphene system. Two extreme cases identified by experiments were chosen, i.e. the argon and helium gasses (Figure 9). Graphene was represented by periodic model with dimensions of 92 $\times$ 92 Å. The z-dimension of the box was set to ~100 Å. Carbons in graphene were simulated as uncharged LJ spheres with parameters proposed by Cheng and Steele.[104] Argon and helium parameters were taken from literature Ref.[138], Ref. [139], respectively. SPC/E water model was used for solvating the system. The initial configurations consisted of 1,567 gas molecules, which were randomly distributed within the simulating box. Obtained values of contact angles 73.2 °, 80.0 ° for helium and argon, respectively, matched the order obtained from experimental measurements. However, the estimations from MD differed in absolute values of the contact angle. It may be explained in part by the: i) size of the studied bubbles (radii of the simulated bubbles were typically around 40 nm); ii) by the different morphology of the surface (a perfectly flat model without terraces); and iii) in part by the fact that the classical force field methods neglect the polarization effects that may be important in such cases involving graphene and it would require further analysis, which was beyond the scope of this work. Nevertheless, MD simulations have confirmed that the variation of the bubble contact angles on graphite is governed by the nature of the gas and its interactions.

In conclusion, it was observed that exfoliated HOPG graphite exhibits an attractive interaction (gasphilic nature) with H_2 and He and weaker interaction (gasphobic nature) with Ar, N_2 and air. Experimental measurements in conjunction with molecular dynamics simulations showed the relation between the gas contact angle and the ratio of gas-graphite and gas–gas interactions.

6 Modeling of Graphene Functionalization[4]

Graphene has attracted great interest because of its remarkable properties and numerous potential applications. A comprehensive understanding of its structural and dynamic properties and those of its derivatives will be required to enable the design and optimization of sophisticated new nanodevices. While it is challenging to perform experimental studies on nanoscale systems at the atomistic level, this is the "native" scale of computational chemistry. Consequently, computational methods are increasingly being used to complement experimental research in many areas of chemistry and nanotechnology, thus providing new insights into the physical and chemical features of complex systems including graphene and graphene derivatives. In the following review we discuss the suitability of various computational methods in simulations regarding graphene as well as the latest trends in the computational chemistry research.

Despite extensive research efforts triggered by numerous potential applications of graphene and its derivatives,[6] only a limited number of graphene-based products have been successfully commercialized to date.

[4]Published as: Pykal M., Jurečka P., Karlický F., Otyepka M., Phys. Chem. Chem. Phys., 2016, 18, p. 6351–6372.

[140] Moreover, the graphene-based technology is still mainly in the research and development stage.[141] Among other purposes, graphene and its derivatives have diverse uses in sensing, ranging from the detection of small molecules[133] to large biomacromolecules,[142, 143] including also DNA translocation[144] and selective molecular sieving.[145] The potential range of applications for graphene can be enhanced enormously by covalent and non-covalent modification (Figure 10).[43] To understand the effects of these modifications, it is necessary to obtain an in-depth understanding of the nature and strength of the interactions between graphene and guest molecules. Computational chemistry is a valuable source of information that can be used to develop such an understanding. Although it provides a valuable insight into complicated scientific problems, one has to choose wisely an appropriate level of theory according to the studied topic. Always there should be chosen a compromise between accuracy and corresponding computational demands that are closely linked with the size of the calculated systems. This can be achieved using either electronic structure methods based on quantum mechanics or with molecular mechanics methods.

Graphene is often modeled as a finite polyaromatic hydrocarbon molecules (PAHs; benzene, coronene, etc.).[146] [22, 147–149] The carbon networks of these model molecules are capped with hydrogen atoms that saturate the dangling bonds at their edges. This affects the distribution of electronic density within the system because the electrons of the hydrogens are drawn to the carbon skeleton, generating a positive electrostatic potential on the hydrogen atoms and a negative electrostatic potential above and below the carbon sheet where the π-electron cloud is located. Consequently, PAHs have significant quadrupole moment that depend on their size (its importance was discussed already in the previous study, or see *Appendix*). This finite quadrupolar potential means that PAHs are imperfect models for the infinite flat periodic sheet of graphene, in which the quadrupole completely vanishes. Moreover, real graphene is corrugated

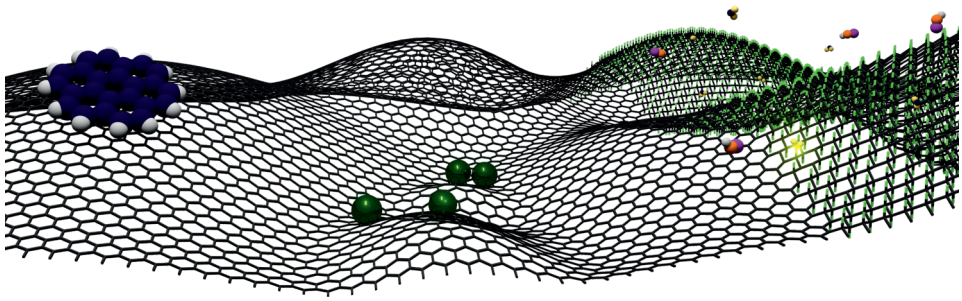

Figure 10: Schematics representing non-covalent and covalent functionalization of graphene.

and the quadrupole moment may be nonzero near its surface. An important advantage of using finite molecular models is that they can be studied using a wide portfolio of electronic structure methods developed for molecular systems. The only limitations come from the size of the system that can be treated in a reasonable timeframe with specific methods and the available computational power. This is in contrast with the empirical methods that allow the use of substantially larger models of freestanding graphene flakes (up to tens of nanometers) and are therefore applicable when studying nanoscale phenomena such as exfoliation and aggregation processes in colloidal dispersions of graphene or the role of structural defects on specific surface area of graphene.[127, 150, 151]

Ideal graphene is an infinite 2D sheet with a regular lattice structure. This periodic graphene model can be studied using numerous methods (using the periodic boundary conditions, usually abbreviated as PBC), most of which are based on DFT and were developed by solid-state physicists to model the physical features of crystals. However, the size of the replicating cell should be large enough to avoid undesired interactions between replicas. Spurious interactions could be particularly problematic if the supercell contains polar molecules or ions, because of the slow decay of Coulombic

forces. It should be noted that the attractive vdW forces in nanomaterials act over longer distances than was originally assumed.[152] In empirical methods the periodical/infinite model help to evade some artifacts that can be caused by the presence of edges, as discussed above. Furthermore, the infinite model may better describe the situations encountered in some experiments, such as those involving measurements on spots of graphene flakes that may be multiple micrometers in diameter. On the other hand, PBC models may be less suitable for studying phenomena such as surface corrugation because the box size limits the scale on which corrugation effects can be studied. In the following text I will focus mainly on the empirical methods and their use and limitations in nanomaterial applications.

The advantage of the molecular mechanics approach over QM models is its simplicity and low computational cost (Figure 11). Unfortunately, its approximations mean that many phenomena cannot be explicitly accounted for by the FFs. The problem of the quadrupole moment and also the other interactions that are challenging or even impossible to describe with a classical force field have been already addressed in the preceding parts of the thesis. As a reminder, these include the charge transport, explicit polarization, and the charge redistribution caused by corrugations of a graphene surface.

The neglect of polarization interactions is perhaps the most serious deficiency of common pairwise additive force fields when modeling graphene and its derivatives. Conventional FFs treat electrostatic interactions using effective partial charges that are constructed to match electrostatic potentials obtained from QM calculations. Consequently, it is impossible for the classical FF to react to changes in the molecular environment or to describe the way different solvents affect various interactions. Ho *et al.*[153] studied the effect of graphene polarization on the structural properties of water molecules at a graphene–water interface. Their results suggested that the explicit inclusion of polarizability had no significant effects on the dynamics of the graphene-water system, and that the effect became even smaller

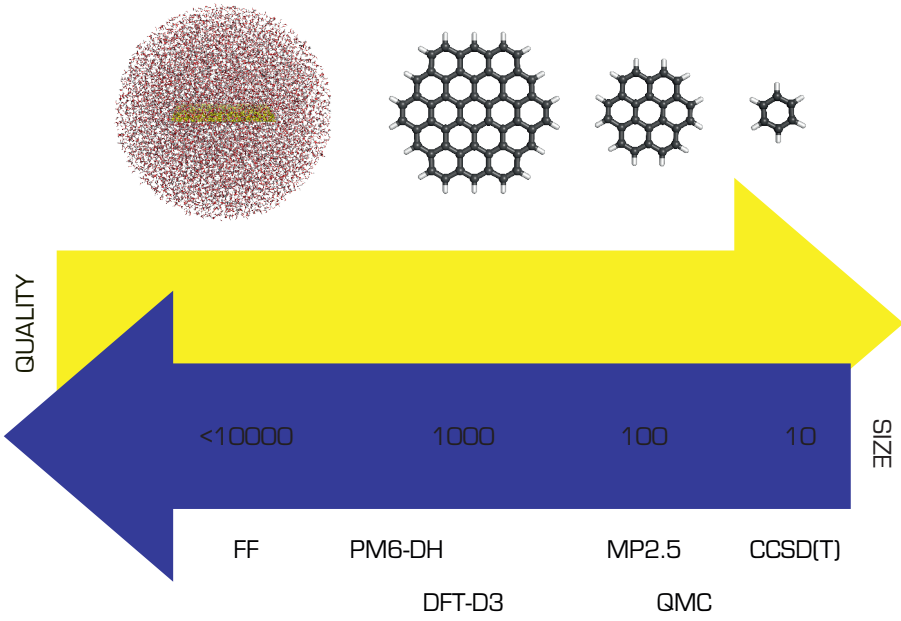

Figure 11: Comparison of several theoretical approaches with respect to the size of the system that can be treated efficiently and the quality of the resulting description (adopted from [154]).

for charged graphene. However, larger effects might be expected for ions and their arrangement near the graphene surface. Another drawback of current force fields is the pairwise additive approximation of the vdW interactions, where the resulting energy is calculated as a sum of contributions from individual pairs of atoms up to the cutoff distance. Many-body terms involving three or more atoms are not explicitly included. Although, as mentioned, force fields are parameterized against experimental data and thus include many-body effects implicitly, in some cases it might be necessary to include at least three-body effects explicitly.[78, 79]

Currently, it is considered that the widely used AMBER FF generally tend to overestimate the base-stacking interactions in nucleic acids.[155, 156] It may be of crucial importance in empirical simulations involving

vdW interactions of graphene and its derivatives as well. Especially when these interactions are mostly the exclusive interactions which are taken into account in graphene modeling (as mentioned earlier, carbons in classical FF approach are treated as uncharged LJ particles). However, this fact has not been thoroughly investigated yet, and there is a need for a deeper analysis of its influence on the simulations concerning graphene.

Computational chemistry provides valuable atomistic insight into the properties of systems that are relevant in bio-disciplines and nanoscience. While computational methods are constantly evolving, they have already succeeded in several tasks and are undoubtedly becoming an integral part of the basic research toolkit. Because of the on-going increases in available computing power, the sizes of the systems amenable to modeling and the lengths of the simulation times that can be handled are both increasing, meaning that computational methods will continue to get more powerful and important.

7 Direct Mapping of Chemical Oxidation of Individual Graphene Sheets through Dynamic Force Measurements at Nanoscale[5]

Graphene oxide is a greatly promising material for diverse application including batteries, sensors, drug delivery and optoelectronics. Typically, graphene oxide is prepared by oxidation of graphene. Nevertheless, the resulting structure of graphene oxide is complex not well-characterized—surface chemistry is not known so far and can vary considerably among the samples, which can dramatically affect its applicability. Here, the oxidation process of graphene during the UV/ozone treatment was studied using the in situ AFM-based dynamic force mapping and computational techniques. It was shown that the graphene edges are most sensitive to the chemical oxidation, from where it propagates further to the surface.

Despite the tremendous graphene's application potential, some of its characteristics make it unsuitable for certain specific uses, for instance in electronics, drug delivery, etc. However, this handicap does not apply to graphene oxide (GO). Due to the presence of oxygen containing groups,

[5]Submitted as: Froning J.P., Lazar P., Pykal M., Quiang L., Mingdong D., Zbořil R., Otyepka M., Nanoscale, 2016.

graphene oxide can easily disperse in aqueous media[46] and exhibits fluorescence over broad range of wavelengths,[50] which opens also the door to biological and medicinal utilization.[157–159] Besides that, GO shows higher reactivity compared to graphene[48, 160] that may help broaden new horizons through its functionalization.[161] Nevertheless, further progress is slowed down due to the complexity of the GO structure. A large number of defects and various functional groups substantially complicate addressing its electronic properties, morphology and reactivity. Moreover, the oxidation mechanism of GO is not fully understood yet and remains highly challenging. Recently, it has been shown by standard force microscopy, that there is a relation between the adhesion and degree of oxidation of graphene making AFM a valuable tool for exploring oxidation processes.[162]

In this work, the morphological changes upon stepwise graphene oxidation at ambient conditions were studied using the AFM-based dynamic force mapping in combination with theoretical methods. XPS showed that ozone primarily affects the carbon flake, whereby the $\mathrm{C/O}$ ratio was increasing with each ozonization cycle until it saturates (whereas the $\mathrm{Si/O}$ ratio of the silica substrate remained constant). The process of graphene oxidation was then simulated using the ReaxFF reactive force field that has been shown to successfully describe bond formation and bond breaking in hydrocarbon-oxygen containing systems.[163] The force field parameters for the MD simulations were chosen to match known parameters for the structural evolution of GO during thermal annealing.[164] Here, we considered a non-periodic graphene sheet, either uncapped or capped with hydrogen atoms that was immersed in rectangular simulation box with atomic oxygen (Figure 12). Because the studied reactions were expected to occur on a timescale larger than accessible with present computational facilities, we ran our simulations at 473, 673 and 873 K, increasing the collision frequency. In the case of hydrogen-capped graphene oxygen containing groups replaced some of the hydrogens on the capped edges of the

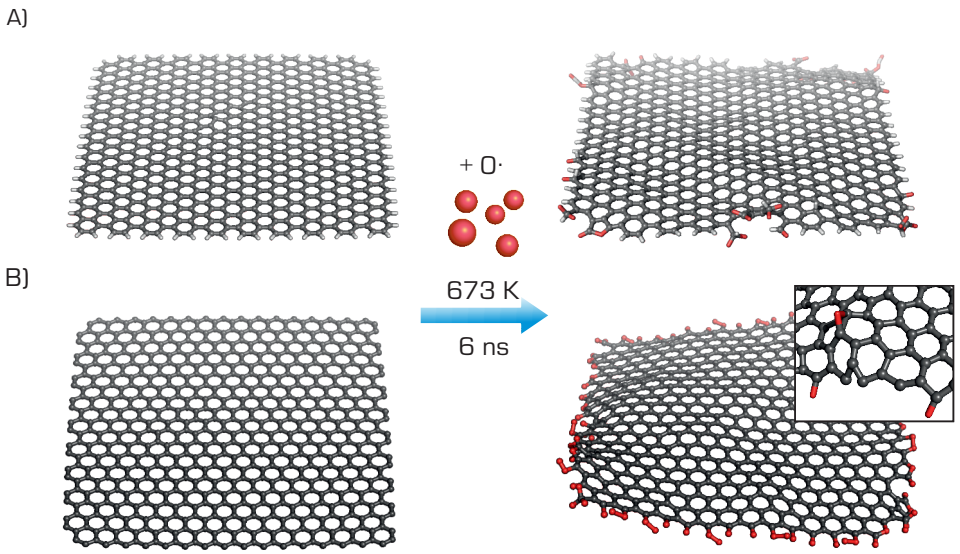

Figure 12: The oxidation of capped graphene by hydrogen atoms (A), and uncapped graphene (B) by atomic oxygen (shown in red; unbound oxygen atoms are omitted for clarity) was modeled by a 6 ns-long reactive MD simulation. The inset shows detail of the edge and an epoxy group on the basal plane.

graphene flake. It was shown that the edges exhibit greatest susceptibility for oxidation, similarly as it has been shown in experiments. The uncapped edges, in the second set of simulations, were fully saturated with various oxygen-containing functional groups in accordance with recent electrochemical observations.[47] Further evolution in the oxidized structure was not observed, only rare events occurred (two events in total per the simulation set, when an epoxy group was formed near of oxidized edge). It could be explained in part by the insufficient simulation timescale that is not able to capture the process of graphene oxidation and in part by the parameters used in these simulations that are not optimal parameterized for this particular problematic, although they have been successfully

used in simulations of the hyperthermal oxygen impact on graphene or HOPG.[165, 166]

In addition, the oxidation of graphene was monitored using the AFM-based techniques. DFT calculations showed that the AFM tip–surface interaction is governed chiefly by non-covalent interactions for both graphene and GO, thus any significant transformation caused by oxidation was not expected. Subsequent dynamic force mapping measurement revealed a different degree of graphene oxidation on the edges and on the basal plane after the first oxidation cycle. It was found that folds and step edges are oxidized preferentially, which was in agreement with reactive MD simulations. Further oxidation led to the gradual leveling of the adhesion contrast between the center of the flake and its edges without significant changes in the graphene topography. After the last treatment cycle the contrast in adhesion of the flake and the substrate was inverted, and several defects in the structure were detected.

In conclusion, we studied the mechanism of graphene oxidation during the UV/ozone treatment. In particular, changes in the topography and chemical composition were examined. The process of oxidation was gradually monitored using the AFM-based dynamic force mapping method under ambient conditions. It was shown by combination of theory and experiment that edges and bended graphenes exhibit higher susceptibility to oxidation than the rest of the flake.

8 Fluorographene—The Youngest Member of Graphene Family[6]

Discovery of two-dimensional materials caused a revolution in nanomaterial science. Nowadays the 2D materials constitute an integral part of material chemistry but they are still in the process of dramatic development. In 2010, fluorographene (graphene fluoride) extended the family of 2D materials and is now considered as the thinnest known insulator with a band gap as large as 8 eV. For a long time, fluorographene was considered as an non-reactive 2D counterpart of teflon®. However, recent studies show that fluorographene can react with numerous reagents yielding interesting new graphene derivatives. Intensive experimental and theoretical effort aim to understanding of properties and reactivity of this chemical structure. If we succeed in controlling the chemical behavior of this material, fluorographene may become a rising star of future material research. In this review we summarize current knowledge and recent advances in fluorographene research.

Shortly after the first isolation,[1] it was demonstrated that graphene possesses anomalous character.[6] However, some specific features of graphene (i.e., zero band gap, hydrophobicity, relative chemical inertness) are not suitable for certain applications. They may be further adjusted by covalent

[6]Published as: Pykal M., Zbořil R., Otyepka M., Chemické listy, 2016, 110, p. 335–343.

or non-covalent functionalization.[43, 167] Especially, the covalent modification may completely change the basic characteristics of the material. Fluorographene, a stoichiometric fluoro-derivate of graphene, represents a remarkable example of this covalent alteration.[59, 60] Binding of fluorine to each carbon atom of graphene change the original semiconductor to the thinnest isolator in the world, making it particularly promising for nano-electronics.[168]

The covalently bound fluorine causes the change in hybridization of the carbon atoms from sp^2 to sp^3, resulting in loss of aromaticity and warping of the structure. In comparison with the unit cell of graphene, the lattice constant of CF is stretched by approximately 1 % and the $C-C$ bond length increases to 1.58 Å (from original 1.42 Å). It was predicted that CF is most stable in the chair conformation, whereby the individual layers in fluorographene are in the AB arrangement (half of the carbon atoms lie above the centers of hexagons). Additional mutual structures were proposed, based on the X-ray diffraction (XRD) and nuclear magnetic resonance (NMR) spectroscopy. First calculations, however, indicated that the energy difference between studied forms is rather small and effect of different layering pattern is almost negligible.[169] (Another geometrical features are summarized on Figure 13.) Young's modulus of CF was measured to be $110 \pm 30\,\mathrm{N\,m^{-1}}$, which is one third of graphene.[59] However, theoretical values are almost half as large.[170] Interestingly, the strength of the $C-F$ bond is changing with the fluorine content in the structure. It was found that the dissociation energy of $C-F$ in partially fluorinated systems is around 50 kcal mol^{-1}, whereas for fully fluorinated structures it reaches up to 112.3 kcal mol^{-1} (which is comparable with the energy of $C-F$ bond in common organic compounds).[62, 171] Individual layers are then held together exclusively by non-covalent vdW interactions, whose value has been calculated equal to $0.19\,\mathrm{J\,m^{-2}}$.[72]

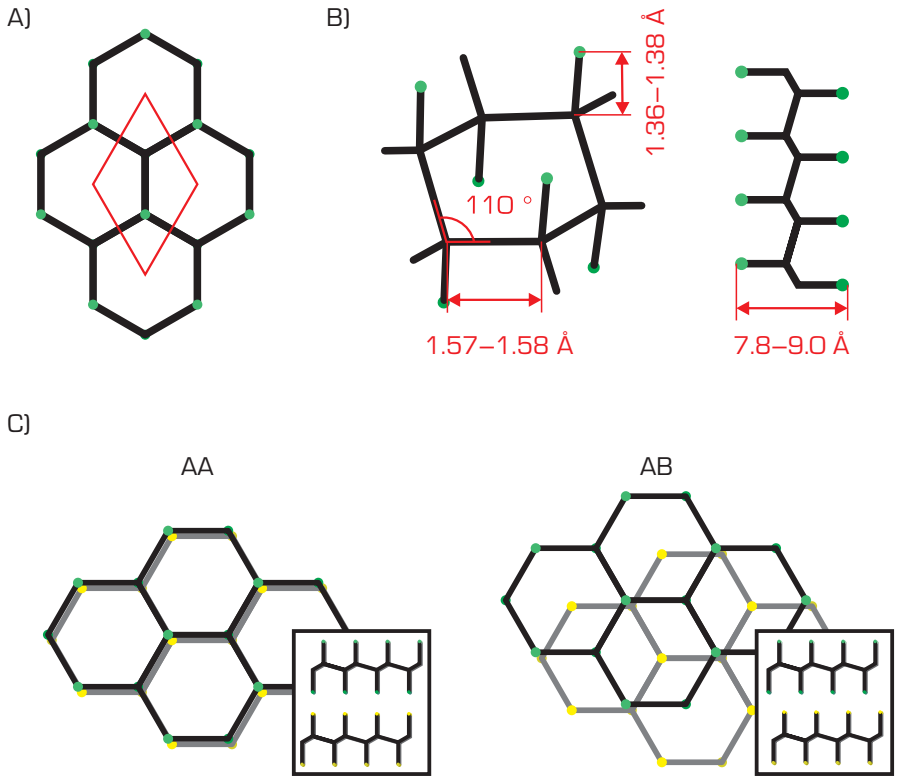

Figure 13: Representation of the hexagonal lattice of fluorographene (fluorine atoms are in green, carbons in black) and its unit cell (indicated by the red line) (A); basic geometrical parameters of CF (B); and AA and AB stacking order of fluorographene layers (C).

The electrical band gap of CF was estimated experimentally from optical absorption spectra or near edge X-ray absorption fine structure (NEXAFS) spectroscopy measurements and is assumed to be higher than 3.0 eV and 3.8 eV, respectively.[59, 60] Moreover, it was shown that band gap rapidly increases with even small amount of fluorines in the structure.[64] Computational methods generally agree on the shape of the electronic band structure showing that CF has the smallest energy gap between valence

and conduction band at the Γ point. However, they differ substantially in estimates of the bang gap. The lowest value, 3.0 eV, was obtained using DFT at the LDA and GGA level.[172] But it is known that these approaches systematically underestimate the band gap[173] and the apparent agreement with experimental values is only coincidental. On the contrary, HF methods tend to overestimate this value.[174] Thus the use of hybrid functionals offers a promising route in this context. Moreover, it was proven that hybrid functionals accurately predict the band gaps of some solid-state and carbon-based materials. In the case of CF, recent HSE06 calculations give a band gap value of 5.1 eV.[61] In addition, using a more demanding GW (Green's function with screened Coulomb interaction) approximation, one gets the even higher value 8.3 eV (on the level GW@HSE06).[61] Nevertheless, thus calculated values cannot be directly compared with the optical absorption spectra measurements, which involve formation of an exciton. This fundamental difference between the very accurate calculations and experiments undoubtedly requires further analysis.

Recently, it turned out that the most interesting is the chemistry of fluorographene. It was thought that similarly as teflon® and other perfluorinated hydrocarbons, CF will be a relatively chemically inter material. It was further supported with high thermal stability.[59] However, latest studies suggested that fluorographene may act as precursor in many substitution reactions[65–67], resulting in a variety of novel graphene derivates (see Figure 14).[62] The first reported was the mentioned reaction with KI at relatively mild conditions (150 °C), when the CF was converted back to graphene (while releasing I_2 from the transient unstable iodographene). Subsequent theoretical calculations regarding other halogen derivates of graphene suggested that only chlorographene and certain mixed halogengraphenes (besides CF) may exist under low temperatures.[60, 175] Furthermore, the reaction with NaSH yielded a novel modification of CF—thiofluorographene.[66] Elemental mapping revealed that fluorine and sulfur atoms are homogeneously distributed across the surface. Following

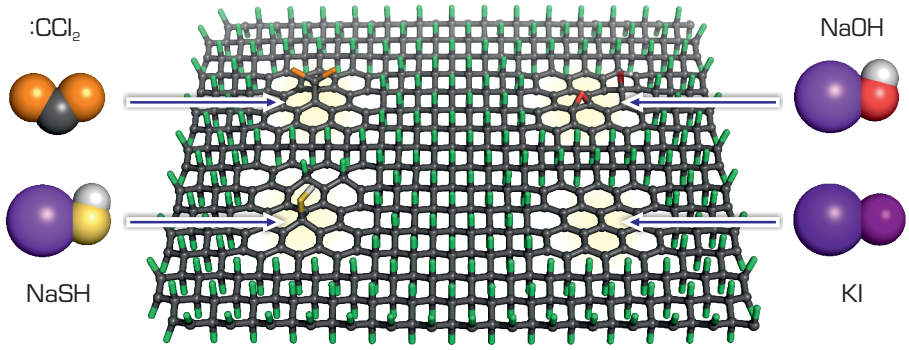

Figure 14: Schematics representing products of reactions of fluorographene with various chemicals; (adopted from [176]).

DFT calculations suggested an adequate structural model. It was shown that fluorine stabilizes otherwise spontaneously desorbing thiol groups; the most stable mutual arrangement of —F and —SH groups was identified the *ortho* (1,2-) configuration. Estimated band gap ranged between 1 and 2 eV that would meet today's technological requirements of the semiconductor industry. An interesting chemistry is also behind the reaction of CF with dichlorocarbene.[65] The $=CCl_2$ groups were again distributed uniformly over the entire CF sheet. In addition, the mechanism of cycloaddition on CF and partially fluorinated graphene was studied through DFT calculations. Because the dichlorocarbene adds on unsaturated bonds, it is belived that reaction occurs in two steps. The physisorbed dichlorocarbene causes defluorination of the precursor, while another molecule is added on the unsaturated bond. However, one cannot exclude the possibility that the elimination of fluorine atoms (generating unsaturated spots) is due to the alkaline conditions that are required for the formation of dichlorocarbene.[62]

Graphene, its derivates and other 2D structures are remarkable nanomaterials that offer great promise for future applications. Quite recently,

the family of 2D materials was extended by fluorographene. This exceptionally interesting chemical was identified that reacts under mild conditions with wide variety of reagents such as NaSH, NaOH, $\mathrm{CCl_2}$, $\mathrm{NaNH_2}$ and $\mathrm{N_2H_4}$ yielding interesting new derivatives. However, the reactivity is not yet well understood and controlled preparation (and thus the chemical behavior) remains still a long-term wish. If one succeeds, fluorographene may cause a similar excitement as that of graphene.

Summary

This thesis focused mainly on the study of interactions of small molecules with carbon-based 2D materials using the combination of various computational chemistry methods. In particular, attention was paid to the liquid-phase exfoliation of graphene, gas–graphene interactions on the interfaces and the intrinsic reactivity of certain graphene derivatives.

In a combined effort of theory and experiment it was shown that exfoliation process may be significantly enhanced by addition of surfactants into the exfoliation bath. Molecular dynamics simulations suggested that the reason of the increased colloid stability and thus the better exfoliation efficacy in chloroform/lecithin solution may arise from the formation of reverse micelles. These reverse micelles, whether attached on graphene surfaces or freely dispersed in solution, are mutually repealing due to the entropic repulsion acting between the exposed hydrophobic lipid tails and stabilizing the exfoliated graphene sheets.

A completely different stabilization mechanism was proposed for two seemingly similar solvents—benzene and hexafluorobenzene. In addition, the significance of electric quadrupole moment on molecular simulations of graphene exfoliation/aggregation was evaluated. The inclusion of electric multipole moments markedly affected the energetic barrier to association (whereas the thermodynamics remained unaltered) which may kinetically stabilize the exfoliated state and prevent the aggregation in C_6F_6 and other solvents.

Subsequently, molecular dynamics simulations were used in order to complement the experiment investigating the gas–HOPG interaction in water medium. From the technological point of view, the gas–graphene interaction is equally important as the liquid–graphene interaction. It was shown that the variance of the gas contact angle is predominantly determined by the gas nature and its interactions. It was observed that helium and hydrogen exhibited an attractive interaction with the graphitic surface, whereas argon, nitrogen and air were attracted by a weaker interaction. The resulting value of the gas contact angle was then given by the ratio of gas-graphite/gas-gas interactions.

In these applications, computational chemistry proved to provide a new valuable insight into diverse systems and processes on the atomic scale. However, orientation among the number of available methods and their applicability may be complicated. An appropriate method must always be selected with regard to the desired requirements and accuracy. Thus, a comprehensive description of various computational methods and conventional models used in simulations of graphene functionalization was provided in our review article. Special emphasis was put on their benefits, limitations and practical applications.

Nevertheless, classical molecular dynamics is occasionally unable to encompass some effects due to its serious approximations. Therefore, the reactivity of graphene oxide was studied using reactive ReaxFF force field. It was shown, again by combining the theoretical calculations and available experimental measurements, that the graphene oxidation is initiated on the edges from where it spreads over the entire surface. It is believed that these advances are likely to contribute to the highly desirable targeted preparation of precisely defined graphene derivatives with the corresponding properties. Recent works showed that the use of fluorographene may be even more advantageous for this purpose, whereby the current progress in fluorographene research was reviewed in the last part of this thesis.

In general, the great potential of computational chemistry was demonstrated, where the main contribution of this work was in providing insight complementary to that obtained by experiment in order to enhance knowledge of particular topics that led to the final interpretation of the collected results.

Shrnutí

Předkládaná práce byla zaměřena převážně na studium interakcí malých molekul s uhlíkovými 2D materiály s využitím různých metod výpočetní chemie. Zejména se věnuje exfoliaci grafenu v kapalné fázi, vzájemnými interakcemi grafenu s molekulami plynu na jeho rozhraních a reaktivitou některých grafenových derivátů.

Společným úsilím experimentálních a teoretických technik bylo ukázáno, že exfoliace grafenu může být podstatně vylepšena přídavkem povrchově aktivních látek do exfoliační lázně. Pomocí molekulových simulací byl navržen mechanismus, který stál za zvýšenou stabilitou koloidu, a tím i za lepší exfoliační účinností, která byla pozorována v roztoku chloroformu s přídavkem lecitinu. Bylo pozorováno, že lecitin v nepolárním prostředí vytváří reverzní micely, ať už na povrchu grafenu nebo volně v roztoku. Ty se pak následně vzájemně odpuzují kvůli entropické repulzi hydrofóbních lipidových řetězců, a tím brání agregaci dispergovaných grafenů.

Jiný stabilizační mechanismum byl pak navržen pro dvojici na první pohled podobných rozpouštědel—benzenu a hexafluorobenzenu. Ve skutečnosti však vykazují zcela rozdílné exfoliační výtěžky. Navíc byl také studován význam vyšších elektrických multipólů na molekulové simulace zabývající se agregací a exfoliací grafenu. Zahrnutí kvadrupólového momentu výrazně ovlivnilo asociační energetickou bariéru hexafluorobenzenu, zatímco termodynamika tohoto procesu zůstala nezměněna. Tato

skutečnost by vedla ke kinetické stabilizaci exfoliovaného stavu a bránila tak agregaci grafenu v C_6F_6 a obdobných rozpouštědlech.

Následně byl použit aparát molekulové dynamiky k doplnění experimentálních poznatků týkajících se interakce mezi různými plyny a HOPG ve vodném prostředí. Z technologického pohledu je tato interakce stejně důležitá jako častěji zmiňovaná interakce kapalina–grafen. Bylo ukázáno, že hodnoty kontaktních úhlů jednotlivých plynů jsou převážně určeny povahou plynů a jejich vzájemnými interakcemi. Helium společně s vodíkem vykazovalo přitažlivou interakci s grafitickým povrchem, zatímco argon, dusík a vzduch byly vázáni slaběji. Výsledné hodnoty kontaktních úhlů pak byly dány poměrem interakcí plyn–grafit a plyn–plyn.

V daných aplikacích bylo ukázano, že výpočetní chemie je schopná poskytnout nový cenný pohled do rozmanitých systémů a procesů, a to až na úrovni jednotlivých atomů. Nicméně, orientace mezi velkým počtem dostupných metod a jejich použitím se může zdát velmi složitá. Zvolená metoda by měla být vždy volena s ohledem na požadavky a očekávanou přesnost. Náš souhrný článek se snaží poskytnout popis jednotlivých metod a modelů, které jsou často používany pro simulace grafenu a jeho modifikací. Zvláštní důraz byl kladen především na výhody, omezení a praktické aplikace jednotlivých přístupů.

Někdy však klasická molekulová dynamika nedokáže obsáhout některé efekty a skutečnosti kvůli svým zjednodušením. Z tohoto důvodu byla studována reaktivita grafen-oxidu pomocí reaktivního silového pole ReaxFF. Opětovným spojením teoretických výpočetních metod a experimentálního měření se ukázalo, že oxidace grafenu je iniciována na jeho okrajích, odkud se pak dále šíří po povrchu. Předpokládá se, že tyto dílčí poznatky by mohly významně přispět k tížené řízené přípravě grafenových derivátů s odpovídajícími vlastnostmi. Nedávné studie ukázaly, že vhodnějším kandidátem pro tyto účely může být fluorografen, přičemž v poslední části práce je shrnut současný pokrok a směr výzkumu týkající se fluorografenu.

Obecně byl prokázán velký potenciál, který tkví ve výpočetní chemii. Hlavní přínos této disertace spočíval v teoretických simulacích a doplnění poznatků získaných ze souvisejících experimentálních měření za účelem hlubšího porozumnění jednotlivým problematikám a lepší interpretaci získaných dat.

List of publications

1. **Pykal M.**, Šafářová K., Machalová Šišková K., Jurečka P., Bourlinos A. B., Zbořil R., Otyepka M., Lipid Enhanced Exfoliation for Production of Graphene Nanosheets, *J. Phys. Chem. C*, **2013**, *117* (22), p. 11800–11803.

2. Kocman M., **Pykal M.**, Jurečka P., Electric Quadrupole Moment of Graphene and its Effect on Intermolecular Interactions, *Phys Chem. Chem. Phys.*, **2014**, *16*, p. 3144–3152.

3. **Pykal M.**, Jurečka P., Karlický F., Otyepka M., Modelling of Graphene Functionalization, *Phys. Chem. Chem. Phys.*, **2016**, *18*, p. 6351–6372.

4. **Pykal M.**, Zbořil R., Otyepka M., Fluorographene—The Youngest Member of Graphene Family, *Chemické listy*, **2016**, *110*, p. 335–343.

5. Froning J.P., Lazar P., **Pykal M.**, Quiang L., Mingdong D., Zbořil R., Otyepka M., Direct Mapping of Chemical Oxidation of Individual Graphene Sheets through Dynamic Force Measurements at Nanoscale, *Submitted*, **2016**.

6. Bartali R., Micheli V., Gottardi G., Lazar P., **Pykal M.**, Otyepka M., Ladani N., Interaction of the Helium, Hydrogen, Air, Argon, Nitrogen Bubbles with Graphite Surface in Water, *Submitted*, **2016**.

References

(1) Novoselov, K. S.; Geim, A. K.; Morozov, S. V.; Jiang, D; Zhang, Y; Dubonos, S. V.; Grigorieva, I. V.; Firsov, A. A. *Science* **2004**, *306*, 666–669.

(2) Landau, L. D. *Phys. Z. Sowjetunion* **1937**, *11*, 26–35.

(3) Peierls, R. *Helvetica Physica Acta* **1934**, *7*, 81–83.

(4) Boehm, H. P.; Clauss, A.; Fischer, G.; Hofmann, U. *Proceedings of the Fifth Conference on Carbon* **1962**, 73–80.

(5) Geim, A. K. *Science* **2009**, *324*, 1530–1534.

(6) Geim, A. K.; Novoselov, K. S. *Nature Materials* **2007**, *6*, 183–191.

(7) Chen, J.-H.; Jang, C.; Xiao, S.; Ishigami, M.; Fuhrer, M. S. *Nature Nanotechnology* **2008**, *3*, 206–209.

(8) Castro Neto, a. H.; Peres, N. M. R.; Novoselov, K. S.; Geim, a. K. *Reviews of Modern Physics* **2009**, *81*, 109–162.

(9) Lee, C.; Wei, X.; Kysar, J. W.; Hone, J. *Science* **2008**, *321*, 385–388.

(10) Zandiatashbar, A.; Lee, G.-H.; An, S. J.; Lee, S.; Mathew, N.; Terrones, M.; Hayashi, T.; Picu, C. R.; Hone, J.; Koratkar, N. *Nat Commun* **2014**, *5*.

(11) Liu, F.; Ming, P.; Li, J. *Physical Review B* **2007**, *76*, 064120.

(12) Balandin, A. a.; Ghosh, S.; Bao, W.; Calizo, I.; Teweldebrhan, D.; Miao, F.; Lau, C. N. *Nano Letters* **2008**, *8*, 902–907.

(13) Pop, E; Mann, D; Wang, Q; Goodson, K; Dai, H. J. *Nano Letters* **2006**, *6*, 96–100.

(14) Balandin, A. A. *Nat Mater* **2011**, *10*, 569–581.

(15) Muller, R. S.; Kamins, T. I.; Chan, M., *Device Electronics for Integrated Circuits*, 3rd edition; Wiley: 2002, p 560.

(16) Malekpour, H.; Chang, K. H.; Chen, J. C.; Lu, C. Y.; Nika, D. L.; Novoselov, K. S.; Balandin, A. A. *Nano Letters* **2014**, *14*, 5155–5161.

(17) Nair, R. R.; Blake, P.; Grigorenko, A. N.; Novoselov, K. S.; Booth, T. J.; Stauber, T.; Peres, N. M. R.; Geim, A. K. *Science* **2008**, *320*, 1308–1308.

(18) Zhu, S.-E.; Yuan, S.; Janssen, G. C.A. M. *EPL* **2014**, *108*, 17007.

(19) Novoselov, K. S.; Falko, V. I.; Colombo, L.; Gellert, P. R.; Schwab, M. G.; Kim, K. *Nature* **2012**, *490*, 192–200.

(20) Bae, S. et al. *Nature Nanotechnology* **2010**, *5*, 574–578.

(21) Kong, L.; Enders, A.; Rahman, T. S.; Dowben, P. a. *Journal of Physics: Condensed Matter* **2014**, *26*, 443001.

(22) Lazar, P.; Karlický, F.; Jurečka, P.; Kocman, M.; Otyepková, E.; Šafářová, K.; Otyepka, M. *Journal of the American Chemical Society* **2013**, *135*, 6372–6377.

(23) Min, S. K.; Kim, W. Y.; Cho, Y.; Kim, K. S. *Nature Nanotechnology* **2011**, *6*, 162–165.

(24) Zhu, Y.; Murali, S.; Cai, W.; Li, X.; Suk, J. W.; Potts, J. R.; Ruoff, R. S. *Advanced Materials* **2010**, *22*, 3906–3924.

(25) Li, Z.; Wang, Y.; Kozbial, A.; Shenoy, G.; Zhou, F.; McGinley, R.; Ireland, P.; Morganstein, B.; Kunkel, A.; Surwade, S. P.; Li, L.; Liu, H. *Nature Materials* **2013**, *12*, 925–931.

(26) Rafiee, J.; Mi, X.; Gullapalli, H.; Thomas, A. V.; Yavari, F.; Shi, Y.; Ajayan, P. M.; Koratkar, N. a. *Nature Materials* **2012**, *11*, 217–222.

(27) Shih, C.-J. J.; Wang, Q. H.; Lin, S.; Park, K.-C. C.; Jin, Z.; Strano, M. S.; Blankschtein, D. *Physical Review Letters* **2012**, *109*, 176101.

(28) Xuekun, L.; Minfeng, Y.; Hui, H.; Rodney, S. R. *Nanotechnology* **1999**, *10*, 269.

(29) Peplow, M. *Nature* **2013**, *503*, 327–329.

(30) Li, X.; Zhang, G.; Bai, X.; Sun, X.; Wang, X.; Wang, E.; Dai, H. *Nature Nanotechnology* **2008**, *3*, 538–542.

(31) Eda, G.; Fanchini, G.; Chhowalla, M. *Nature Nanotechnology* **2008**, *3*, 270–274.

(32) Coleman, J. N. *Advanced Functional Materials* **2009**, *19*, 3680–3695.

(33) Bourlinos, A. B.; Georgakilas, V.; Zbořil, R.; Steriotis, T. a.; Stubos, A. K. *Small* **2009**, *5*, 1841–1845.

(34) Ciesielski, A.; Samori, P. *Chemical Society Reviews* **2014**, *43*, 381–398.

(35) Hernandez, Y. et al. *Nature Nanotechnology* **2008**, *3*, 563–568.

(36) Coleman, J. N. *Accounts of Chemical Research* **2013**, *46*, 14–22.

(37) O'Neill, A.; Khan, U.; Nirmalraj, P. N.; Boland, J.; Coleman, J. N. *The Journal of Physical Chemistry C* **2011**, *115*, 5422–5428.

(38) Bolotin, K. I.; Sikes, K. J.; Jiang, Z.; Klima, M.; Fudenberg, G.; Hone, J.; Kim, P.; Stormer, H. L. *Solid State Communications* **2008**, *146*, 351–355.

(39) Huang, H.; Chen, W.; Chen, S.; Wee, A. T. S. *ACS Nano* **2008**, *2*, 2513–2518.

(40) Singh, V.; Joung, D.; Zhai, L.; Das, S.; Khondaker, S. I.; Seal, S. *Progress in Materials Science* **2011**, *56*, 1178–1271.

(41) Li, X.; Cai, W.; An, J.; Kim, S.; Nah, J.; Yang, D.; Piner, R.; Velamakanni, A.; Jung, I.; Tutuc, E.; Banerjee, S. K.; Colombo, L.; Ruoff, R. S. *Science* **2009**, *324*, 1312–1314.

(42) Li, X.; Magnuson, C. W.; Venugopal, A.; An, J.; Suk, J. W.; Han, B.; Borysiak, M.; Cai, W.; Velamakanni, A.; Zhu, Y.; Fu, L.; Vogel, E. M.; Voelkl, E.; Colombo, L.; Ruoff, R. S. *Nano Letters* **2010**, *10*, 4328–4334.

(43) Georgakilas, V.; Otyepka, M.; Bourlinos, A. B.; Chandra, V.; Kim, N.; Kemp, K. C.; Hobza, P.; Zbořil, R.; Kim, K. S. *Chemical Reviews* **2012**, *112*, 6156–6214.

(44) Eigler, S.; Dotzer, C.; Hof, F.; Bauer, W.; Hirsch, A. *Chemistry – A European Journal* **2013**, *19*, 9490–9496.

(45) Chen, D.; Feng, H.; Li, J. *Chemical Reviews* **2012**, *112*, 6027–6053.

(46) Dreyer, D. R.; Park, S.; Bielawski, C. W.; Ruoff, R. S. *Chemical Society Reviews* **2010**, *39*, 228–240.

(47) Eng, A. Y. S.; Chua, C. K.; Pumera, M. *Nanoscale* **2015**, *7*, 20256–20266.

(48) Erickson, K.; Erni, R.; Lee, Z.; Alem, N.; Gannett, W.; Zettl, A. *Advanced Materials* **2010**, *22*, 4467–4472.

(49) Thostenson, E. T.; Li, C.; Chou, T.-W. *Composites Science and Technology* **2005**, *65*, 491–516.

(50) Loh, K. P.; Bao, Q.; Eda, G.; Chhowalla, M. *Nature Chemistry* **2010**, *2*, 1015–1024.

(51) Compton, O. C.; Nguyen, S. T. *Small* **2010**, *6*, 711–723.

(52) Pei, S.; Cheng, H.-M. *Carbon* **2012**, *50*, 3210–3228.

(53) Poh, H. L.; Šaněk, F.; Ambrosi, A.; Zhao, G.; Sofer, Z.; Pumera, M. *Nanoscale* **2012**, *4*, 3515–3522.

(54) Brodie, B. C. *Philosophical Transactions of the Royal Society of London* **1859**, *149*, 249–259.

(55) Hofmann, U.; König, E. *Zeitschrift für anorganische und allgemeine Chemie* **1937**, *234*, 311–336.

(56) Staudenmaier, L. *Berichte der deutschen chemischen Gesellschaft* **1898**, *31*, 1481–1487.

(57) Hummers, W. S.; Offeman, R. E. *Journal of the American Chemical Society* **1958**, *80*, 1339–1339.

(58) Kovtyukhova, N. I.; Ollivier, P. J.; Martin, B. R.; Mallouk, T. E.; Chizhik, S. A.; Buzaneva, E. V.; Gorchinskiy, A. D. *Chemistry of Materials* **1999**, *11*, 771–778.

(59) Nair, R. R. et al. *Small* **2010**, *6*, 2877–2884.

(60) Zbořil, R.; Karlický, F.; Bourlinos, A. B.; Steriotis, T. a.; Stubos, A. K.; Georgakilas, V.; Šafářová, K.; Jančík, D.; Trapalis, C.; Otyepka, M. *Small* **2010**, *6*, 2885–2891.

(61) Karlický, F.; Otyepka, M. *Journal of Chemical Theory and Computation* **2013**, *9*, 4155–4164.

(62) Dubecký, M.; Otyepková, E.; Lazar, P.; Karlický, F.; Petr, M.; Čépe, K.; Banáš, P.; Zbořil, R.; Otyepka, M. *The Journal of Physical Chemistry Letters* **2015**, *6*, 1430–1434.

(63) Chen, G.; Shi, Z.; Yu, J.; Wang, Z.; Xu, J.; Gao, B.; Hu, X. *Thermochimica Acta* **2014**, *589*, 63–69.

(64) Robinson, J. T.; Burgess, J. S.; Junkermeier, C. E.; Badescu, S. C.; Reinecke, T. L.; Perkins, F. K.; Zalalutdniov, M. K.; Baldwin, J. W.; Culbertson, J. C.; Sheehan, P. E.; Snow, E. S. *Nano Letters* **2010**, *10*, 3001–3005.

(65) Lazar, P.; Chua, C. K.; Holá, K.; Zbořil, R.; Otyepka, M.; Pumera, M. *Small* **2015**, *11*, 3790–3796.

(66) Urbanová, V.; Holá, K.; Bourlinos, A. B.; Čépe, K.; Ambrosi, A.; Loo, A. H.; Pumera, M.; Karlický, F.; Otyepka, M.; Zbořil, R. *Advanced Materials* **2015**, *27*, 2305–2310.

(67) Whitener, K. E.; Stine, R.; Robinson, J. T.; Sheehan, P. E. *The Journal of Physical Chemistry C* **2015**, *119*, 10507–10512.

(68) Sato, Y.; Itoh, K.; Hagiwara, R.; Fukunaga, T.; Ito, Y. *Carbon* **2004**, *42*, 3243–3249.

(69) Lundie, M.; Šljivančanin, Ž.; Tomić, S. *Journal of Physics: Conference Series* **2014**, *526*, 012003.

(70) Montes-Navajas, P.; Asenjo, N. G.; Santamaría, R.; Menéndez, R.; Corma, A.; García, H. *Langmuir* **2013**, *29*, 13443–13448.

(71) Withers, F.; Dubois, M.; Savchenko, A. K. *Physical Review B* **2010**, *82*, 073403.

(72) Lazar, P.; Otyepková, E.; Karlický, F.; Čépe, K.; Otyepka, M. *Carbon* **2015**, *94*, 804–809.

(73) Wang, X.; Dai, Y.; Gao, J.; Huang, J.; Li, B.; Fan, C.; Yang, J.; Liu, X. *ACS Applied Materials & Interfaces* **2013**, *5*, 8294–8299.

(74) Mazánek, V.; Jankovský, O.; Luxa, J.; Sedmidubský, D.; Janoušek, Z.; Šembera, F.; Mikulics, M.; Sofer, Z. *Nanoscale* **2015**, *7*, 13646–13655.

(75) Hobza, P.; Špirko, V.; Selzle, H. L.; Schlag, E. W. *The Journal of Physical Chemistry A* **1998**, *102*, 2501–2504.

(76) Jeziorski, B.; Moszynski, R.; Szalewicz, K. *Chemical Reviews* **1994**, *94*, 1887–1930.

(77) Eisenschitz, R.; London, F. *Zeitschrift für Physik* **1930**, *60*, 491–527.

(78) Distasio JR., R. A.; von Lilienfeld, O. A.; Tkatchenko, A. *Proceedings of the National Academy of Sciences of the United States of America* **2012**, *109*, 14791–14795.

(79) Grimme, S.; Antony, J.; Ehrlich, S.; Krieg, H. *The Journal of Chemical Physics* **2010**, *132*, 154104.

(80) Møller, C.; Plesset, M. S. *Physical Review* **1934**, *46*, 618–622.

(81) Hübner, O.; Glöss, A.; Fichtner, M.; Klopper, W. *The Journal of Physical Chemistry A* **2004**, *108*, 3019–3023.

(82) Grimme, S. *The Journal of Chemical Physics* **2003**, *118*, 9095.

(83) Distasio JR., R. A.; Head-Gordon, M. *Molecular Physics* **2007**, *105*, 1073–1083.

(84) Jurečka, P.; Hobza, P. *Journal of the American Chemical Society* **2003**, *125*, 15608–15613.

(85) Riley, K. E.; Pitonák, M.; Jurečka, P.; Hobza, P. *Chemical Reviews* **2010**, *110*, 5023–5063.

(86) Grimme, S. *Wiley Interdisciplinary Reviews: Computational Molecular Science* **2011**, *1*, 211–228.

(87) Hobza, P.; Šponer, J.; Reschel, T. *Journal of Computational Chemistry* **1995**, *16*, 1315–1325.

(88) Kristyán, S.; Pulay, P. *Chemical Physics Letters* **1994**, *229*, 175–180.

(89) Grimme, S. *Journal of Computational Chemistry* **2004**, *25*, 1463–1473.

(90) Jurečka, P.; Černý, J.; Hobza, P.; Salahub, D. R. *Journal of Computational Chemistry* **2007**, *28*, 555–569.

(91) Grimme, S. *Journal of Computational Chemistry* **2006**, *27*, 1787–1799.

(92) Tkatchenko, A.; Scheffler, M. *Physical Review Letters* **2009**, *102*, 073005.

(93) Dion, M.; Rydberg, H.; Schröder, E.; Langreth, D. C.; Lundqvist, B. I. *Physical Review Letters* **2004**, *92*, 246401.

(94) White, D. N. J. *Journal of Computer-Aided Molecular Design* **1997**, *11*, 517–521.

(95) Anisimov, V. M.; Vorobyov, I. V.; Roux, B.; MacKerell, A. D. *Journal of Chemical Theory and Computation* **2007**, *3*, 1927–1946.

(96) Iori, F.; Corni, S. *Journal of Computational Chemistry* **2008**, *29*, 1656–1666.

(97) Hughes, Z. E.; Tomásio, S. M.; Walsh, T. R. *Nanoscale* **2014**, *6*, 5438–5348.

(98) Foloppe, N.; MacKerell Jr., A. D. *Journal of Computational Chemistry* **2000**, *21*, 86–104.

(99) Jorgensen, W. L.; Maxwell, D. S.; Tirado-Rives, J. *Journal of the American Chemical Society* **1996**, *118*, 11225–11236.

(100) Oostenbrink, C.; Villa, A.; Mark, A. E.; Van Gunsteren, W. F. *Journal of Computational Chemistry* **2004**, *25*, 1656–1676.

(101) Wang, J.; Cieplak, P.; Kollman, P. A. *Journal of Computational Chemistry* **2000**, *21*, 1049–1074.

(102) Ulbricht, H.; Moos, G.; Hertel, T. *Physical Review Letters* **2003**, *90*, 095501.

(103) Girifalco, L.; Hodak, M.; Lee, R. *Physical Review B* **2000**, *62*, 13104–13110.

(104) Cheng, A.; Steele, W. a. *The Journal of Chemical Physics* **1990**, *92*, 3867–3873.

(105) Sun, H *Journal of Physical Chemistry* **1998**, *5647*, 7338–7364.

(106) Stuart, S.; Tutein, A.; Harrison, J. *The Journal of Chemical Physics* **2000**, *112*, 6472–6486.

(107) Brenner, D. W.; Shenderova, O. a.; Harrison, J. a.; Stuart, S. J.; Ni, B.; Sinnott, S. B. *Journal of Physics: Condensed Matter* **2002**, *14*, 783–802.

(108) Van Duin, A. C. T.; Dasgupta, S.; Lorant, F.; Goddard, W. A. *Journal of Physical Chemistry A* **2001**, *105*, 9396–9409.

(109) Nielson, K. D.; van Duin, A. C. T.; Oxgaard, J.; Deng, W.-Q.; Goddard, W. A. *The Journal of Physical Chemistry A* **2005**, *109*, 493–499.

(110) Strachan, A.; Kober, E. M.; van Duin, A. C. T.; Oxgaard, J.; Goddard, W. A. *The Journal of Chemical Physics* **2005**, *122*, 054502.

(111) Singh, S. K.; Costamagna, S; Neek-Amal, M.; Peeters, F. M. *The Journal of Physical Chemistry C* **2014**, *118*, 4460–4464.

(112) Van Duin, A. C. T.; Merinov, B. V.; Jang, S. S.; Goddard, W. A. *The Journal of Physical Chemistry A* **2008**, *112*, 3133–3140.

(113) Han, S. S.; Kang, J. K.; Lee, H. M.; van Duin, A. C. T.; Goddard, W. A. *The Journal of Chemical Physics* **2005**, *123*, 114703.

(114) Mortier, W. J.; Ghosh, S. K.; Shankar, S. *Journal of the American Chemical Society* **1986**, *108*, 4315–4320.

(115) Paupitz, R; Autreto, P. A. S.; Legoas, S. B.; Srinivasan, S. G.; van Duin, A. C. T.; Galvão, D. S. *Nanotechnology* **2013**, *24*, 035706.

(116) Avouris, P. *Nano Letters* **2010**, *10*, 4285–4294.

(117) May, P.; Khan, U.; O'Neill, A.; Coleman, J. N. *Journal of Materials Chemistry* **2012**, *22*, 1278.

(118) Hansen, C. M., *Hansen Solubility Parameters: A User's Handbook*, Second Edition; CRC Press: 2007.

(119) Bourlinos, A. B.; Georgakilas, V.; Zbořil, R.; Steriotis, T. a.; Stubos, A. K.; Trapalis, C. *Solid State Communications* **2009**, *149*, 2172–2176.

(120) Lotya, M.; Hernandez, Y.; King, P. J.; Smith, R. J.; Nicolosi, V.; Karlsson, L. S.; Blighe, F. M.; De, S.; Wang, Z.; McGovern, I. T.; Duesberg, G. S.; Coleman, J. N. *Journal of the American Chemical Society* **2009**, *131*, 3611–3620.

(121) Lotya, M.; King, P. J.; Khan, U.; De, S.; Coleman, J. N. *ACS Nano* **2010**, *4*, 3155–3162.

(122) Smith, R. J.; Lotya, M.; Coleman, J. N. *New Journal of Physics* **2010**, *12*, 125008.

(123) Ang, P. K.; Jaiswal, M.; Lim, C. H.Y. X.; Wang, Y.; Sankaran, J.; Li, A.; Lim, C. T.; Wohland, T.; Barbaros, O.; Loh, K. P. *ACS Nano* **2010**, *4*, 7387–7394.

(124) Liu, S.-J.; Wen, Q.; Tang, L.-J.; Jiang, J.-H. *Analytical Chemistry* **2012**, *84*, 5944–5950.

(125) Bongiorno, D; Ceraulo, L; Ferrugia, M *Arkivoc* **2004**, *part (v)*, 251–262.

(126) Konatham, D.; Striolo, A. *Nano Letters* **2008**, *8*, 4630–4641.

(127) Shih, C.; Lin, S. *Journal of the American Chemical Society* **2010**, *132*, 14638–14648.

(128) Whitehouse, D. B.; Buckingham, A. D. *Journal of the Chemical Society, Faraday Transactions* **1993**, *89*, 1909–1913.

(129) Kästner, J.; Thiel, W. *The Journal of Chemical Physics* **2005**, *123*, 144104.

(130) Lu, Y.-H.; Yang, C.-W.; Fang, C.-K.; Ko, H.-C.; Hwang, I.-S. *Scientific Reports* **2014**, *4*, 7189–7189.

(131) McCreery, R. L.; McDermott, M. T. *Analytical Chemistry* **2012**, *84*, 2602–2605.

(132) Patel, A. N.; Collignon, M. G.; Oconnell, M. A.; Hung, W. O. Y.; McKelvey, K.; MacPherson, J. V.; Unwin, P. R. *Journal of the American Chemical Society* **2012**, *134*, 20117–20130.

(133) Schedin, F; Geim, a. K.; Morozov, S. V.; Hill, E. W.; Blake, P; Katsnelson, M. I.; Novoselov, K. S. *Nature Materials* **2007**, *6*, 652–655.

(134) Pittoni, P. G.; Wang, R. J.; Yu, T. S.; Lin, S. Y. *Journal of the Taiwan Institute of Chemical Engineers* **2014**, *45*, 3062–3068.

(135) Erbil, H. Y.; Demirel, A. L.; Avcii, Y.; Mert, O. *Science* **2003**, *299*, 1377–1380.

(136) Stanton, M. M.; Ducker, R. E.; MacDonald, J. C.; Lambert, C. R.; Grant McGimpsey, W. *Journal of Colloid and Interface Science* **2012**, *367*, 502–508.

(137) Good, R. J.; Srivatsa, N. R.; Islam, M.; Huang, H. T. L.; Van Oss, C. J. *Journal of Adhesion Science and Technology* **1990**, *4*, 1–617.

(138) Martin-Calvo, A.; Garcia-Perez, E.; Garcia-Sanchez, A.; Bueno-Perez, R.; Hamad, S.; Calero, S. *Physical Chemistry Chemical Physics* **2011**, *13*, 11165–11174.

(139) Hirschfelder, J. O.; Curtiss, C. F.; Bird, R. B., *Molecular Theory of Gases and Liquids*; Wiley: New York, 1954.

(140) Secor, E. B.; Hersam, M. C., ed. by LLC., S.-A. C.

(141) Years in two dimensions. Editorial, T. *Nature Nanotechnology* **2014**, *9*, 725.

(142) Rodrigo, D.; Limaj, O.; Janner, D.; Etezadi, D.; Garcia de Abajo, F. J.; Pruneri, V.; Altug, H. *Science* **2015**, *349*, 165–168.

(143) Shao, Y.; Wang, J.; Wu, H.; Liu, J.; Aksay, I. a.; Lin, Y. *Electroanalysis* **2010**, *22*, 1027–1036.

(144) Traversi, F; Raillon, C; Benameur, S. M.; Liu, K; Khlybov, S; Tosun, M; Krasnozhon, D; Kis, A; Radenovic, A *Nature Nanotechnology* **2013**, *8*, 939–945.

(145) Koenig, S. P.; Wang, L.; Pellegrino, J.; Bunch, J. S. *Nature Nanotechnology* **2012**, *7*, 728–732.

(146) Rubeš, M.; Nachtigall, P.; Vondrásek, J.; Bludský, O. *Journal of Physical Chemistry C* **2009**, *113*, 8412–8419.

(147) Medeiros, P. V.; Gueorguiev, G.; Stafström, S. *Carbon* **2015**, *81*, 620–628.

(148) Podeszwa, R. *The Journal of Chemical Physics* **2010**, *132*, 044704.

(149) Zhao, Y.; Truhlar, D. G. *Journal of Physical Chemistry C* **2008**, *112*, 4061–4067.

(150) Lin, S.; Shih, C.-J.; Strano, M. S.; Blankschtein, D. *Journal of the American Chemical Society* **2011**, *133*, 12810–12823.

(151) Qin, Z.; Taylor, M.; Hwang, M.; Bertoldi, K.; Buehler, M. J. *Nano Letters* **2014**, *29*, 7271–7282.

(152) Gobre, V. V.; Tkatchenko, A. *Nature communications* **2013**, *4*, 2341.

(153) Ho, T. a.; Striolo, A. *The Journal of Chemical Physics* **2013**, *138*, 054117.

(154) Pykal, M.; Jurečka, P.; Karlický, F.; Otyepka, M. *Physical Chemistry Chemical Physics* **2016**, *18*, 6351–6372.

(155) Banáš, P.; Mládek, A.; Otyepka, M.; Zgarbová, M.; Jurečka, P.; Svozil, D.; Lankaš, F.; Šponer, J. *Journal of Chemical Theory and Computation* **2012**, *8*, 2448–2460.

(156) Norberg, J.; Nilsson, L. *Biophysical Journal* **1995**, *69*, 2277–2285.

(157) Mokdad, A.; Dimos, K.; Zoppellaro, G.; Tuček, J.; Perman, J. A.; Malina, O.; Andersson, K. K.; Ramanatha Datta, K. K.; Froning, J. P.; Zbořil, R. *RSC Advances* **2015**, *5*, 76556–76566.

(158) Shi, W.; Fan, H.; Ai, S.; Zhu, L. *New Journal of Chemistry* **2015**, *39*, 7054–7059.

(159) Zhu, H.; Gao, L.; Jiang, X.; Liu, R.; Wei, Y.; Wang, Y.; Zhao, Y.; Chai, Z.; Gao, X. *Chemical Communications* **2014**, *50*, 3695–3698.

(160) Park, S.; An, J.; Jung, I.; Piner, R. D.; An, S. J.; Li, X.; Velamakanni, A.; Ruoff, R. S. *Nano Letters* **2009**, *9*, 1593–1597.

(161) Georgakilas, V.; Tiwari, J. N.; Kemp, K. C.; Perman, J. A.; Bourlinos, A. B.; Kim, K. S.; Zbořil, R. *Chemical Reviews* **2016**, *116*, 5464–5519.

(162) Ding, Y.-H.; Zhang, P.; Ren, H.-M.; Zhuo, Q.; Yang, Z.-M.; Jiang, X.; Jiang, Y. *Applied Surface Science* **2011**, *258*, 1077–1081.

(163) Chenoweth, K.; van Duin, A. C. T.; Goddard, W. A. *The Journal of Physical Chemistry A* **2008**, *112*, 1040–1053.

(164) Bagri, A.; Mattevi, C.; Acik, M.; Chabal, Y. J.; Chhowalla, M.; Shenoy, V. B. *Nature Chemistry* **2010**, *2*, 581–587.

(165) Goverapet Srinivasan, S.; van Duin, A. C. T. *The Journal of Physical Chemistry A* **2011**, *115*, 13269–13280.

(166) Poovathingal, S.; Schwartzentruber, T. E.; Srinivasan, S. G.; van Duin, A. C. T. *The Journal of Physical Chemistry A* **2013**, *117*, 2692–2703.

(167) Criado, A.; Melchionna, M.; Marchesan, S.; Prato, M. *Angewandte Chemie International Edition* **2015**, *54*, 10734–10750.

(168) Ho, K.-I.; Huang, C.-H.; Liao, J.-H.; Zhang, W.; Li, L.-J.; Lai, C.-S.; Su, C.-Y. *Scientific Reports* **2014**, *4*, 5893.

(169) Han, S. S.; Yu, T. H.; Merinov, B. V.; van Duin, A. C. T.; Yazami, R.; Goddard, W. A. *Chemistry of Materials* **2010**, *22*, 2142–2154.

(170) Leenaerts, O.; Peelaers, H.; Hernández-Nieves, A. D.; Partoens, B.; Peeters, F. M. *Physical Review B* **2010**, *82*, 195436.

(171) Sandford, G. *Tetrahedron* **2003**, *59*, 437–454.

(172) Samarakoon, D. K.; Chen, Z.; Nicolas, C.; Wang, X.-Q. *Small* **2011**, *7*, 965–969.

(173) Karlický, F.; Otyepka, M. *Annalen der Physik* **2014**, *526*, 408–414.

(174) Karlický, F.; Kumara Ramanatha Datta, K.; Otyepka, M.; Zbořil, R. *ACS Nano* **2013**, *7*, 6434–6464.

(175) Şahin, H.; Ciraci, S *The Journal of Physical Chemistry C* **2012**, *116*, 24075–24083.

(176) Pykal, M.; Zbořil, R.; Otyepka, M. *Chemické Listy* **2016**, *110*, 335–343.

A Lipid Enhanced Exfoliation for Production of Graphene Nanosheets

THE JOURNAL OF PHYSICAL CHEMISTRY C

Article

pubs.acs.org/JPCC

Lipid Enhanced Exfoliation for Production of Graphene Nanosheets

Martin Pykal,[†] Klára Šafářová,[†] Karolína Machalová Šišková,[†] Petr Jurečka,[†] Athanasios B. Bourlinos,[‡] Radek Zbořil,[†] and Michal Otyepka[†,*]

[†]Regional Centre of Advanced Technologies and Materials, Department of Physical Chemistry, Faculty of Science, Palacký University Olomouc, 17. Listopadu 12, 771 46 Olomouc, Czech Republic

[‡]Physics Department, University of Ioannina, 45110 Ioannina, Greece

Supporting Information

ABSTRACT: Liquid-phase exfoliation of graphite is a widely used method to obtain graphene nanosheets, and therefore the development of a simple and efficient exfoliation procedure remains challenging. Here, we present a one-step method of graphene exfoliation in lecithin/chloroform solution. The graphene nanosheets produced by the lecithin assisted exfoliation method were analyzed by microscopy techniques, including statistical analysis of atomic force microscopy (AFM) images and Raman spectroscopy, which both indicate the presence of few-layer graphene nanosheets, including substantial content of three-layer sheets. Molecular dynamics simulations on the time scale of 0.5+ μs suggested that stability of the obtained colloid may originate from formation of lecithin reverse hemimicelles and micelles, which prevents the aggregation of exfoliated graphene flakes by entropic repulsion of the lipid hydrophobic chains.

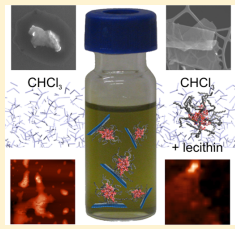

INTRODUCTION

Defect-free graphene nanosheets have great potential in nanoelectronics, solar cells, and mechanical reinforcement of polymers.[1,2] In particular, the AB-stacked bilayer and trilayer graphene is believed to have great potential for future nanoelectronic devices.[3−6] The liquid-phase exfoliation of graphite in a solvent under mild sonication presents a widespread technique for the efficient production of solvent-processable, high quality graphene nanosheets.[7,8] Interestingly, solvent extraction may be further assisted by the presence of exfoliants dissolved in the liquid-phase and having strong affinity to the graphene surface through noncovalent interactions, like certain surfactant or polymer additives.[9,10] Generally, these additives improve the exfoliation yield and help to split the thick graphite plates into the thinnest possible flakes (<5 nm). Typical examples of effective exfoliants include long alkyl-chain surfactants having a hydrophobic tail and a polar headgroup.[11,12] To the best of our knowledge, no report in the literature refers to lecithin as an efficient exfoliant of graphene. Lecithin is a natural occurring phospholipid with two pending hydrophobic alkyl chains and a polar headgroup in its structure. The choice of lecithin becomes even more attractive when considering the fact that phospholipids are a major component of all cell membranes. Accordingly, lecithin−graphene hybrids should display good biocompatibility and low toxicity in (bio)applications.[13,14]

Here, we present efficient liquid-phase exfoliation of graphite in chloroform−lecithin solutions leading to few-layer graphene nanosheets. Chloroform is an excellent solvent for lecithin as well as a good dispersion medium for graphene.[15] Here, through the combination of theoretical and experimental approaches, we show that the exfoliation efficacy can be significantly improved by addition of lipids, namely lecithin. The theoretical calculations suggest that the enhanced exfoliation efficiency may stem from the formation of lecithin reverse micelles and hemimicelles in chloroform depending on the concentration of lipids. The reverse micelles stick to the exfoliated graphene nanosheets and simultaneously prevent self-association by entropically based forces. The exfoliation efficacy of graphene nanosheet preparation was quantified by statistical analysis of AFM images.

METHODS

Graphene Preparation. In a typical preparation, 1 g graphite powder (Aldrich) was suspended in 200 mL chloroform containing a 2-g portion of dissolved lecithin (Aldrich). The suspension was sonicated in an ultrasound bath for 3 h (130 W) and then left for 1−2 days to settle out any insoluble particles. The supernatant colloidal dispersion (0.03−0.05 mg mL^{-1}) was collected and evaporated until dry in a hood at room temperature. The solid residue was treated with 25 mL chloroform to dissolve excess lecithin. Subsequently, the insoluble fraction was separated from the freely soluble lecithin by centrifugation. The obtained gray solid (namely graphene nanosheets) was finally suspended in 5 mL chloroform by mild sonication. The exfoliation yield with respect to graphite is ca. 0.5%. In a blank experiment, 1 g graphite was directly exfoliated in 200 mL chloroform without lecithin under sonication, as above. The suspension was left to settle for 1−2 days, and the supernatant phase was collected for comparative analysis. In the

Received: February 4, 2013
Revised: May 6, 2013
Published: May 10, 2013

absence of lecithin, the supernatant constitutes a suspension of fine graphite particles in chloroform, clearly seen by the naked eye. The suspended particles immediately separate by centrifugation, leaving behind a colorless solvent.

Characterization. SEM micrographs were taken on a Hitachi 6600 FEG microscope (resolution: SE—1.3 nm) with an accelerating voltage of 15 kV. The distance between the sample and detector was 7.5 mm. TEM was carried out on a JEOL 2010 microscope operating at 160 kV with a point-to-point resolution of 1.9 Å. AFM images were taken on an NTEGRA (NT-MDT) microscope. All AFM experiments were carried out in semicontact mode with standard NSG10 tips in air at room temperature. Raman scattering spectra were recorded on a DXR Raman microscope (Thermo Scientific), equipped with a thermoelectrically cooled (down to −50 °C) CCD camera, using a 633 nm (1.96 eV) excitation wavelength of an He—Ne laser and a 10× objective. The laser power at the sample was adjusted to 4.0 mW. Spectral acquisition was repeated 100 times with 2 s accumulation time. Raman spectra were collected by employing a triplet spectrograph with a full range grating (spectral dispersion: average 2 cm^{-1} per CCD pixel element) and using a 50 μm slit aperture. Spot size was approximately 1 μm^2. Software Omnic 8 for Dispersive Raman was used for the spectra acquisition and their initial processing, such as, e.g., baseline correction. Any smoothing of the spectra was avoided. Final processing and peak fitting of Raman spectra were performed in Origin 7.0.

Simulation Procedure. All MD simulations were carried out using the Gromacs 4.5 software package[16] using the generalized AMBER force field (GAFF) parameters for 1,2-dioleoyl-*sn*-glycero-3-phosphocholine (DOPC) and graphene carbon atoms, which were treated as uncharged Lennard—Jones spheres. OPLS rigid united atom parameters[17] were used for chloroform molecules. The equations of motion were integrated every 2 fs under periodic boundary conditions with PME electrostatics. The velocity rescaling Berendsen thermostat was used to maintain a constant temperature in the system and pressure was coupled to an anisotropic Berendsen barostat (NpT ensemble, 300 K; 1 bar). The system was equilibrated for 10 ns after initial restrained minimization. The production runs were 500+ ns long and snapshots were collected every 20 ps for subsequent analysis.

Simulations of Micelle Formation in Chloroform. The initial structure of the monolayer was prepared from the DOPC bilayer proposed by Siu et al.[18] available at the Lipidbook server.[19] One half of the original structure, i.e., 36 lipid molecules, was solvated with 1737 chloroform molecules (equilibrated box size 5 × 4.6 × 13 nm).

Simulations of DOPC on Graphene Surface. In the case of DOPC attached to periodic graphene, 12 lipid molecules were placed on the periodically repeated graphene sheet (4.9 × 4.6 nm) and solvated by 1183 chloroform molecules (equilibrated box size 4.9 × 4.7 × 8.2 nm).

RESULTS AND DISCUSSION

Missing information about the mechanism of graphene stabilization in nonpolar environment and in the presence of lipids prompted us to employ computer simulations to fill this gap. We would like to note that previous simulations dealing with interaction of graphene with surfactants were carried out in water environment (see, for example, refs 20 and 21). We carried out molecular dynamics (MD) simulations on 0.5 μs time scale to investigate how the presence of lecithin can enhance the exfoliation process. Natural lecithin is a complex system mostly composed of phosphocholines, and therefore we simplified lecithin by DOPC in our simulations. The molecular dynamics simulations of DOPC solutions in chloroform show that DOPC forms reverse micelles spontaneously on a 100-ns time scale (Figure S1 of the Supporting Information, SI), which is in agreement with experimental observations for similar solvents.[22] The core of reverse micelles contains polar DOPC heads, and the hydrophobic tails are exposed to chloroform (Figure S1 of the SI). We further analyzed the interaction of DOPC with graphene surface in chloroform. Two different starting geometries were built: one with hydrophobic tails oriented toward the graphene (Figure 1A), and the other one

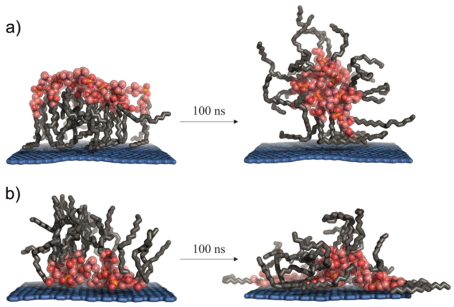

Figure 1. Simulations demonstrating formation of reverse DOPC (lecithin model) micelle (A) and hemimicelle (B) on graphene surface in chloroform. The simulations starting with DOPC molecules oriented with its nonpolar tails or with the polar heads toward the graphene are shown. Chloroform molecules are omitted for clarity.

with polar heads oriented toward the graphene (Figure 1B). In both simulations, the reverse micelles were formed on the graphene surface and remained attached to the graphene sheet, leaving a large part of the hydrophobic tails exposed to solvent and free to sample their conformational space. As we will discuss below, this may play an important role in stabilizing the graphene flakes in the exfoliated state by preventing their aggregation.

Let us assume that some reverse micelles are present in solution and some are attached (and/or formed) on the surface of the freshly exfoliated graphene nanosheets. When approaching each other, the micelles repel due to the volume restriction effect, which prevents their aggregation.[23] The volume restriction effect originates from the restriction of the conformational space of exposed hydrophobic tails upon contact with other micelles. A similar effect should also be expected between the micelles and the exfoliated graphene sheets, as well as between the hemimicelles present on the graphene sheets and other graphene sheets. According to kinetic theory of graphene aggregation, the resulting increase of the association barrier may significantly stabilize the dispersion.[24] Thus, the presence of the lecithin reverse micelles in solution and on the graphene surface may prevent self-aggregation of the exfoliated graphene by creating association barriers of entropic origin.

It should be noted that lecithin might also play a role in the exfoliation process itself, for instance by stabilizing the exfoliation intermediates during ultrasound agitation, and

thermodynamic stabilization of the exfoliated flakes cannot be ruled out as well. Thus, the above-described hypothesis may not be the only contribution to the lecithin effect on the exfoliation efficiency.

Motivated by the results from the simulations, we exfoliated graphene in chloroform with and without the presence of lecithin. As a first remark, the short-range exfoliation of graphite in chloroform (without lecithin) results in a fine yet stable suspension of thick plates (hazy suspension), and AFM images of the dried sample showed mostly thick particles (see Figure S2 of the SI). On the contrary, exfoliation in the presence of lecithin affords a clear, optically transparent colloid with a concentration of 0.03−0.05 mg mL^{-1}. Such concentrations compare well with those obtained from other liquid-phase exfoliation processes.[25] Albeit the rather low exfoliation yield in presence of lecithin (0.5%), the method is size-selective, leading to graphene nanosheets with narrow plate thickness (see AFM below). The exfoliated samples were further analyzed by scanning electron microscopy (SEM), transmission electron microscopy (TEM), atomic-force microscopy (AFM), and Raman spectroscopy. All of these techniques unequivocally show that if lecithin is present during the exfoliation process, high quality graphene, few-layer nanosheets are gained (Figures 2 and 3). The statistical analysis of 350 AFM images documents

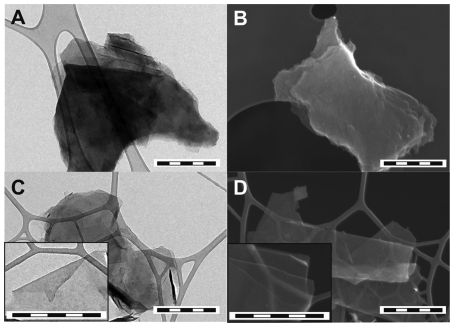

Figure 2. TEM (left) and SEM (right) images of graphitic flakes exfoliated in pure chloroform (A, B), and few-layer graphene nanosheets exfoliated under the presence of lecithin (C, D). The scale bar represents 500 nm.

that the produced graphene nanosheets are few-layer graphene flakes with a mean height value of 3.3 ± 1.1 nm (Figure 3), which approximately corresponds to 7−8 layers.

Raman spectroscopic measurements confirmed the presence of three- and few-layer graphene sheets in the sample[26] and also indentified spectral features of lecithin (Figure 4). On 3 out of 21 analyzed spots, the minimum number of peaks necessary to correctly fit G′ peak was six, indicating three-layer graphene (Figure S3 of the SI).[27] The remaining places contained few-layer graphene or a mixture of various heights. Thus, both AFM distributions and Raman spectroscopy confirm a certain portion of the three-layer graphene flakes.

■ CONCLUSIONS

We present a one-step method of graphene preparation by liquid-phase exfoliation in the low boiling point solvent chloroform under the presence of lecithin. Molecular dynamics

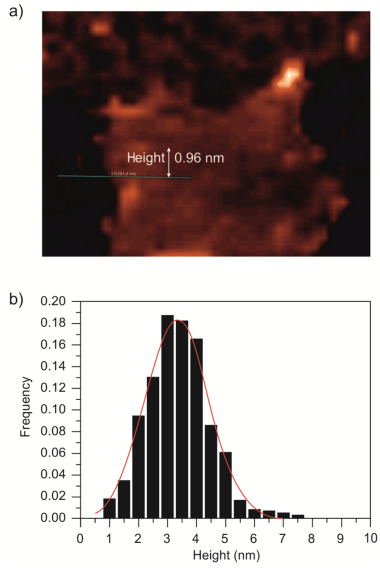

Figure 3. AFM image (A) showing a graphene nanoflake and statistical analysis of AFM measurements (B) showing a histogram of the flake height of graphene sheets prepared by lecithin-assisted exfoliation of graphite in chloroform.

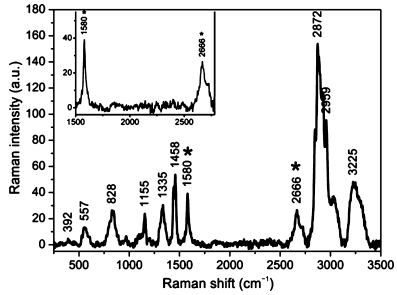

Figure 4. Raman spectrum of few-layer graphene exfoliated by lecithin solution in chloroform showing characteristic lecithin features. Inset: The region of 1500−2800 cm^{-1}, where G and G′ bands of graphene appears (labeled by asterisks) is magnified.

simulations suggest that the higher stability of exfoliated graphene nanosheets under the presence of lecithin may be due to the formation of reverse micelles and their attachment to graphene. The micelles repel each other by volume restriction effect and prevent aggregation of graphene sheets. The microscopic techniques together with Raman measurement show that few-layer (up to 3.9 nm) graphene nanosheets are produced with a notable content of three-layer graphene. The liquid-phase production of graphene sheets has good efficacy and may benefit from a potentically good biocompatibility of

arising lecithin−graphene composites, because lecithin is naturally occurring in animals.

■ ASSOCIATED CONTENT

Supporting Information

Experimental details (preparation, SEM, TEM, AFM, and Raman measurements) and additional figures. This material is available free of charge via the Internet at http://pubs.acs.org.

■ AUTHOR INFORMATION

Corresponding Author

*Phone: +420 585 634 756; fax: +420 585 634 761; e-mail: michal.otyepka@upol.cz.

Notes

The authors declare no competing financial interest.

■ ACKNOWLEDGMENTS

This research was supported by grants P208/10/1742 (P.J.) and P208/12/G016 (M.O., R.Z., K.S.) from the Grant Agency of the Czech Republic and by a student project PrF_2013_028 of Palacký University Olomouc. Further funding was provided by the Operational Program Research and Development for Innovations—European Regional Development Fund (Project No. CZ.1.05/2.1.00/03.0058 of the Ministry of Education, Youth and Sports of the Czech Republic).

■ REFERENCES

(1) Avouris, P. Graphene: Electronic and Photonic Properties and Devices. *Nano Lett.* **2010**, *10*, 4285−4294.

(2) May, P.; Khan, U.; O'Neill, A.; Coleman, J. N. Approaching the Theoretical Limit for Reinforcing Polymers with Graphene. *J. Mater. Chem.* **2012**, *22*, 1278.

(3) Ohta, T.; Bostwick, A.; Seyller, T.; Horn, K.; Rotenberg, E. Controlling the Electronic Structure of Bilayer Graphene. *Science* **2006**, *313*, 951−954.

(4) Zhang, Y. B.; Tang, T.; Girit, C.; Hao, Z.; Martin, M. C.; Zettl, A.; Crommie, M. F.; Shen, Y. R.; Wang, F. Direct Observation of a Widely Tunable Bandgap in Bilayer Graphene. *Nature* **2009**, *459*, 820−823.

(5) Zhou, S. Y.; Gweon, G. H.; Fedorov, A. V.; First, P. N.; de Heer, W. A.; Lee, D. H.; Guinea, F.; Castro Neto, A. H.; Lanzara, A. Substrate-Induced Bandgap Opening in Epitaxial Graphene. *Nat. Mater.* **2007**, *6*, 916−916.

(6) Craciun, M. F.; Russo, S.; Yamamoto, M.; Oostinga, J. B.; Morpurgo, A. F.; Tarucha, S. Trilayer Graphene Is a Semimetal with a Gate-Tunable Band Overlap. *Nat. Nanotechnol.* **2009**, *4*, 383−388.

(7) Coleman, J. N. Liquid-Phase Exfoliation of Nanotubes and Graphene. *Adv. Funct. Mater.* **2009**, *19*, 3680−3695.

(8) Coleman, J. N. Liquid Exfoliation of Defect-Free Graphene. *Acc. Chem. Res.* **2013**, *46*, 14−22.

(9) Lotya, M.; Hernandez, Y.; King, P. J.; Smith, R. J.; Nicolosi, V.; Karlsson, L. S.; Blighe, F. M.; De, S.; Wang, Z.; McGovern, I. T.; et al. Liquid Phase Production of Graphene by Exfoliation of Graphite in Surfactant/Water Solutions. *J. Am. Chem. Soc.* **2009**, *131*, 3611−3620.

(10) Bourlinos, A. B.; Georgakilas, V.; Zboril, R.; Steriotis, T. a.; Stubos, A. K.; Trapalis, C. Aqueous-Phase Exfoliation of Graphite in the Presence of Polyvinylpyrrolidone for the Production of Water-Soluble Graphenes. *Solid State Commun.* **2009**, *149*, 2172−2176.

(11) Lotya, M.; King, P. J.; Khan, U.; De, S.; Coleman, J. N. High-Concentration, Surfactant-Stabilized Graphene Dispersions. *ACS Nano* **2010**, *4*, 3155−3162.

(12) Smith, R. J.; Lotya, M.; Coleman, J. N. The Importance of Repulsive Potential Barriers for the Dispersion of Graphene Using Surfactants. *New J. Phys.* **2010**, *12*, 125008.

(13) Ang, P. K.; Jaiswal, M.; Lim, C. H. Y. X.; Wang, Y.; Sankaran, J.; Li, A.; Lim, C. T.; Wohland, T.; Barbaros, O.; Loh, K. P. A Bioelectronic Platform Using a Graphene−Lipid Bilayer Interface. *ACS Nano* **2010**, *4*, 7387−7394.

(14) Liu, S.-J.; Wen, Q.; Tang, L.-J.; Jiang, J.-H. Phospholipid−Graphene Nanoassembly As a Fluorescence Biosensor for Sensitive Detection of Phospholipase D Activity. *Anal. Chem.* **2012**, *84*, 5944−5950.

(15) O'Neill, A.; Khan, U.; Nirmalraj, P. N.; Boland, J.; Coleman, J. N. Graphene Dispersion and Exfoliation in Low Boiling Point Solvents. *J. Phys. Chem. C* **2011**, *115*, 5422−5428.

(16) Hess, B.; Kutzner, C.; van der Spoel, D.; Lindahl, E. GROMACS 4: Algorithms for Highly Efficient, Load-Balanced, And Scalable Molecular Simulation. *J. Chem. Theory Comput.* **2008**, *4*, 435−447.

(17) Jorgensen, W. L.; Briggs, J. M.; Contreras, M. L. Relative Partition Coefficients for Organic Solutes from Fluid Simulations. *J. Phys. Chem.* **1990**, *94*, 1683−1686.

(18) Siu, S. W. I.; Vácha, R.; Jungwirth, P.; Böckmann, R. Biomolecular Simulations of Membranes: Physical Properties from Different Force Fields. *J. Chem. Phys.* **2008**, *128*, 125103.

(19) Domański, J.; Stansfeld, P. J.; Sansom, M. S. P.; Beckstein, O. Lipidbook: A Public Repository for Force-Field Parameters Used in Membrane Simulations. *J. Membr. Biol.* **2010**, *236*, 255−258.

(20) Titov, A. V.; Král, P.; Pearson, R. Sandwiched Graphene-Membrane Superstructures. *ACS Nano* **2010**, *4*, 229−234.

(21) Wu, D.; Yang, X. Coarse-Grained Molecular Simulation of Self-Assembly for Nonionic Surfactants on Graphene Nanostructures. *J. Phys. Chem. B* **2012**, *116*, 12048−12056.

(22) Bongiorno, D.; Ceraulo, L.; Ferrugia, M. 1H-NMR and FT-IR Study of the State of Melatonin Confined in Membrane Models: Location and Interactions of Melatonin in Water Free Lecithin and AOT Reversed Micelles. *Arkivoc* **2004**, No. part (v), 251−262.

(23) Konatham, D.; Striolo, A. Molecular Design of Stable Graphene Nanosheets Dispersions. *Nano Lett.* **2008**, *8*, 4630−4641.

(24) Shih, C.; Lin, S.; Strano, M. S.; Blankschtein, D. Understanding the Stabilization of Liquid-Phase-Exfoliated Graphene in Polar Solvents: Molecular Dynamics Simulations and Kinetic Theory of Colloid Aggregation. *J. Am. Chem. Soc.* **2010**, *132*, 14638−14648.

(25) Hernandez, Y.; Nicolosi, V.; Lotya, M.; Blighe, F. M.; Sun, Z.; De, S.; McGovern, I. T.; Holland, B.; Byrne, M.; Gun'Ko, Y. K.; et al. High-Yield Production of Graphene by Liquid-Phase Exfoliation of Graphite. *Nat. Nanotechnol.* **2008**, *3*, 563−568.

(26) Reina, A.; Jia, X.; Ho, J.; Nezich, D.; Son, H.; Bulovic, V.; Dresselhaus, M. S.; Kong, J. Large-Area, Few-Layer Graphene Films on Arbitrary Substrates by Chemical Vapor Deposition. *Nano Lett.* **2009**, *9*, 30−35.

(27) Malard, L. M.; Pimenta, M. a.; Dresselhaus, G.; Dresselhaus, M. S. Raman Spectroscopy in Graphene. *Phys. Rep* **2009**, *473*, 51−87.

B Electric Quadrupole Moment of Graphene and its Effect on Intermolecular Interactions

PCCP

PAPER

View Article Online
View Journal | View Issue

Electric quadrupole moment of graphene and its effect on intermolecular interactions

Cite this: *Phys. Chem. Chem. Phys.*, 2014, **16**, 3144

Mikuláš Kocman, Martin Pykal and Petr Jurečka*

Carbon atoms in aromatic compounds exhibit a permanent electric quadrupole moment due to the aromatic π electron distribution. In the case of small aromatic hydrocarbons, this quadrupole contributes significantly to their intermolecular interactions, but when the honeycomb lattice is expanded to infinity, the quadrupolar field sums to zero and its significance vanishes. Therefore, electrostatic interactions with graphene are often omitted in force field molecular modeling. However, for a finite sheet, the electrostatic field decays only slowly with increasing size and is always non-negligible near edges. In addition, in a corrugated graphene sheet, the electrostatic field near the surface does not vanish completely and remains sizeable. In the present study, we investigated the magnitude of the graphene quadrupolar field as a function of model size and graphene corrugation, and estimated the error resulting from its neglect in molecular dynamics simulations. Exfoliation energies in benzene and hexafluorobenzene were calculated using the potential of mean force method with and without explicit quadrupoles. The effect on exfoliation energies was found to be quite small. However, the quadrupole moment may be important for graphene sheet association (aggregation) as it affects barrier heights, and consequently kinetics of association. Our results indicate that quadrupolar interactions may need to be considered in molecular modeling when graphene is corrugated or bent.

Received 6th November 2013,
Accepted 2nd December 2013

DOI: 10.1039/c3cp54701a

www.rsc.org/pccp

1. Introduction

Recent progress in graphene-related nanotechnologies has fuelled interest in theoretical modeling of graphene-based materials. Different levels of theory can provide important information about various material properties, its behavior and chemistry.[1] Electronic, mechanical, optical and other properties related to electronic structure are usually obtained from quantum chemical calculations. Detailed atomistic information about dynamical processes occurring on longer time scales, such as interactions with biomolecules or the surrounding environment, is typically modeled using molecular mechanics and force fields. The chosen level of theory determines the computational cost and also accuracy of the resulting description of individual properties and features.

The feature of graphene that is of interest in this article is its electric quadrupole moment. Whereas quantum mechanical treatments are in general capable of providing an accurate description of the graphene quadrupolar field, in empirical force fields, it is usually ignored. Typically, carbon atoms in force field calculations are treated as van der Waals spheres and are not assigned any charge or multipole moment. As we will discuss below, ignoring the quadrupole moment is in most applications a reasonable approximation. However, in some cases, this neglect may result in error, the importance of which is difficult to prejudge. Here, we focus on modeling the quadrupole moment of graphene using empirical potentials and molecular dynamics (MD) simulations and discuss its influence on intermolecular interactions with finite and corrugated graphene sheets. Note that there are other important sources of errors in force field calculations which we do not consider here, such as lack of explicit polarization in pairwise additive potentials. Although the effect of missing polarization is expected to be important, it is beyond the scope of this work, which aims to estimate errors that result solely from neglecting the quadrupolar interaction in force field calculations. Another problem is that not only quadrupolar, but also dipolar electric field may arise in real graphene upon its deformation. This effect, however, cannot be modeled by a classical force field, therefore we also do not consider it here.

Let us first examine the origin of graphene's quadrupole moment in more detail. Molecules of aromatic hydrocarbons have strong molecular electric quadrupole moments arising from two different sources. First, carbon atoms in aromatic rings exhibit a permanent quadrupole moment due to the aromatic π electron distribution. High electron densities above and below the graphene layer generate a quadrupolar field characterized by a negative Q_{zz} component of the quadrupolar tensor perpendicular to the aromatic ring (z direction in Fig. 1a).

Regional Centre of Advanced Technologies and Materials, Department of Physical Chemistry, Faculty of Science, Palacky University, 17. listopadu 12, 77146 Olomouc, Czech Republic. E-mail: petr.jurecka@upol.cz

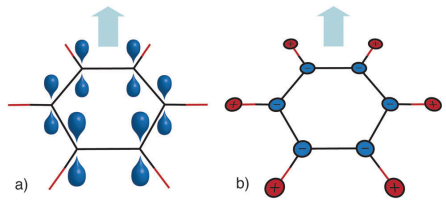

Fig. 1 Two components of the quadrupole moment in a benzene molecule. Similar components contribute to the quadrupole of finite graphene flakes.

Henceforth, we will refer to this contribution as the "atomic quadrupole". The remaining elements of the quadrupolar tensor are much smaller and vanish on the inner carbon atoms for larger molecules (see also ref. 2). Second, in aromatic hydrocarbons, a molecular quadrupole may arise due to the polarity of C–H bonds. For instance, in benzene, the Q_{zz} molecular component due to partial charges on hydrogen and carbon atoms is of the same sign as the atomic quadrupole (Fig. 1b). We will refer to this component as the "CH polarity quadrupole". Note that a quadrupole of the latter type may also arise due to other substitutions. For instance, hexafluorobenzene exhibits a CF polarity quadrupole, with a Q_{zz} sign opposite to that of the CH polarity quadrupole. In smaller polyaromatic molecules the atomic and CH polarity quadrupoles are comparable in magnitude.[2]

In an infinite and perfectly planar graphene sheet, the quadrupolar contributions arising from individual carbon atoms add up in such a way that the overall electrostatic potential (ESP) near the surface vanishes completely. However, here we are interested in finite and possibly corrugated graphene leaves. In a small polyaromatic molecule, the atomic quadrupolar contributions sum to create a molecular electrostatic potential similar to the one depicted in Fig. 2. The ESP of larger graphene flakes has similar features. We will now consider the long-range and short-range parts of the ESP of finite graphene flakes separately and discuss how they change with model size.

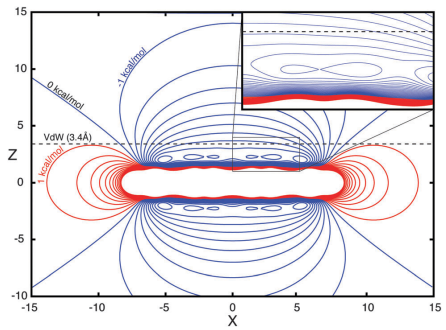

Fig. 2 Electrostatic potential around a small polyaromatic molecule (coronene). The dotted line is plotted 3.4 Å above the graphene surface, *i.e.*, at a typical vdW distance.

In the long range limit, *i.e.*, at distances that are large compared to the size of the graphene flake itself, ESP decays as R^{-3}. Here, the electrostatic field in the z direction (see Fig. 2) is characterized by a macroscopic quadrupole, Q_{zz}^{Macro}, which is simply the sum of the individual carbon atomic quadrupoles, Q_{zz} ($Q_{zz}^{\mathrm{Macro}} = NQ_{zz}$). It should be noted that the R^{-3} decay in the z direction can only be observed very far from the graphene surface, for instance at tens of μm for μm-sized flakes, *i.e.*, far from the vdW contact region. Although the macroscopic quadrupole has not been reported for a single graphene flake, a value of $Q_{zz} = (-3.03 \pm 0.10) \times 10^{-40}$ Cm^2 per carbon atom has been calculated from macroscopic quadrupole measured by Whitehouse and Buckingham for graphite particles.[3] We assumed that this value also applied for the graphene atomic quadrupole.

When approaching the graphene flake surface, the distance dependence of the electrostatic potential weakens (see also the discussion below). The region corresponding to the weaker distance dependence of the electrostatic potential is very wide, ranging from the surface to about one fifth of the flake diameter in the z direction. In this work, we focused mainly on the contact vdW region about 3.4 Å above the surface (indicated by a dashed line in Fig. 2). As the size of the graphene flake increases, the electrostatic potential in this region asymptotically approaches zero, as noted above. Thus, despite bearing a sizeable macroscopic quadrupole moment, the quadrupolar contribution to intermolecular interactions at its surface almost vanishes for large perfectly planar graphene flakes.

Closer to the graphene surface, at the distances typical for vdW interactions, a periodically varying microscopic field arises due to the atomic structure of the surface. The inset of Fig. 2 shows this periodic component as a mild undulation in the ESP contours when passing from one carbon atom to another. Albeit rather weak, the periodic quadrupolar component has been shown to influence the adsorption of gases on a graphite surface.[4–6] According to Vernov and Steele,[4] it has little effect on the adsorption energies but substantially alters barriers to the free translation and location of energy minima of N_2 and H_2O molecules on graphite. Later, Do and Do[5] considered the polarization of an adsorbed fluid (argon) by the periodic quadrupolar field and showed that dipoles induced in the adsorbed gas repel each other and reduce the stability of the adsorbed layer (surface mediation effect). In this article, we do not discuss the periodic component (although it is included in our simulations) but rather focus on the strength of the quadrupolar potential as a function of the finite flake size and corrugation.

To investigate the importance of quadrupolar interactions of graphene flakes with the surrounding medium, we chose to model liquid phase exfoliation in two solvents that differ in the sign of their Q_{zz} quadrupole tensor components, namely benzene and hexafluorobenzene (C_6F_6). Liquid phase exfoliation is a process in which solubilized graphene mono- and multi-layers are produced upon sonication of graphite in suitable solvents. This process is an important potential method for the

large scale and low cost production of medium sized graphene flakes. The key to this technology is finding an efficient, cheap and environment friendly solvent for solubilizing graphene to concentrations above 1 mg ml^{-1}, which is currently challenging.[7] A number of solvents for graphene solubilization have been studied experimentally[8,9] and theoretically.[10,11] It has been suggested that the best solvents are those whose surface energies are close to that of graphene itself (68 mJ m^{-2}),[12] thus minimizing mixing enthalpy. Even better predictions are obtained by using Hansen solubility parameters;[13] approximate values of $\delta_{D,G} \sim 18$ $MPa^{1/2}$, $\delta_{P,G} \sim 10$ $MPa^{1/2}$ and $\delta_{H,G} \sim 7$ $MPa^{1/2}$ have been suggested by Coleman's group,[14] leading to the discovery of a number of new efficient solvents for graphene.[12]

Benzene and C_6F_6 represent a particularly interesting pair of exfoliation solvents. They have reasonably similar Hansen solubility parameters (benzene: $\delta_{D,G} \sim 18.0$ $MPa^{1/2}$, $\delta_{P,G} \sim 0.0$ $MPa^{1/2}$ and $\delta_{H,G} \sim 2.0$ $MPa^{1/2}$; C_6F_6: $\delta_{D,G} \sim 16.9$ $MPa^{1/2}$, $\delta_{P,G} \sim 0.0$ $MPa^{1/2}$ and $\delta_{H,G} \sim 0.0$ $MPa^{1/2}$),[13] and therefore are expected to exhibit similar exfoliation efficiencies. Nevertheless, experiments have shown that whereas C_6F_6 is quite a good exfoliation solvent, benzene is a rather poor one.[9] Interestingly, benzene and C_6F_6 differ in their quadrupole moment, which is of similar magnitude but has opposite sign. Therefore, we decided to test whether this fact can explain the observed difference in exfoliation efficiencies of these two solvents. In molecular mechanics, this could easily be tested by comparing simulations with and without atomic quadrupoles placed on the graphene model.

Our paper is organized as follows. First, we analyze the electrostatic potential at different locations near to graphene flakes as a function of size and corrugation. Then, we estimate Gibbs energy changes of graphene flake exfoliation with and without a quadrupole moment by pulling a free graphene leaf from the surface. After that, the influence of a quadrupole on the solvation energy of graphene leaves of different sizes in different solvents is estimated using alchemical transformation of the quadrupole in a solvent. Finally we estimate exfoliation/association barrier heights by pulling fixed coplanar sheets in different solvents.

2. Methods

Several different structures were chosen to represent graphene flakes and supporting graphene in this study. Graphene flakes were represented by circumcoronene (denoted as C54) or by a larger 35 × 35 Å rectangular flake with 478 carbon atoms (denoted as C478). The periodic supporting graphene was modeled as a 50 × 50 Å rectangular graphene flake (C1008) in simulations including circumcoronene and as a 70 × 70 Å graphene flake (C2040) in simulations including C478. A single graphene sheet was used to model the graphite support. Exfoliation energies of graphite were shown to be somewhat higher (by about 18%),[15] but this should not affect our results because we are interested in the relative effect of the electrostatic component rather than the exfoliation energy itself.

Molecular dynamics simulations were performed within the Gromacs 4.5 software package.[16] After equilibration in the NPT ensemble (P = 1.0 bar, T = 298.15 K), production runs were performed in the NVT ensemble (T = 298.15 K). All atom GAFF force field parameters[17] were used for carbon atoms in circumcoronene and graphene flakes and the SPC/E model was used for water.[18] Parameters for C_6F_6 were taken from the literature,[19] and for benzene, GAFF parameters were used for vdW spheres and RED[20] parameters were used for charges. The integration step for all simulations was 2 fs and the interval for data collection was set to 0.5 ps. The cutoff distance for the direct electrostatics and vdW potential was set to 10 Å. The particle mesh Ewald method was used to calculate the indirect electrostatic potential beyond the cutoff distance. Bonds to hydrogen atoms were constrained during the MD simulations using the non-iterative LINCS algorithm.

The quadrupole moment of the graphene surface was represented by a pair of virtual sites placed above and below each carbon atom. The charges and distances of the virtual sites were chosen to reproduce the experimental value of the graphite quadrupole moment $Q_{zz} = (-3.03 \pm 0.10) \times 10^{-40}$ Cm^2 measured by Whitehouse and Buckingham.[3] A positive charge ($0.52e$) was placed at each carbon atom and two negative charges ($-0.26e$) were placed 0.6 Å above and below the graphene plane. The same values were used for all molecules in the present study.

2.1. Alchemical transformation

Alchemical transformation was used to estimate the effect of the quadrupole moment on solvation energies of graphene flakes in benzene, C_6F_6 and water. The method is based on thermodynamic integration (TI) of derivatives of the Hamiltonian with respect to a mixing parameter lambda, which was used to interpolate the state with and without the quadrupole moment. We used the 5-point Gaussian quadrature. Each simulation for a given lambda was equilibrated for 2.5 ns and the sampling period for data collection was 7.5 ns.

2.2. Graphene peeling

The potential of mean force (PMF) for peeling of the C54 and C478 molecules from an infinite graphene support was calculated using restrained MD simulations in an explicit solvent. As a reaction coordinate, we chose the z-coordinate of one of the outer carbon atoms, which was slowly pulled in the normal direction from the graphene surface. The reaction coordinate was divided into 43 windows separated by 0.48 Å (C54) or 165 windows separated by 0.34 Å (C478). For each window, 16 ns (C54) or 6 ns (C478) MD simulations were carried out. The umbrella integration method[21] was used to reconstruct the PMF of peeling.

2.3. Thermodynamic integration

The PMF of exfoliation of two carbon sheets (C54) constrained to be coparallel was calculated using constrained MD simulations in benzene and C_6F_6 explicit solvents. The 14 Å long reaction coordinate was divided into 52 windows with unequal spacing in order to improve sampling of the regions with rapidly changing force. Each window was equilibrated for 2.5 ns and 7.5 ns was used for data collection. The total force

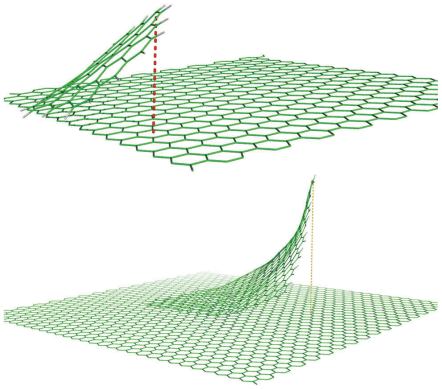

Fig. 3 Peeling of graphene flakes (C54 and C478) from an infinite graphene sheet.

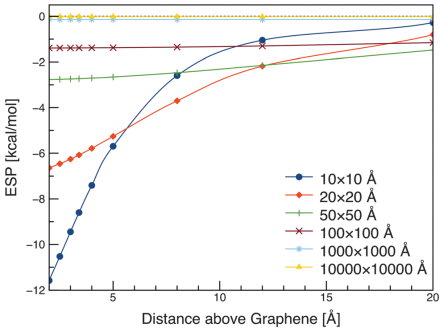

Fig. 4 Electrostatic quadrupolar potential above the surface of a graphene sheet as a function of the distance from the surface, and size of the sheet.

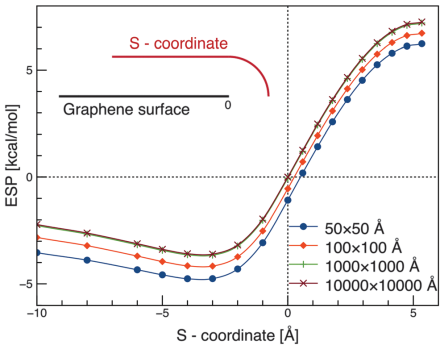

Fig. 5 Electrostatic potential next to the surface (3.4 Å) of a graphene sheet near to an edge as a function of the distance from the edge (*S*-coordinate) and size of the sheet. The *S*-coordinate is negative above graphene and positive when leaving the flake.

acting on the center of mass of a C54 sheet was collected every 0.5 ps. The average force in each window was integrated using the cubic spline method.

3. Results and discussion

3.1. Electrostatics of finite graphene sheets

A typical size of a graphene flake exfoliated by sonication is about 1 μm^2, which corresponds to about 40 million carbon atoms. Flakes are usually irregularly shaped, with straight edges; a rectangular flake would have less than 10 000 atoms along its edge (1 μm, 10 000 Å). Fig. 4 illustrates how the electrostatic potential above the center of a graphene sheet decays as a function of the distance from the surface, *z*. Results are shown for rectangular sheets with several edge sizes, *a*, ranging from 10 to 10 000 Å. With increasing size of the flake, the distance dependence of the potential near to the surface weakens and its amplitude decreases. To estimate the relative importance of this potential for intermolecular interactions, we can compare it with the strength of typical vdW interactions, which dominate binding in graphite: each carbon atom contributes about 1.4 kcal mol^{-1} (or 61 meV per atom) to the cohesion energy of graphite.[22] Fig. 4 shows that for sheets smaller than 100 × 100 Å, the electrostatic interaction with a unit charge is more than 1 kcal mol^{-1}, which is comparable to the dispersion interaction with a carbon-like atom. On the other hand, for sheets larger than 1000 × 1000 Å, the electrostatic interaction with a unit charge is much weaker than 1 kcal mol^{-1} and for a 1 μm flake, it becomes negligible. Interaction of this quadrupolar field with uncharged molecules will usually be even weaker.

Next, we examined the potential near the graphene edge. Fig. 5 shows a plot of the electrostatic potential as a function of the distance from the flake edge. The electrostatic potential was calculated 3.4 Å above the surface, corresponding to typical vdW distances. Results for different sizes of flakes, *a*, are plotted in different colors. These results show that for a very large flake, the potential near the edge converges to a finite value of about −3.6 kcal mol^{-1} and for smaller flakes, it is even larger. Thus, electrostatic interactions with graphene edges may be important even for relatively large planar sheets. This may result in different adsorption properties of the edges as compared to the rest of the surface.

3.2. Electrostatics of corrugated graphene

Unlike the ideal planar model described above, real graphene exhibits out-of-plane undulations, often called corrugation. The corrugation height has been estimated from experiment as about 1 nm and the length of the "wave" roughly between 5 and 10 nm for free graphene *in vacuo*.[23] As a result of this corrugation, cancellation of the electrostatic quadrupole in real

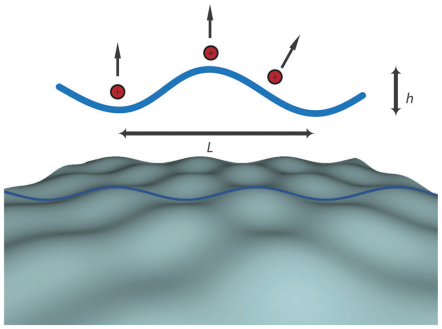

Fig. 6 The model of undulated graphene. Corrugation was represented as an undulation of height h = 1 nm and length L = 8 nm. The electrostatic potential was calculated 3.4 Å above the surface at three distinct locations, *i.e.*, the "valley", the "peak", and the inflex point.

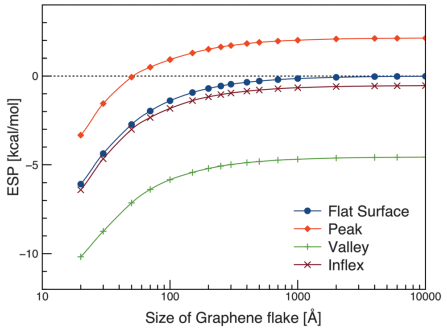

Fig. 8 Electrostatic potential close to the surface (3.4 Å) of a corrugated graphene sheet as a function of the sheet size. Potential above the peak (red), valley (green) and in the inflex of a ripple (violet) is compared with the potential above a perfectly planar sheet of the same size.

graphene is expected to be imperfect. We attempted to estimate the effect of the graphene undulation on the electrostatic potential near to the surface (3.4 Å above the surface). We chose to examine three distinct locations on the undulated landscape, the "peak", the inflex point and the "valley" (see Fig. 6). Corrugation was modeled as sinusoidal in both the x and y directions with an undulation height of 1 nm and 8 nm period.

Fig. 7 shows ESP at these three locations as a function of distance from a rectangular flake (1000 × 1000 Å). For comparison, we also show ESP of a perfectly planar flake of the same size (blue line). As expected, the potential next to the corrugated graphene was predicted to be substantially larger than that above the planar sheet. The absolute value was largest in the valley, somewhat smaller above the peak and very small near the inflex. Interestingly, whereas ESP was always negative above the planar carbon sheets, it was positive at the top of the peak, then changed sign near the inflex and acquired a negative value in the valley. It also decayed more rapidly with distance than ESP of a planar sheet.

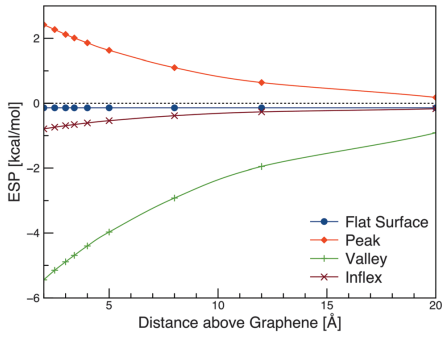

Fig. 7 Electrostatic potential as a function of distance from a corrugated graphene sheet (1000 × 1000 Å) above the peak (red), valley (green) and in the inflex (violet) of a ripple compared with the potential above a perfectly planar sheet of the same size.

Fig. 8 shows ESP above a rectangular graphene flake as a function of its size. The most important difference compared to planar graphene is that the potential does not converge to zero but to a finite value with increasing sheet size. For our simple model, ESP converged to about 2 kcal mol^{-1} per unit charge above the peak and about −4.5 kcal mol^{-1} per unit charge in the valley. Note that this value is only a very rough estimate because corrugation in real graphene is irregular and probably highly environment-dependant. Nevertheless, it is fairly large and may potentially make a sizeable contribution to the total interaction energy when graphene interacts with polar or charged molecules.

The quadrupolar electrostatic potential of corrugated graphene can be compared with that of benzene and polyaromatic molecules (Fig. 9). Among polyaromatic hydrocarbons, ESP was found to be largest for coronene and only somewhat smaller for benzene, circumcoronene (C-coronene) and dicircumcoronene (DC-coronene) (3.4 Å above surface in the middle of the molecule). The value for graphitic carbon is taken from Whitehouse and Buckingham.[3] In the case of corrugated graphene, the value of ESP in the valley was comparable to that of benzene, and the values above the peak and near the edge were smaller in magnitude, but still significant. Because benzene's quadrupole is known to play a very important role in its intermolecular interactions, it is likely that quadrupolar electrostatic interactions are also important for molecular interactions with corrugated graphene.

Electric field of graphene's quadrupole may become sizeable not only near edges or due to corrugation but every time the graphene sheet is disturbed from planarity. This happens at graphene folds or wrinkles but also in processes in which the

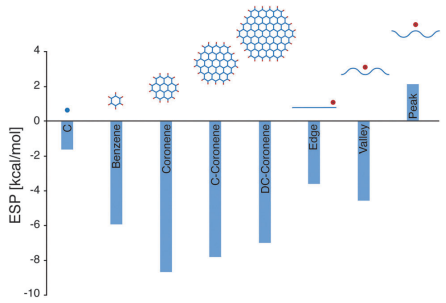

Fig. 9 Comparison of ESP near a graphene edge and of corrugated graphene with ESPs of aromatic hydrocarbons (calculated 3.4 Å above the surface, in the middle of the molecule).

graphene sheet is mechanically stressed, *e.g.*, during sonication induced exfoliation. In all these cases, quadrupolar interactions may need to be considered. Here we should note that when graphene is deformed, rearrangement of its electronic density may also generate dipole moment and other multipoles, which may significantly contribute to the total electric field. However, because these effects cannot be estimated at the force field level, we do not discuss them here. The magnitude of the quadrupolar contribution described in this work may be easily compared with other effects when their estimates become available.

3.3. Role of the quadrupole in MD simulations

The quadrupole moment of carbon atoms in graphene is usually neglected in MD simulations with classical force fields. Therefore, it is important to determine what role it may play and whether neglecting it is a safe approximation. In the present work, we focused mainly on interactions with benzene and C_6F_6, which differ in sign of their molecular quadrupole (Q_{zz}). In particular, we examined whether different exfoliation capabilities of these two solvents may be explained by interactions with the graphene quadrupole. We also attempted to estimate the quadrupole contribution to solvation energies of small graphene flakes by alchemical transformation and TI, and the PMF of graphene exfoliation considering two different exfoliation coordinates. Some calculations were also performed in water.

3.3.1. Potential of mean force of graphene peeling. The mechanism of liquid phase exfoliation is not yet fully understood and many different pathways may be possible. One idealized pathway is that the leaving sheet is gradually peeled from the support. To model this process, we pulled two small model molecules (circumcoronene and the rectangular flake C478) from the support by one of the outer carbon atoms (see Fig. 3 in Methods) and calculated PMF of this process by the umbrella integration technique (Fig. 10).

The PMF of peeling in C_6F_6 exhibited a deep minimum at the contact distance (about 3.4 Å) and then increased monotonically

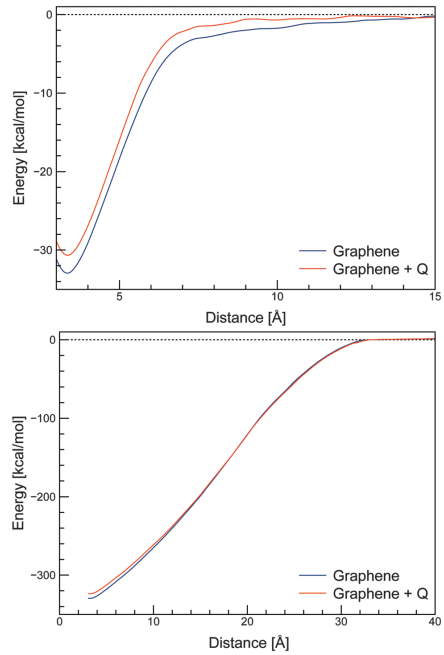

Fig. 10 Calculated PMF of exfoliation of circumcoronene (top) and C478 (bottom) in C_6F_6. A distance of about 3.4 Å corresponds to a stacked bilayer.

and reached the exfoliated state without a barrier. The exfoliated state was predicted to be thermodynamically unstable, consistent with results of MD simulations for other organic solvents.[10] The stabilization energy per carbon atom was about −0.61 kcal mol^{-1} for the circumcoronene model and −0.69 kcal mol^{-1} for C478. When quadrupoles were included on the peeled leaves, the exfoliated state was stabilized by electrostatics and the stabilization energies changed by 0.04 kcal mol^{-1} (from −0.61 to −0.57 kcal mol^{-1}) for C54 and by 0.01 kcal mol^{-1} (from −0.69 to −0.68 kcal mol^{-1}) for the C478 flake. Apparently, the quadrupolar contribution is relatively small in C_6F_6 and tends to decrease with the size of the simulated flake. Therefore, neglect of quadrupole moment is probably a reasonable approximation in this case.

3.3.2. Quadrupole contribution to solvation. The contribution of the quadrupolar moment to graphene's solvation energy was estimated by thermodynamic integration of alchemical transformation. Here we gradually grew atomic quadrupoles and integrated the accompanying change of Gibbs energy. To obtain a deeper insight, we simulated growth of both the natural graphene atomic quadrupoles (denoted as Q), and quadrupoles of the same absolute value but of opposite sign

Table 1 Change in Gibbs energy of solvation when quadrupoles are introduced, ΔG, for C54 and C478 in different solvents

	Circumcoronene (54 C atoms)		35 × 35 Å (478 C atoms)	
ΔG (kcal mol^{-1})	$0 \rightarrow Q$	$0 \rightarrow -Q$	$0 \rightarrow Q$	$0 \rightarrow -Q$
C_6F_6	−2.6	0.2	−8.6	0.4
C_6H_6	−0.1	−2.2		
Water	−4.9			

(denoted as $-Q$). The graphene flake models were not constrained, and thus were free to form ripples. Table 1 shows results for circumcoronene (C54) and the C478 flake, in water, benzene and C_6F_6.

Comparison of the simulations with reversed quadrupoles (Q and $-Q$) indicated competing electrostatic and polarization contributions to solvation. The polarization contribution (here only orientation solvent polarization) is always stabilizing. On the other hand, electrostatic interactions can be either stabilizing or destabilizing, depending on the orientation of the solute and solvent quadrupoles (we assume prevailing coplanar solvent orientation with the surface). Here, the interaction is stabilizing for the natural quadrupole on C54 (Q) in C_6F_6 and the opposite quadrupole ($-Q$) in benzene. The electrostatic and polarization contributions to solvation were apparently of similar magnitude, which resulted in almost complete cancellation in the cases where the electrostatic component was destabilizing (C54(Q) in benzene and C54($-Q$) in C_6F_6).

For benzene and C_6F_6, the quadrupolar contribution to solvation was relatively small and decreased with the flake size (contributions per C atom for C54 and C478 were −0.05 and −0.02, respectively, see Table 1). We did not calculate the total solvation energy directly, but a rough estimate can be obtained from the above estimated exfoliation energy and interaction energy ($\Delta G_{solv} \approx \Delta G_{exf} + E_{int}$). This gives about −22 kcal mol^{-1} for C54. Thus, the quadrupolar contribution to solvation in C_6F_6 was estimated to be only about 12% and is expected to be much smaller for larger graphene flakes. Higher results for water indicate that electrostatic interactions are more important in polar solvents, as expected. Nevertheless, it appears that neglecting quadrupolar interactions in force field calculations introduces only a relatively minor error in solvation energies and is probably a justified approximation.

3.3.3. Potential of mean force of coparallel flakes. The PMF of graphene plates can provide important information relevant to stability of graphene colloid in a given solvent.[10] Here, the graphene flakes were modeled using two circumcoronene molecules, which were kept planar and coparallel. One of the circumcoronenes bore atomic quadrupoles, whereas the other did not. The circumcoronene without quadrupoles represented a flat support, for which the electrostatic field cancels out due to its planarity. The circumcoronene with atomic quadrupoles mimicked the approaching (or leaving) graphene sheet, which may be corrugated or bent, and thus exhibit a local quadrupolar field. For comparison, we also calculated PMF for a model in which both circumcoronene molecules were without quadrupoles, as in the classical force field.

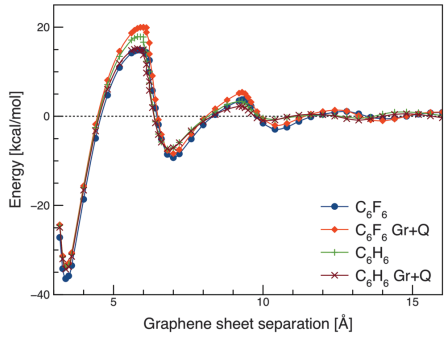

Fig. 11 PMF of separation of two circumcoronene molecules calculated in C_6F_6 with (red) and without quadrupoles (blue) and in benzene with (brown) and without quadrupoles (green) on the approaching circumcoronene.

Fig. 11 shows PMF in two different solvents, benzene and C_6F_6, calculated both with and without atomic quadrupoles on the approaching molecule. The exfoliation energy in C_6F_6 was very similar to that obtained in the peeling calculation described above (Fig. 10), *i.e.*, about 0.67 kcal mol^{-1} per carbon atom. Interestingly, the exfoliation energies in benzene and C_6F_6 were very similar. This means that the experimentally observed difference between the exfoliation efficiencies in the two solvents cannot be explained by thermodynamic stabilization of the exfoliated state. Nevertheless, the good stability of the graphene dispersion in C_6F_6 may be partly explained by kinetic considerations, as discussed below.

Inclusion of quadrupoles had notable effects on several characteristics of the PMF curves. Consistent with the results shown above (using a different exfoliation trajectory, Fig. 10), the exfoliation energy in C_6F_6 decreased only slightly (by about 3 kcal mol^{-1}, or 5%) when quadrupoles were included. However, inclusion of quadrupoles had a more pronounced effect on the barrier heights. Let us consider an association barrier at around 6 Å, which separates the solvent separated minimum at around 7 Å from the contact minimum at 3.4 Å. The height of this barrier has been shown to play an important role in kinetic theory of graphene colloid aggregation because it contributes to colloid stability.[10] When quadrupoles were neglected, benzene provided a slightly larger barrier height than C_6F_6, which suggests slower aggregation in benzene. Interestingly, when quadrupoles were considered, the height of this barrier increased by 4.2 kcal mol^{-1} (17%) in C_6F_6, whereas in benzene it decreased by 2.7 kcal mol^{-1} (11%) (note that these are rough estimates only as they are model-dependent). As a result, the expected association rate would be slower in C_6F_6 than in benzene when quadrupoles are included, as opposed to the situation when quadrupoles are neglected.

Because of the sensitivity of reaction rates to barrier heights, the almost 7 kcal mol^{-1} change may lead to a significant decrease of the aggregation rate in C_6F_6, resulting in better kinetic stability of graphene colloid in this solvent. Thus, kinetic aspects may partially explain the experimentally observed better exfoliation capabilities of C_6F_6, which cannot be explained by thermodynamic considerations, as discussed above.

4. Conclusions

In this study, we investigated the effect of graphene's electric quadrupole moment arising from its π electron distribution on intermolecular interactions. The magnitude of the graphene quadrupolar field was studied as a function of model size and corrugation. For an infinite and perfectly planar graphene sheet, the quadrupolar field near the surface vanishes with increasing sheet size, and therefore does not contribute to intermolecular interactions. However, in small graphene sheets the electric quadrupolar field decreases with increasing sheet size only slowly and may have a significant effect for small flakes, nanoribbons or near the edges of flakes. In corrugated graphene, the quadrupolar field does not vanish even for infinite sheets, and in the valleys of the corrugation, it reaches values comparable to those known for a benzene molecule. Because cancellation of the quadrupolar field near a graphene surface is disturbed by the curvature of the surface, significant electrostatic contributions may be expected near to graphene bends and folds. These results indicate that quadrupolar interactions may need to be considered when modeling intermolecular interactions with corrugated or bent graphene.

The effect of neglecting quadrupoles was tested in MD simulations of graphene exfoliation/aggregation in two similar solvents, benzene and C_6F_6. Inclusion of explicit quadrupoles made only a small contribution to the solvation energy of exfoliated flakes, of the order of a few percent. Although the electrostatic contribution thermodynamically favors solubilization of graphene in C_6F_6 when compared to benzene, stabilization is too small to explain the striking difference between the observed exfoliation efficiencies of these two solvents. However, considering quadrupoles had a marked effect on the PMF of graphene aggregation. Without quadrupoles, benzene exhibited a higher association barrier than C_6F_6, but when quadrupoles were included, the barrier height in C_6F_6 became substantially higher than that in benzene. Because the aggregation barrier height contributes to the kinetic stability of the exfoliated state, quadrupolar interactions may need to be taken into account when accurate modeling of graphene aggregation is needed.

It should be noted that current pairwise additive empirical potentials also neglect other effects which may play important roles in molecular interactions with graphene, such as polarization, charge redistribution in graphene upon corrugation, or charge transfer between interacting molecules. Some of these effects may be sizeable and comparable in magnitude with the quadrupolar contribution. The main purpose of this work was to isolate the quadrupolar contribution and estimate its magnitude separate from the above mentioned effects.

In conclusion, corrugated or bent graphene exhibits an electric quadrupole moment that may be important for intermolecular interactions. Our results will help to assess errors due to omission of quadrupolar electrostatic interactions in force field MD simulations and improve the general understanding of the importance of quadrupolar moments in molecular interactions with graphene.

Acknowledgements

This work was supported by grant P208/10/1742, from the Grant Agency of the Czech Republic. Further funding was provided by the Operational Program Research and Development for Innovations of the European Regional Development Fund *via* projects CZ.1.05/2.1.00/03.0058 and CZ.1.07/2.3.00/20.0017 administered by the Ministry of Education, Youth and Sports of the Czech Republic and a student project of Palacky University (PrF_2013_028).

References

1 V. Georgakilas, M. Otyepka, A. B. Bourlinos, V. Chandra, N. Kim, K. C. Kemp, P. Hobza, R. Zboril and K. S. Kim, *Chem. Rev.*, 2012, **112**, 6156–6214.
2 G. R. Jenness and K. D. Jordan, *J. Phys. Chem. C*, 2009, **113**, 10242–10248.
3 D. B. Whitehouse and A. D. Buckingham, *J. Chem. Soc., Faraday Trans.*, 1993, **89**, 1909.
4 A. Vernov and W. A. Steele, *Langmuir*, 1992, **8**, 155–159.
5 D. D. Do and H. D. Do, *Colloids Surf., A*, 2007, **300**, 50–59.
6 D. Nicholson, R. F. Cracknell and N. G. Parsonage, *Mol. Simul.*, 1990, **5**, 307–314.
7 U. Khan, A. O'Neill, M. Lotya, S. De and J. N. Coleman, *Small*, 2010, **6**, 864–871.
8 J. N. Coleman, *Adv. Funct. Mater.*, 2009, **19**, 3680–3695.
9 A. B. Bourlinos, V. Georgakilas, R. Zboril, T. A. Steriotis and A. K. Stubos, *Small*, 2009, **5**, 1841–1845.
10 C. Shih, S. Lin, M. S. Strano and D. Blankschtein, *J. Am. Chem. Soc.*, 2010, **132**, 14638–14648.
11 A. Schlierf, H. Yang, E. Gebremedhn, E. Treossi, L. Ortolani, L. Chen, A. Minoia, V. Morandi, P. Samorì, C. Casiraghi, D. Beljonne and V. Palermo, *Nanoscale*, 2013, **5**, 4205–4216.
12 J. N. Coleman, *Acc. Chem. Res.*, 2013, **46**, 14–22.
13 C. Hansen, *Hansen Solubility Parameters: A User's Handbook*, CRC Press, Boca Raton, Florida, 2nd edn, 2007, p. 544.
14 Y. Hernandez, M. Lotya, D. Rickard, S. D. Bergin and J. N. Coleman, *Langmuir*, 2010, **26**, 3208–3213.
15 L. A. Girifalco and R. A. Lad, *J. Chem. Phys.*, 1956, **25**, 693.

16 D. Van Der Spoel, E. Lindahl, B. Hess, G. Groenhof, A. E. Mark and H. J. C. Berendsen, *J. Comput. Chem.*, 2005, **26**, 1701–1718.
17 J. Wang, R. M. Wolf, J. W. Caldwell, P. A. Kollman and D. A. Case, *J. Comput. Chem.*, 2004, **25**, 1157–1174.
18 H. J. C. Berendsen, J. R. Grigera and T. P. Straatsma, *J. Phys. Chem.*, 1987, **91**, 6269–6271.
19 D. Dellis, I. Skarmoutsos and J. Samios, *J. Mol. Liq.*, 2010, **153**, 25–30.
20 F.-Y. Dupradeau, A. Pigache, T. Zaffran, C. Savineau, R. Lelong, N. Grivel, D. Lelong, W. Rosanski and P. Cieplak, *Phys. Chem. Chem. Phys.*, 2010, **12**, 7821–7839.
21 J. Kästner and W. Thiel, *J. Chem. Phys.*, 2005, **123**, 144104.
22 R. Zacharia, H. Ulbricht and T. Hertel, *Phys. Rev. B: Condens. Matter Mater. Phys.*, 2004, **69**, 155406.
23 J. C. Meyer, A. K. Geim, M. I. Katsnelson, K. S. Novoselov, T. J. Booth and S. Roth, *Nature*, 2007, **446**, 60–63.

C Modelling of Graphene Functionalization

PCCP

PERSPECTIVE

View Article Online
View Journal | View Issue

Cite this: *Phys. Chem. Chem. Phys.*, 2016, **18**, 6351

Modelling of graphene functionalization

Martin Pykal, Petr Jurečka, František Karlický and Michal Otyepka*

Received 22nd June 2015,
Accepted 19th August 2015

DOI: 10.1039/c5cp03599f

www.rsc.org/pccp

Graphene has attracted great interest because of its remarkable properties and numerous potential applications. A comprehensive understanding of its structural and dynamic properties and those of its derivatives will be required to enable the design and optimization of sophisticated new nanodevices. While it is challenging to perform experimental studies on nanoscale systems at the atomistic level, this is the 'native' scale of computational chemistry. Consequently, computational methods are increasingly being used to complement experimental research in many areas of chemistry and nanotechnology. However, it is difficult for non-experts to get to grips with the plethora of computational tools that are available and their areas of application. This perspective briefly describes the available theoretical methods and models for simulating graphene functionalization based on quantum and classical mechanics. The benefits and drawbacks of the individual methods are discussed, and we provide numerous examples showing how computational methods have provided new insights into the physical and chemical features of complex systems including graphene and graphene derivatives. We believe that this overview will help non-expert readers to understand this field and its great potential.

1. Introduction

Graphene[1] is a two dimensional material consisting of a hexagonal (honeycomb) lattice of covalently bound sp^2 carbon atoms that are sandwiched between two π-electron clouds. Despite extensive research efforts triggered by numerous potential applications of graphene and its derivatives (Fig. 1),[2] only a limited number of graphene-based products have been successfully commercialized to date. The graphene-based technology is still mainly in the research and development stage (for a more detailed discussion, please see the October 2014 issue of *Nature Nanotechnology*[3]). Among other purposes, it has diverse uses in sensing, ranging from the detection of small molecules[4] to large biomacromolecules,[5,6] including also DNA translocation[7] and selective molecular sieving.[8] The potential range of applications for graphene can be enhanced enormously by covalent and non-covalent modification.[9] Covalent modification entails the formation of chemical bonds between graphene and

Regional Centre of Advanced Technologies and Materials, Department of Physical Chemistry, Faculty of Science, Palacký University Olomouc, tř. 17. listopadu 12, 771 46 Olomouc, Czech Republic. E-mail: Michal.Otyepka@upol.cz; Fax: +420 585 634 761; Tel: +420 585 634 756

Martin Pykal

Martin Pykal is a PhD student at the Palacký University, Olomouc. His main areas of interest are molecular dynamics simulations of graphene and other carbon nanostructures and their interactions with small biomolecules.

Petr Jurečka

Petr Jurečka is currently an associate professor at the Palacký University and a researcher at the Regional Centre of Advanced Technologies and Materials (RCPTM) in Olomouc, Czech Republic. He received his PhD degree in physical chemistry from Charles University and Institute of Organic Chemistry and Biochemistry in Prague in 2004 for theoretical studies of intermolecular interactions. His current work focuses on molecular modelling of nucleic acids, development of empirical force fields for nucleic acids, and intermolecular interactions in nanomaterials.

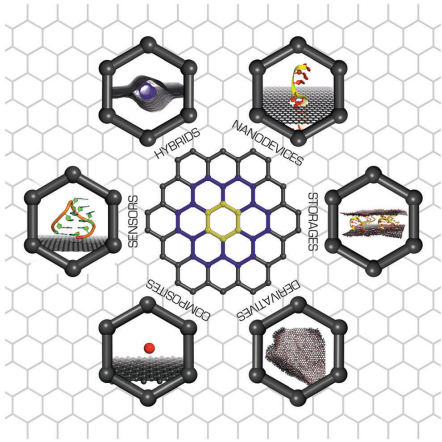

Fig. 1 Areas where graphene and its derivatives may have valuable applications.

some modifiers, which significantly change the structure and the hybridization of its carbon atoms. Such changes have profound effects on the material's physicochemical properties.[10] Conversely, non-covalent modification entails the adsorption of a modifier onto the graphene surface *via* weak non-covalent forces. Such adsorption also changes the structure and properties, but to a lesser degree than the covalent modification; the magnitude of the changes is proportional to the modifier's binding energy. It should however be noted that the transition between covalent and non-covalent modification is rather smooth. To understand the effects of these modifications, and their behaviour in sensing applications, it is necessary to obtain an in-depth understanding of the nature and strength of the interactions between graphene and guest molecules. Computational chemistry is a valuable source of information that can be used to develop such an understanding.

Modelling of the interactions between graphene and guest molecules or modifiers can provide important insights into the effects of graphene modifications. This can be achieved using either electronic structure methods based on quantum mechanics, which explicitly account for the electronic structure of the studied molecular systems, or with molecular mechanics methods (also known as empirical force fields) that simplify molecular systems by representing them as collections of covalently bound van der Waals spheres. This perspective provides an overview of electronic structure and empirical methods (Sections 3 and 4) that can be used in computational studies on graphene modifications, extended with basic simulation methods for nuclear degrees of freedom (Section 5). We also provide some guidance for non-experts to explain which methods are applicable in particular contexts and how suitable they are for predicting the behaviour and properties of functionalized graphene and graphene derivatives. Finally we present numerous illustrative examples of computational studies that have enhanced our understanding of modified graphene (Section 6).

2. Graphene models

2.1 Finite molecular models of graphene

Graphene is often modelled as a finite polyaromatic hydrocarbon (PAH)[11–14] such as coronene ($C_{24}H_{12}$) or circumcoronene ($C_{54}H_{18}$), both of which are shown in Fig. 2.[15,16] The carbon networks of these model molecules are capped with hydrogen atoms that saturate the dangling bonds at their edges. This affects the distribution of electronic density within the system because the electrons of the hydrogens are drawn to the carbon skeleton, generating a positive electrostatic potential on the

František Karlický

František Karlický graduated in 2004 at the University of Ostrava, Czech Republic. He obtained a PhD degree in physical chemistry from the Prague Institute of Chemical Technology in 2009 and his PhD work was focused on the development of methods for solving the Schrödinger equation for many-body bosonic systems. He is now an assistant professor at the Department of Physical Chemistry and a junior researcher at the Regional Centre of Advanced Technologies and Materials, Palacký University, Olomouc. His research interests include modelling of carbon nanostructures, transition metal complexes and atomic clusters.

Michal Otyepka

Michal Otyepka received his PhD degree in physical chemistry at the Palacký University, Olomouc (2004). Currently, he is a head of the Department of Physical Chemistry and vice-director of the Regional Centre of Advanced Technologies and Materials, both at the Palacký University, Olomouc, Czech Republic. His research is mostly focused on modelling of biomacromolecules, 2D materials and their interactions, and chemistry of graphene derivatives. In 2014, he received Impulse from Neuron fund to support science.

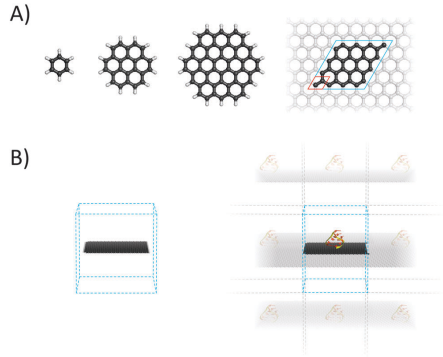

Fig. 2 (A) Some aromatic hydrocarbons that are commonly used as non-periodic models of graphene in quantum calculations (benzene, coronene and circumcoronene), and a supercell of 32 carbon atoms from a periodic graphene model, with a unit cell highlighted in red. (B) Simulation boxes for empirical models containing a finite graphene flake (left) and a periodic graphene sheet with a small adsorbed RNA molecule (right). In techniques based on periodic boundary conditions, the supercell/simulation box is replicated throughout the space.

hydrogen atoms and a negative electrostatic potential above and below the carbon sheet where the π electron cloud is located. Consequently, polyaromatic hydrocarbons have significant quadrupole moments that depend on their size (Fig. 3).[17] This finite quadrupolar potential means that PAHs are imperfect models for the infinite flat periodic sheet of graphene, in which the quadrupolar potential completely vanishes. It should be noted, however, that real graphene is corrugated and the quadrupolar potential may be nonzero near its surface (Fig. 3). An important advantage of using finite molecular models is that they can be studied using a wide portfolio of electronic structure

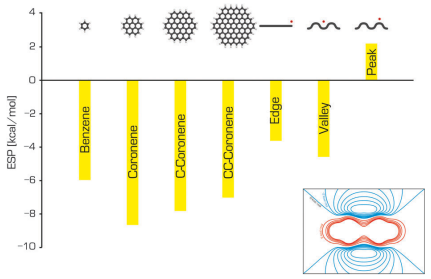

Fig. 3 The electrostatic potentials of benzene, coronene, circumcoronene and circumcircumcoronene (calculated in the middle of the molecule, 3.4 Å above the surface), and the electrostatic potentials at specific positions relative to a graphene sheet (adapted from ref. 17). The inset shows the ESP around the benzene molecule; the red and blue contours represent positive and negative potentials, respectively.

methods developed for molecular systems. The only limitations come from the size of the system that can be treated in a reasonable timeframe with specific methods, and the available computational power. A systematic study by Hobza and coworkers showed that the interaction energies of tetracyanoethylene and tetracyanoquinodimethane with various PAHs decreased convergently as the size of PAH increased.[18]

Empirical methods (Section 4) allow the use of substantially larger models of graphene flakes (up to tens of nanometers), and are therefore applicable when studying nanoscale phenomena such as exfoliation and aggregation processes in colloidal dispersions of graphene.[19] In such cases edge effects as well as the effects of the system's quadrupole moment may become important.[17] Shih and coworkers[20] studied the stability and mechanisms of the aggregation process in exfoliated graphene solutions in several frequently used polar solvents. Based on their simulations and kinetic theory, they proposed a model of graphene aggregation in which the dominant barrier to aggregation was associated with the energetic cost of eliminating a single layer of solvent molecules confined between two graphene sheets oriented in parallel. Colloidal dispersions of graphene were also investigated by Lin *et al.*,[21] who examined the morphology and kinetics of self-assembled structures of surfactants and graphene sheets. Their findings suggest that the surfactant molecules stabilized the colloidal graphene dispersion and prevented the re-formation of new two- and three-layered graphene aggregates. Freestanding graphene was also considered in a study on wrinkles on the graphene surface and their effect on the specific surface area.[22] The results indicated that wrinkles could only change the specific surface area by 2% at most, regardless of their shape, the nature of the defects that were present, or the strain acting on the area.

2.2 Periodic graphene

Ideal graphene is an infinite two-dimensional (2D) sheet with a regular lattice structure. Such a material can be straightforwardly modelled using periodic boundary conditions (Fig. 2) in which a unit cell including two carbon atoms is replicated across space. This periodic graphene model can be studied using numerous methods, most of which are based on density functional theory (DFT) and were developed by solid-state physicists to model the physical features of crystals. When studying the adsorption of guest molecules (adsorbates) to graphene, the size of a replicating cell, which is known as the supercell, is dictated by the size and target concentration of the adsorbate because it is important to avoid unwanted interactions between replicas. Since the periodic boundary conditions are typically implemented over the three-dimensional (3D) space, graphene (which is generally assumed to lie in the *xy* plane) and its complexes are modelled using 3D unit cells with a large vertical length (~1.5 nm) to avoid spurious vertical interactions between replicas. Spurious interactions could be particularly problematic if the supercell contains polar molecules or ions, because of the slow decay of Coulombic forces. It should be noted that the attractive van der Waals (vdW) forces

in nanomaterials act over longer distances than was originally assumed.[23]

Periodic models can also be used with empirical methods (Section 4). One of their advantages is that they help to avoid some artefacts that can be caused by the presence of edges. An example is the quadrupole moment, which should be considered when working with finite graphene models such as those discussed above. The electronic band structure of graphene and its derivatives can only reasonably be studied using periodic models because models that do not account the inherent extended nature of graphene neglect correlation contributions from the bands close to the Dirac point. Furthermore, the infinite model may better describe the situations encountered in some experiments, such as those involving measurements on spots of graphene flakes that may be multiple micrometers in diameter. In such cases, the presence of edge effects in a simulated finite sheet could introduce undesirable bias. An infinite periodic boundary condition (PBC) model was used to study the mechanism by which graphene dispersions are stabilized in the presence of lipids, revealing that the lipids present a kinetic barrier to graphene aggregation by forming reverse micelles on the graphene surface.[24] On the other hand, PBC models may be less suitable for studying phenomena such as surface corrugation because the box size limits the scale on which corrugation effects can be studied. Another potential drawback of the periodic model that may be encountered with certain simulation configurations relates to sandwiched structures in which two graphene sheets are separated by a fixed distance; this can lead to unphysical conditions such as unreasonable pressures. It should also be noted that not every software package for performing empirical computations supports periodic models.

As mentioned above, both finite and infinite (periodic) graphene models can be described using either quantum chemical (electronic structure) or molecular mechanical (empirical) methods. The potential applications of each are delineated by the Born–Oppenheimer approximation, which enables the separation of electronic and nuclear motions inside a molecular system. Phenomena involving changes in electronic states should be modelled using electronic structure methods that explicitly account for electronic motions. Molecular mechanics can be used to model phenomena in which the electronic structure does not change or changes only slightly, such as changes in conformational states or physisorption.

3. Electronic structure methods

3.1 Methods for studying non-covalent complexes of graphene

We have already mentioned that graphene can be modified either covalently or non-covalently. However, the mode of adsorbate binding may in reality lie somewhere between these two extremes. To model such situations it is necessary to use theoretical methods that accurately describe both covalent and non-covalent forces. It should be stressed that the accurate description of non-covalent forces is quite challenging for current theoretical methods. To avoid lengthy descriptions of the many electronic structure methods that could potentially be used to describe the electronic and physical–chemical properties of graphene, we will focus here on methods that can be used to predict its non-covalent interactions with reasonable confidence. The fidelity of theoretical methods for chemical modifications of graphene will be discussed only with reference to specific cases. It is generally accepted that individual sheets of graphene are bound by London dispersion forces in graphite. London forces originate from non-local electron correlation effects.[25] Any electronic structure theory must therefore account properly for these non-local correlation effects in order to reliably predict the properties of non-covalent graphene complexes such as their binding energies and geometries.

3.2 Wavefunction based methods

The Hartree–Fock (HF) method fails to describe electron correlation effects because it neglects the correlation between electrons of opposite spin. It is therefore necessary to use post-HF methods to address this deficiency. The second-order Møller–Plesset perturbation method (MP2) accounts for a large fraction of the electron correlation effect, but it has some drawbacks. First, it is significantly more computationally demanding than the HF method and tends to overestimate the binding energies of non-covalent complexes that are bound mostly by London dispersive forces. Several methods that derive from MP2 but offer greater accuracy have been developed. The spin-component scaled MP2 (SCS-MP2)[26] and SCS(MI)-MP2[27] methods are of particular note because they predict binding energies significantly more accurately than MP2 without any additional computational cost. The CCSD method itself is not suitable for the accurate description of dispersion bonded complexes. However, its spin-component scaled variants SCS-CCSD[28] and SCS(MI)-CCSD, the latter of which is optimized for the study of molecular interactions,[29] provide remarkably accurate results with a very good accuracy/computational cost ratio. The scaled MP2/MP3 method including higher-order correlation effects (*e.g.*, MP2.5)[30] can also be useful for obtaining very accurate binding energies for non-covalent complexes at an affordable computational cost. The current gold standard for predicting the binding energies of non-covalent complexes is undoubtedly the coupled cluster method including single, double and perturbative triple excitations – CCSD(T). Unfortunately, CCSD(T) calculations are so computationally demanding that only small systems of less than $\sim$35 atoms can be studied in this way (Table 1). Significant speedups of CCSD and CCSD(T) calculations have been achieved using the recently-introduced domain based local pair-natural orbital (DLPNO) approximation, yielding the modified DLPNO-CCSD[31] and DLPNO-CCSD(T)[32] methods. However, further testing of these methods may be required before they can be considered suitable for routine use. More detailed information on the performance of various methods for modelling non-covalent complexes can be found in a recent review.[33]

Wavefunction-based methods are always used in conjunction with a finite basis set. In the literature, combinations of a

Table 1 Overview of electronic structure methods (see the text for abbreviations) that can be used to study complexes of graphene. Methods applicable to finite and periodic models are indicated with an "×". For each method, the size of the model (in terms of its number of atoms) that can be treated, the computational cost, and the quality of the results obtained are indicated by sets of asterisks, with one asterisk indicating small models/low computational costs/good quality results, and four asterisks indicating large systems/huge costs/best quality results

Method	Finite	PBC	Size	Cost	Quality
WFT					
MP2	×	×	**	**	*
SCS(MI)-MP2	×	×	**	**	**
MP2.5	×	—	**	***	***
CCSD(T)	×	—	*	****	****
DFT					
M06-2X	×	×	***	**	**
DFT-D2, DFT-D3[a]	×	×	***	**	**
DFT-TS[a]	×	×	***	**	**
vdW-DF, vdW-DF2	×	×	***	***	**
optB88-vdW	×	×	***	***	**
RPA	×	×	*	****	***
Other					
QMC	×	×	**	****	****
PM6-DH, SCC-DFTB-D	×	×	****	*	*

[a] The real performance and cost of DFT-D2, -D3, and -TS methods are determined by the underlying functional; hybrids are more expensive than GGA functionals.

method and a basis set are typically denoted in the form of a method/basis set – for example, SCS(MI)-MP2/cc-pVTZ, where cc-pVTZ stands for the correlation consistent polarized valence triple-zeta basis set developed by Dunning and coworkers.[34] Many different basis sets have been developed, and a detailed description of their construction and applicability would be beyond the scope of this review; the interested reader can find more detailed information elsewhere.[35] However, it should be noted that the chosen basis set can significantly affect the quality of the results obtained in any quantum chemical calculation. It is generally accepted that larger basis sets provide better results. This idea resulted in the development of extrapolation schemes,[36–38] which estimate the results for an infinite basis set that is referred to as the complete basis set (CBS). Calculations performed at the CCSD(T)/CBS level of theory provide very accurate estimates for quantities such as the interaction energies of non-covalent complexes.[33,39,40] When CBS extrapolation cannot be performed and small or medium size basis sets are used, which is usually the case, it is important to apply a correction for the basis set superposition error (BSSE) (Fig. 4) such as the counterpoise (CP) correction of Boys and Bernardi.[41] The BSSE arises from the fact that the basis sets used to describe non-covalent complexes are necessarily larger than those used for their individual components (in the simple case of a dimeric complex, the basis set for the dimer will necessarily be twice the size of that for the separated monomer). Failure to correct the BSSE inevitably leads to an overestimation of binding energies. However, the CP correction is imperfect and frequently overestimates the BSSE,[42] so some authors use either the fractional BSSE correction or combine the CP with special extrapolation schemes.[38,43]

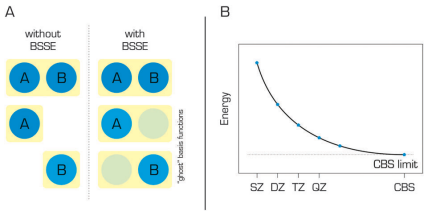

Fig. 4 (A) The interaction energy of two atoms or molecules is typically calculated as the energy difference between the complex (A + B) and its components (A and B). In the counterpoise correction, the energy of each subsystem is calculated in the basis set of the whole complex, using "ghost" basis functions located at the original positions of the atomic centres of the other subsystem without the associated charges and electrons. (B) The convergence of energy with increasing basis set size (*i.e.* going from the minimal single-zeta (SZ) basis set to the double-(DZ), triple-(TZ) and quadruple zeta (QZ) sets) can be used to extrapolate the energy at the complete basis set (CBS) limit.

The post-HF methods were primarily developed for the study of molecular systems and they are readily applied to molecules and their assemblies. On the other hand, their applicability under periodic boundary conditions is currently very limited.[44] The MP2 method has been implemented in a way that is compatible with the periodic boundary approach[45–48] but calculations using this implementation are impractical for graphene because of its zero band gap. The CCSD method has been implemented in the VASP code for periodic boundary simulations[49] but this update has not yet been released to the public.

3.3 Density functional methods

Classical DFT methods based on the local density approximation (LDA), the generalized gradient approximation (GGA), or hybrid functionals do not account for non-local electron correlation effects, which are critical for the correct description of London dispersion forces.[50–52] In LDA the binding caused by a too strong exchange contribution to the exchange–correlation functional is very different from the dynamical correlation effects promoting dispersion interactions. Several strategies have been developed to describe London dispersion forces within the framework of DFT. These include the empirically corrected DFT methods (abbreviated as DFT-D). The first DFT-D methods were based on summation over pair-wise c_{ij}/r_{ij}^6 terms (where c_{ij} represents an empirical dispersion coefficient for the electron pair ij at a distance of r_{ij}), which were multiplied by a damping function (whose parameterization critically influences the accuracy of DFT-D) to avoid double counting of dispersive contributions,[53,54] which is necessary because DFT natively accounts for local electron–electron correlation. After the initial success of the DFT-D method[53,55] a series of more sophisticated methods with better performance were introduced including DFT-D2,[56] DFT-D3[57] and DFT-TS.[58] In addition, it was shown that many-body dispersion methods that go beyond pair-wise vdW interactions are required to improve the description of

non-covalent interactions involving graphene.[59,60] Dispersion can also be accounted for by combining DFT and MP2 calculations, the latter of which naturally account for long-range correlation.[61] Such methods are called double hybrids because they include some portion of HF exchange in addition to the MP2 correlation. Double hybrid methods can be very accurate.[62,63] However, like MP2 calculations, they cannot be applied to periodic graphene. Note also that double hybrids somewhat underestimate long-range dispersion, although this can be corrected for by introducing empirical dispersion correction terms.[64]

An alternative strategy resulted in the development of non-local density functionals that account directly for dispersive correlation effects. Approaches of this type include the vdW-DF method of Dion *et al.*,[65] its improved successor vdW-DF2,[66] the reparameterized version optB88-vdW,[67] and the VV10 method of Vydrov *et al.*[68] It should be noted that functionals which account for electron–electron correlation effects can be systematically improved by exploiting the adiabatic connection fluctuation–dissipation theorem[69] as clearly explained by Tkatchenko.[70] Yet another way of modelling mid-range intermolecular interactions accurately with DFT is to use one of the highly parameterized local, GGA or meta-GGA DFT functionals developed by Truhlar and coworkers, which are called the Minnesota functionals (*e.g.* M06-2X[71]). These functionals provide surprisingly good results at affordable cost (The comparison with other methods is shown in Table 1). The ability of some of these methods to predict the energies of interaction between graphene-based materials and molecular hydrogen has been investigated by Kocman *et al.*[72] London dispersive forces can also be described using the random phase approximation (RPA) method, which accounts for electron–electron correlation effects from first principles. The RPA provides rather accurate predictions of surface adsorption behavior[73–75] and bulk material properties.[76,77] However, it is very computationally demanding. Finally, the GW approximation[78] has been used for accurate quasiparticle electronic band structure calculations. This many-body method corrects DFT using a self-energy operator consisting of Green's function (G) and the screened Coulomb interaction (W), and thereby inherently accounts for electron–electron correlation effects.

The height of the activation barrier to a given chemical modification of graphene can be related to the kinetics of the corresponding process using the Eyring equation. To accurately predict activation barriers, it is necessary to address the problem of the electron self-interaction error (SIE) in DFT exchange functionals.[79] This can be achieved by admixing HF or exact exchange in DFT functionals. DFT functionals containing HF exchange are known as hybrid functionals. An ideal DFT method capable of accurately describing thermodynamics, kinetics and non-covalent interaction should thus be free of SIE and account for non-local electron correlation effects. This could potentially be achieved in various ways, for example by combining RPA with exact exchange.[80,81] However, this would not be trivial to achieve, and careful testing of such approaches would be essential.

3.4 Quantum Monte Carlo methods

Quantum Monte Carlo (QMC) represents another strategy for solving the electronic Schrödinger equation from first principles. QMC methods are explicit many-body approaches based on the real-space random sampling of the electron configuration space. Two QMC methods are in common use, variational Monte Carlo (VMC) and diffusion Monte Carlo (DMC). The VMC method relies on the variational principle and stochastic integration of a quantum-mechanical total energy expectation value. Its main advantage is the ability to sample complicated wave functions including explicit correlation and to improve them variationally. A more powerful alternative to VMC is the fixed-node DMC method (FN-DMC), which relies on the projection (or enhancement) of the ground-state component from a given input trial electronic wave function in imaginary time. In combination with real-space sampling (that is a complete basis set, *i.e.* electrons can visit any point in the real space), FN-DMC provides exact solutions within the boundaries imposed by the fixed-node ($\Psi_T = 0$) condition of the input trial state Ψ_T. The fixed-node approximation is the one of multiple possible strategies for simulating Pauli exchange repulsion. FN-DMC thus efficiently accounts for electron–electron correlation effects from first principles. It should be noted that the QMC results are less sensitive to the one-electron basis sets used to construct trial wave functions since the electron correlations are simulated explicitly rather than by using many-body expansions in terms of one-particle states, as is the case in traditional wave function theory. QMC results have associated error bars that only converge slowly ($\propto 1/\sqrt{K}$ for calculations with K independent sampling points), but the method's computational cost typically scales as a low-order polynomial (of order 3–4), which is significantly better than the scaling of CCSD(T)/CBS (of order 7) and thus enables studies of larger systems with comparable accuracy (as demonstrated in ref. 82). Moreover, QMC methods can be efficiently parallelized and implemented for both finite and periodic boundary conditions (Table 1). Consequently, they have great potential for use in electronic structure calculations on graphene and related compounds. In recent years, QMC methods have been used to study small conjugated hydrocarbons (benzene/coronene) and their interactions with atoms/molecules[72,82–86] and for explicit modelling of periodic graphene/graphite.[84,87,88] For more details on QMC, we direct the reader to a pair of recent reviews (and references included therein).[89,90]

3.5 Semiempirical methods

Since the advent of quantum chemistry, there has been a continuous effort to develop fast electronic structure methods capable of treating large systems containing hundreds of atoms. One way of doing this is to introduce additional approximations to the HF method (Section 3.2) in the form of semiempirical parameters, which are derived by approximation or fitting to experimental results or data from higher-level calculations. Semiempirical methods such as AM1,[91] PM3[92] and PM6[93] are very widely used in chemical research. In physics, the tight-binding (TB) semiempirical method is a

similar approximate approach for predicting the electronic structure of periodic materials.[94,95] In the TB approach, the wave function of a complex system is constructed as a superposition of the wave functions for isolated atoms located at the positions of the corresponding nuclei within the system of interest. It has been used successfully to describe graphene and its derivatives,[96] achieving accuracies that rival higher level methods while enabling the simulation of systems comprising hundreds of atoms. For instance, ballistic transport in transistors based on the functionalized graphene[97] were reported on the basis of the energy band calculation by high-level methods for graphane and graphone, subsequently fitted with a three-nearest neighbour sp^3 tight-binding Hamiltonian. More recently, the TB approximation was used to study the electronic structures and optical properties of micrometer-scale partially and fully fluorinated graphene systems comprising 2400 × 2400 carbon atoms at GW accuracy.[98] The TB approximation has also been generalized, leading to the development of density functional-based tight binding (DFTB).[99] DFTB was subsequently improved by the incorporation of self-consistent redistribution of Mulliken charges (SCC-DFTB)[100] to account for the Coulomb interaction between charge fluctuations, and by the addition of an empirical dispersion correction (SCC-DFTB-D).[101] SCC-DFTB accounts for long-range electrostatic forces and self-interaction contributions, and has been used to investigate the correlation between the hydrogen superlattice structure on graphene and the band gap opening,[102] and to explore the properties of graphene nanodots inside fluorographene.[103]

The approximations made in the creation of current semi-empirical methods mean that they cannot accurately describe non-covalent interactions. This problem can be addressed by introducing empirical dispersion corrections (D) in the same way as was done for DFT in the creation of the DFT-D methods. In keeping with the established nomenclature, the suffix -D is appended to semiempirical methods corrected in this way, which include AM1-D and PM3-D.[104] The latter of these two methods was successfully used to model the interactions of small molecules with aromatic systems[105] and graphite.[106] Hobza and coworkers developed the semiempirical method PM6-DH, which incorporates an additional correction term to describe hydrogen-bonding[107] as a function of H-bond length, donor–H···acceptor angle and partial charges on the H and acceptor atoms. Additional variants of the DH correction, *e.g.*, DH+[108] and DH2,[109] which avoid double counting of the dispersion energy, are also available. These methods were used to model the adsorption of various molecules on graphene with quite good accuracy.[110–112] A variant of the TB method incorporating an *a posteriori* dispersion correction has also been introduced, which performed well in the modelling of hydrogen physisorption on PAH and graphene and in predicting the bulk properties of graphite.[113]

4. Empirical methods

Whereas advanced quantum chemical methods provide highly accurate descriptions of systems comprising a few tens of atoms, molecular mechanics (MM) can be used to perform calculations on systems comprising thousands of atoms (Fig. 5) such as nucleic acids, proteins, and nanostructures. Of course, this advantage is counterbalanced by many simplifications and limitations resulting from the omission of the electronic degrees of freedom: molecular mechanics only accounts for the motions of nuclei. In molecular mechanics, the system is considered to be an ensemble of beads and springs that are held together by simple harmonic forces. The core of the molecular mechanics calculation is a force field (also known as an empirical potential) consisting of a set of equations and some associated parameters that are used to describe the system's energetics. The resulting energy E_{ff} is calculated as the sum of several terms (eqn (1)) whose form and number is determined by the method's degree of simplification:

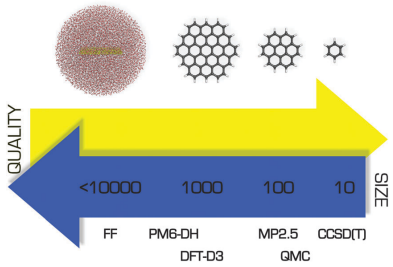

Fig. 5 Comparison of several theoretical approaches with respect to the size of the system that can be treated efficiently and the quality of the resulting description.

$$E_{\mathrm{ff}} = E_{\mathrm{bonded}} + E_{\mathrm{vdW}} + E_{\mathrm{elec}} + (E_{\mathrm{pol}}) + (E_{\mathrm{other\,terms}}), \quad (1)$$

here, E_{bonded} represents the contributions to the total energy from bonding terms (bond stretching, angle bending, and torsion angle twisting), while E_{vdW} and E_{elec} represent the non-bonding van der Waals and electrostatic terms, respectively. Further optional terms for polarization, E_{pol}, and other additional energy terms (for instance dispersive many-body terms) are included in brackets. Non-covalent interactions are accounted for using simple expressions for the Coulombic (electrostatic) and van der Waals forces:

$$E_{\mathrm{vdW}} = 4\varepsilon_{ij}\left[\left(\frac{\sigma_{ij}}{r_{ij}}\right)^{12} - \left(\frac{\sigma_{ij}}{r_{ij}}\right)^{6}\right], \quad (2)$$

$$E_{\mathrm{elec}} = \frac{q_i q_j}{\varepsilon r_{ij}}, \quad (3)$$

Here, ε_{ij} and σ_{ij} are the Lennard-Jones (LJ) parameters, r_{ij} is the interatomic distance, ε is the relative permittivity and q_i and q_j are the partial electric charges. The first listed LJ parameter, ε_{ij}, specifies the well depth, which determines how strongly two particles interact; σ_{ij} represents the distance at which the potential between the two particles is zero. The calculations can be performed with explicitly modelled solvent molecules,

which are often essential when studying phenomena such as molecular recognition, protein folding,[114] or liquid-phase exfoliation.[115]

4.1 Current empirical force fields

Numerous force fields for various kinds of structures have been developed over the past few decades.[116–119] Force fields are often very specialized and designed to target quite narrow groups of molecules. The greatest number of empirical calculations are performed on biological systems and so efforts to develop and refine force fields have largely focused on proteins, nucleic acids, and so on. While the transferability of parameters from one molecule to another is one of the principal assumptions of molecular mechanics models, their validity is far from clear when transferring parameters from biomolecules to nanomaterials. Fortunately, several modified force field parameters have been developed specifically for simulating graphene. Table 2 compares the non-bonded parameters for aromatic carbon atoms from the three most widely used biomolecular force fields to those from several modified potentials that were developed for modelling carbon allotropes and which have been used by various groups. Since in most cases the carbon atoms in graphene are treated as uncharged Lennard-Jones spheres, the molecular mechanics descriptions of the interactions between graphene and other molecules are governed exclusively by these non-bonded van der Waals parameters. Clearly, the listed force fields differ quite significantly with respect to these parameters, so it is important to choose a force field carefully if planning to use molecular mechanics to study graphene or its derivatives.

4.2 Approximations employed by empirical force fields

The advantage of the molecular mechanics approach over QM models is its simplicity and low computational cost (Fig. 5). Unfortunately, its approximations mean that many phenomena cannot be explicitly accounted for by the FFs. The problem of the quadrupole moment has already been mentioned, but there are other interactions that would be challenging or impossible to describe with a classical force field. These include the charge transport involved in many of graphene's intermolecular interactions, explicit polarization, and the charge redistribution caused by wrinkling of a graphene surface.

Table 2 Non-bonded parameters for aromatic carbon atoms from different force fields used in molecular dynamics simulations of graphene and graphene derivatives

Force field	σ [Å]	ε [kcal mol^{-1}]
Parm 99[116]	3.39967	0.0860
OPLS[117]	3.55000	0.0700
CHARMM27[118]	3.55005	0.0700
Ulbricht *et al.*[120]	3.78108	0.0608
Girifalco *et al.*[121]	3.41214	0.0551
Cheng and Steele[122]	3.39967	0.0557
COMPASS[123 a]	3.48787	0.0680

[a] Uses 9-6 LJ potential.

The neglect of polarization interactions is perhaps the most serious deficiency of common pairwise additive force fields when modelling graphene and its derivatives. Conventional FFs treat electrostatic interactions using effective partial charges that are constructed to match electrostatic potentials obtained from QM calculations. The point charges are located on the atomic centres and are constant (*i.e.* conformation- and time-independent). Consequently, it is impossible for the FF to react to changes in the molecular environment or to describe the way different solvents affect various interactions. In some force fields this problem is partly solved by adding an explicit term for electronic polarization. The contribution of polarization may be especially important in the case of nanomaterials, and it can be accounted for in several ways. A frequently used and technically simple option is the classical Drude model (the so-called "charge on spring" model), where an additional particle is attached to the atom. The particle has its own charge and, along with its attached atom, generates an induced dipole moment that depends on the external field. More detailed descriptions of the Drude model and its implementation can be found elsewhere.[124] The Drude methodology was used by Ho *et al.*,[125] who studied the effect of graphene polarization on the structural properties of water molecules at a graphene–water interface. Their results suggested that the explicit inclusion of polarizability had no significant effects on the dynamics of the graphene–water system, and that the effect became even smaller for charged graphene. However, larger effects might be expected for ions and their arrangement near the graphene surface. A similar way of including polarizability is the rigid rod model.[126] Like the Drude model, this approach involves attaching a virtual interaction site to the atom, but the assigned charge is kept at a fixed distance and is only permitted to rotate. The GRAPPA force field, which was specifically designed for simulations of water–graphitic interfaces, uses the rigid rod model.[127] A third way of including polarization is to assign atomic polarizabilities to the atoms and then calculate the resulting induced dipoles, whose orientation is determined by the external field felt at each atomic site in the molecule. This approach was used by Schyman *et al.*[128] in a study on the adsorption of water and ions on carbon surfaces including graphene, where the results obtained from polarizable and non-polarizable force fields were compared to quantum calculations. The authors suggested that the use of the polarizable force field substantially improved the description of graphene-like surfaces in the condensed phase.

Another drawback of current force fields is the pairwise additive approximation of the van der Waals interactions, where the resulting energy is calculated as a sum of contributions from individual pairs of atoms up to the cutoff distance. Many-body terms involving three or more atoms are not explicitly included. Although force fields are parameterized against experimental data and thus include many-body effects implicitly, in some cases it might be desirable to include at least three-body effects explicitly. In particular, many-body effects may be important for describing the behaviour of colloidal dispersions of nanomaterials or the intermolecular interactions of graphene sheets and nanotubes.[57,129]

Classical force fields do not allow bond cleavage and formation because they model bonds with harmonic potentials. This is sufficient for the study of various non-covalent modifications of graphene and other materials. However, a model capable of describing bond cleavage/formation is required for the study of any process involving chemical change such as chemisorption or chemical reactions. In such cases it is necessary to use methods that explicitly account for the system's electronic structure. Unfortunately, such methods can only be applied to relatively small model systems (Fig. 5). Empirical reactive force fields such as AIREBO,[130] REBO,[131] and ReaxFF[132] were developed to enable the study of large reacting molecular systems. These force fields use the standard force field approximations but also include terms for bond formation and dissociation. A more detailed description of individual reactive force fields is beyond the scope of this review and can be found in the specialized literature.[133,134]

5. Nuclear motion

As electronic structure is within Born–Oppenheimer approximation solved separately and it was described in Sections 3 and 4, this section discusses methods that account for nuclear motion and can be used to estimate the associated physical–chemical quantities. Thermodynamic quantities (internal energy, enthalpy, entropy, *etc.*) for processes involving nuclear motion are typically obtained from molecular dynamics (MD) and Monte Carlo (MC) simulations that involve sampling configurational space. While the first method average time sequence of the required quantity, the latter collects values of the quantity corresponding to random configuration walk.[135] Simulation methods that describe the studied system in terms of position and momentum vectors can be naturally extended to quantum versions (quantum MC and quantum MD) based on the nuclear wave function/density matrix as a central point.

5.1 Molecular dynamics

Molecular dynamics (MD) simulations usually use the laws of classical mechanics such as Newton's equations of motion to study the time evolution (dynamics) of a system:

$$\boldsymbol{F}_i = m_i \frac{\mathrm{d}^2}{\mathrm{d}t^2}\boldsymbol{r}_i(t), \quad i = 1, 2, \ldots, n. \tag{4}$$

The force $\boldsymbol{F}_i$ acting on each atom i (which has a mass m_i and position $\boldsymbol{r}_i$) due to its interactions with other particles can be determined at any time t during the simulation assuming that each atom's initial position and velocity is known. The force is enumerated as the negative gradient of the potential energy surface (PES)

$$\boldsymbol{F}_i = -\nabla_i E(\boldsymbol{r}_1, \boldsymbol{r}_2, \ldots, \boldsymbol{r}_n). \tag{5}$$

Classical molecular dynamics is a method, which uses PES given as the predefined potential; either based on empirical data (force field) or on independent electronic structure calculations. The term *ab initio* molecular dynamics (AIMD)[136] is used if the electronic energy is acquired during the MD run. AIMD has also been referred to as first principles MD, quantum chemical MD, on-the-fly MD, direct MD, potential-free MD and quantum MD.

Once the resulting force is known, new positions and velocities at time $t + \delta t$ are obtained by numerical solution of the equations. It is essential to select an appropriate time step δt. If a large time step is chosen the system may become unstable due to growing inaccuracies in the integration procedure. Time steps of 1–2 fs are typically used in classical MD simulations. This means that with current computer power it is possible to study dynamics on time scales of up to several microseconds. Perhaps the biggest benefit of this technique is its unique ability to provide information on the studied system at the atomistic level with femtosecond temporal resolutions. Moreover, specific techniques (for instance thermodynamic integration, potential of mean force, free energy perturbation, Jarzynski equality, *etc.*)[137] have been developed for use alongside MD to estimate the thermodynamic properties of the studied systems, making MD simulations potentially useful for investigating the thermodynamic changes accompanying the non-covalent functionalization of graphene.

Sometimes, it is not possible to neglect quantum effects associated with movements of atoms and molecules (see Section 6.8 for examples). In such cases it is necessary to work with a nuclear wave function known as a wavepacket in vibrational dynamics, which must be discretized and propagated.[138] The system-bath approximation is typically used when simulating quantum objects on graphene. In this approximation, the quantum system is represented by a wavepacket and the initial classical surface is implemented in a way that accounts for lattice dynamics and corrugation. A recent study on the physisorption of atomic hydrogen on graphitic surfaces[139] compared four different quantum mechanical techniques: close coupling wavepacket (CCWP) and reduced density matrix (RDM) propagation methods as well as the perturbation (PT) and effective Hamiltonian (EH) theories. All four methods' descriptions of hydrogen sticking were in reasonably good agreement. The CCWP and RDM methods described desorption well, but only the RDM method correctly captured the decay of the total trapped population. On the other hand, the PT and EH methods were around two orders of magnitude faster than CCWP and RDM. In the case of chemisorption, which involves stronger atom–surface coupling, perturbation methods cannot be accurate and CCWP or RDM should be used;[140] the latter may be preferable because it can describe many phonon processes. An alternative approach to fully quantum problems based on Feynman's path integral from statistical quantum mechanics can also be formulated. Path integral molecular dynamics (PIMD)[141] has been used successfully to study the adsorption of hydrogen on graphene and coronene.[142]

5.2 Monte Carlo methods

Monte Carlo methods are based on stochastic sampling, *i.e.* random walks (*cf.* Section 3.4). Monte Carlo methods can be divided into methods which assume that classical mechanics is applicable (and energy is a continuous variable) and those

which are based on the idea of discrete quantum energy levels.[143] While the classical Monte Carlo (CMC) methods are less widely used than classical molecular dynamics in the modelling of graphene systems, quantum Monte Carlo (QMC) methods are commonly used to model strongly quantum interactions with graphene/graphite. The diffusion Monte Carlo (DMC) method is typically used to compute the ground vibrational state (T = 0 K) of quantum systems on graphene. Thermodynamic properties at nonzero temperatures are computed using path-integral Monte Carlo (PIMC) methods,[144] which directly sample the density matrix using the path integral approach and replace integrals with averages over samples, as is also done in PIMD.

6. Selected applications

6.1 Interactions of graphenes

Accurate descriptions of interactions with graphene are essential for understanding the structure and dynamics of graphene-like systems. The graphene–graphene interaction is of fundamental importance in many areas. Two graphene sheets can be stacked in a number of ways that differ in terms of the relative shifts of their basal planes. More attention is paid to the most stable AB-stacked arrangement, where half of the carbon atoms in the one layer sit directly above the centres of the hexagonal rings of the second layer. Nevertheless, determining the interlayer binding (cohesive) energy of graphene/graphite remains a significant challenge for theoreticians and experimentalists.[145–149] Recently published benchmark data from thermal desorption spectroscopy suggested a value of 61 meV per atom[150] and prompted further in-depth theoretical investigations into the interlayer cohesive energy and vdW interactions in graphene-like systems.[151–155] AB-stacked graphene is also an attractive object of study because it is potentially amenable to band gap tuning.[156]

Methods for modulating the band gap of graphene and its derivatives are highly desired because they make it possible to tune the material's electronic properties and could facilitate the design of a new generation of electronic devices. There are a number of ways in which the band gap of graphene could potentially be modified. One is to apply strain to the graphene.[157,158] Alternatively, the adsorption of certain molecules on graphene induces symmetry breaking and hence band gap opening.[159] It has been demonstrated that non-covalent functionalization of graphene with Br_2 opens a relatively large band gap that can be further adjusted by using ultraviolet light to decompose the adsorbed Br_2 molecules.[160] A third option is the covalent modification of graphene. Fan *et al.* calculated that the electronic properties of graphene can be tuned by doping with either boron/nitrogen or joint BN domains.[161] It was however shown that the chemical nature of B/N dopants in graphene significantly changes the final doping effect (Fig. 6).[162] It has also been suggested that the reaction of graphene with atomic hydrogen is able to reversibly (by annealing) convert this highly conductive species completely into graphane, which is an insulator.[163] Moreover, Singh and co-workers[164] interspaced small saturated graphene islands in the graphane host and showed that the energy gap of these islands is determined by their size. Specifically, DFT calculations indicated that smaller islands had larger energy gaps. Another way of engineering the band gap of graphene is to use graphene nanoribbons of different widths; the narrower the ribbon, the wider the gap.[165,166] This approach could be particularly useful in printing processes. Graphene fluorination opens the band gap in a similar way to hydrogenation,[167,168] and it has been suggested that the magnitude of the band gap could be tuned by adjusting the degree of fluorination[169,170] or by replacing fluorine with heavier halogens.[171]

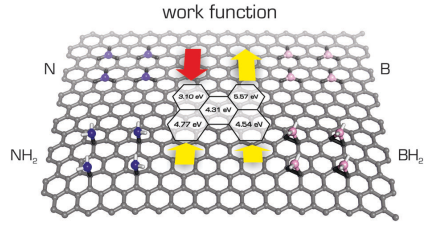

Fig. 6 The work functions (W_fs) calculated using the PBE0 functional of B/N-doped graphenes vary with the chemical nature of doping.[162] The W_f value of pristine graphene 4.31 eV (shown in the middle) increases in substitutionally B-doped graphene to 5.57 eV and decreases to 3.10 eV in substitutionally N-doped graphene. On the other hand, the W_f values increase in both graphenes with added $-NH_2$ and $-BH_2$ groups to 4.77 and 4.54 eV, respectively.

6.2 Interactions of graphene with small molecules

Graphene was quickly identified as a powerful adsorbent[172] whose interactions with various molecules often induce specific physicochemical responses that could be exploited in new types of sensors.[4,5,173] Moreover, non-covalent functionalization of the graphene surface substantially increases its potential range of applications.[9] Therefore the interactions of graphene with small molecules have been studied extensively, both experimentally and computationally, in order to obtain information on the strength and nature of such interactions (for some examples see Fig. 7). Using DFT symmetry adapted perturbation theory (DFT-SAPT),[174] which enables the decomposition of interaction energy into meaningful components, *i.e.*, coulombic, polarization, dispersion terms *etc.*, Lazar and coworkers showed that the adsorption of organic molecules was driven mostly by London dispersive forces.[12] The same conclusion had previously been drawn in a study on the adsorption of water molecules to graphene.[175] The adsorbates, which bind to graphene weakly *via* London dispersion forces, change its electronic structure only slightly but reduce the mobility of its electrons,[176] which can be exploited in sensing applications.[4] Recently, Zhou *et al.*[177] studied the physisorption of benzene and benzene derivatives on graphene, and suggested that the benzene derivatives adsorb

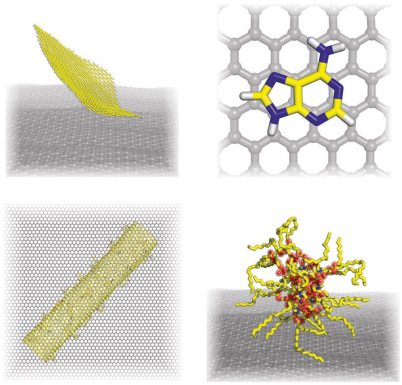

Fig. 7 Screenshots from molecular dynamics simulations of various processes taking place on a graphene surface: graphene exfoliation (top left), nucleobase adsorption (top right), graphene···carbon nanotube assembly (bottom left), and the formation of a reverse lecithin micelle on a graphene surface.

more strongly than pure benzene regardless of their substituents' electronic properties.

Molecules adsorbed on graphene may also affect its electronic properties by donating (n-doping) or withdrawing (p-doping) electrons and thereby shifting its Fermi level.[178,179] The same also applies for graphene supports. DFT calculations provide clear information about electron fluxes and can directly determine which adsorbates/supports donate/withdraw electrons to/from graphene. This feature was also exploited to design graphene devices with a reasonably wide band gap, which can be used in graphene-based transistors.[180,181] Such devices can be created from bilayer graphene sandwiched in between $FeCl_3$ and K (Fig. 8). Calculations using the vdW-DF functional identified

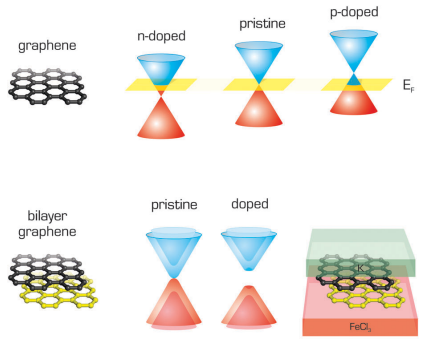

Fig. 8 Band structure of single layer graphene showing p- and n-type doping with respect to the Fermi level, and band gap opening in bilayer graphene caused by doping.

$FeCl_3$ as an electron acceptor capable of providing p-doped graphene and K as a donor providing n-doped graphene.[182]

Many studies have investigated the binding energies of adsorbates to graphene using a very diverse portfolio of theoretical techniques. Unfortunately, the development of this field has been hampered by a lack of reliable experimental data, which makes it difficult to benchmark the performance of individual methods. Adsorption enthalpies are particularly suited for such comparisons because they correspond to well-defined processes, which can be modelled in a straightforward manner. Enthalpies are usually measured by temperature programmed desorption on highly oriented pyrolitic graphite (HOPG)[183] or inverse gas chromatography on few-layered graphene.[12,184] Calculations suggest that adsorption energies on single layer graphene are around ~10% higher than those on few-layered graphene.[184] The adsorption enthalpies derived from *ab initio* MD simulations using the vdW-DF (optB88-vdW) functional were in good agreement with experimental data, suggesting that this non-local functional describes the binding energies of dispersion-bound molecules to graphene reasonably well. It is worth noting that force field simulations (using the OPLS-AA force field) also accurately predicted the relative binding enthalpies of the studied molecules, indicating that the same force field could be used to obtain preliminary estimates for the interaction energies of large molecules with graphene. If highly accurate predictions of binding energies of biomacromolecules to graphene are required, one should include contributions stemming from many-body terms.[129]

Preferred binding sites on the surface and energy differences between various binding sites can be estimated directly from theoretical calculations. Such information is important for understanding the friction on the graphene surface. Single atom adsorbates can bind at three sites (Fig. 9) referred to as on top (above the carbon atom perpendicular to the graphene sheet), on bond (above the carbon–carbon bond) and on hollow (above the centre of a "carbon hexagon"). Large molecules may have an even larger number of such high symmetry sites, as shown for tetracyanoethylene.[185] Calculations can predict

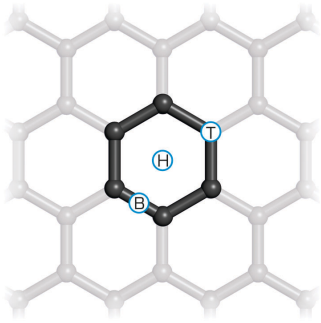

Fig. 9 On bond (B), top (T), and hollow (H) adsorption sites on graphene.

adsorption energies to individual sites and using the Boltzmann distribution law, the occupancy of individual sites can be estimated. Characterizing the potential energy surface of adsorbates sliding over the graphene increases the scope for understanding the friction that is generated. For example, calculations of this profile explained the contraintuitive increase in friction observed in a Pt atomic force microscopy tip moving over a graphene surface after fluorination.[186]

The strength of adsorption may depend not only on the adsorbate but also on its concentration and topology (the relative positions of individual adsorbates on the graphene surface). This indicates that the adsorbates significantly change the electronic structure of graphene and its binding involves some degree of covalent binding (chemisorption). The binding of fluorine or hydrogen atoms to graphene illustrates this phenomenon well.[10] The bond dissociation energy of fluorine atoms at low concentration is only around 50 kcal mol^{-1} whereas in fully fluorinated graphene (fluorographene or graphene fluoride) it is 112 kcal mol^{-1}.[187] The attachment of a fluorine atom to a carbon atom changes its sp^2 hybridization state to sp^3, inducing local structural buckling (*cf.* Fig. 10). The degree of structural changes correlates with the strength of binding, which is reflected in the high resolution XPS spectrum of the corresponding atom. Consequently, high resolution XPS spectra can be used to decipher information about the binding of such atoms.[188]

The abovementioned information indicates that there is no sharp distinction between physisorption (non-covalent functionalization) and chemisorption (covalent functionalization) to graphene. In general, the interaction curve of a given adsorbate with graphene will feature two minima: one corresponding to physisorption (also known as the precursor state) and the other to chemisorption.[140,142,189] These minima may be separated by an activation barrier (Fig. 10).

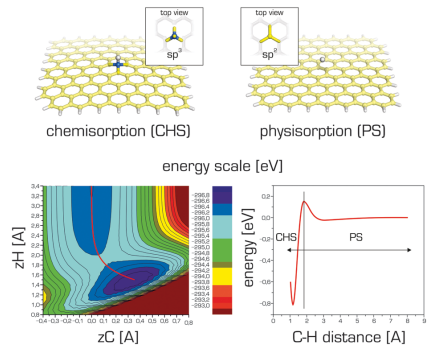

Fig. 10 The potential energy surface (calculated using PBE-D2) for hydrogen adsorption on graphene features two separate energy minima corresponding to physisorbed (PS) and chemisorbed (CHS) complexes. *z*H and *z*C denote the *z*-coordinates of the hydrogen nucleus and the closest carbon atom, respectively.

Density functional theory and molecular dynamics were successfully used together to explore the adsorption of the amino acid leucine on graphene,[190] revealing that under certain conditions leucine molecules adsorb spontaneously from solution. Moreover, it was suggested that the properties of the graphene could be tuned by controlling the orientation of the leucine molecules when they adsorbed. The adsorption of a somewhat larger tripeptide on graphene was studied by Camden *et al.*[191] It was shown that the presence of water at the interface strongly influenced the peptide's binding and conformation, suggesting that the inclusion of explicit solvent molecules may be essential for a proper description of the properties of peptide systems on graphene. Furthermore, some organic molecules could form highly ordered self-assembled monolayers (SAM) and bilayers on the graphene surface. O'Mahony and coworkers[192] used MD techniques to study the formation of alkylamine SAMs and the effect of different layer terminations on the adsorption of proteins on these platforms. It was suggested that alkylamine SAM assemblies could be used for instance for protein immobilization and exploited in targeted binding of specific molecules.

Molecular dynamics simulations appear to be useful for studying the wetting properties of graphene (and are widely used for this purpose), which are the subject of considerable ongoing debate.[193,194] The surface tension of graphene should be measured on free standing graphene, which is still quite challenging to achieve experimentally because graphene is usually prepared on a support and may be contaminated by adsorbates from the atmosphere.[195] On the other hand, such conditions are readily accessible in molecular simulations, which can estimate the contact angle on pure and free standing graphene.[196] The hydrophobicity of graphene is crucial for many of its potential applications (in nanomedicine, sensing, filtration, surface coatings *etc.*) and depends on many variables such as the purity[195] of the graphene sheet and the presence of defects[197,198] as well as the nature of the underlying support, whose wetting properties may affect (and be affected by) that of the graphene; this phenomenon is referred to as the wetting transparency of graphene.[199,200] Li and coworkers[201] suggested that graphene and other graphitic surfaces may even be slightly hydrophilic due to the adsorption of hydrocarbons commonly present in the air. Detailed studies on this behaviour could lead to the design of novel functional devices.[202]

6.3 Interactions of graphene with biomacromolecules

A molecular-level understanding of nucleic acids' and proteins' conformational behaviour near graphene-like supports may be important in the design and optimization of new nanoscale devices. Such interactions could be important in nanomedicine, where graphene or its derivatives could act as enzymatic inhibitors,[203] or in sensing since a variety of graphene-based sensors relying on different physicochemical principles have been proposed (Fig. 11).[204] One should bear in mind that molecules proposed for sensing applications have to preserve their native structure upon adsorption to graphene to maintain their function. It was shown that it is theoretically feasible to construct

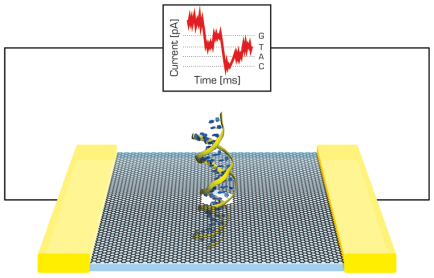

Fig. 11 DNA passing through the graphene nanopore may induce changes in the current, which could be used in DNA sequencing.

very sensitive graphene devices for ssDNA sequencing as a rapid and cost-effective alternative to current techniques.[205] Moreover, MD simulations of nucleic acid bases in solution suggest that graphene–base interactions are stronger than base–base stacking.[206] It has also been observed that DNA bases interact strongly with graphene[207–209] and that interactions with graphene can induce short DNA duplexes to partially unfold, mainly from the ends.[207] Such behaviour has also been reported for double stranded siRNA.[210]

6.4 Graphene and metals

The interactions of metals with graphene are very interesting, and complex. Naturally, graphene interacts with solid metals[211] in electrical circuits,[212] in graphene coated metals[213] and during its synthesis by chemical vapour deposition.[214–218] The interactions of metal nanoparticles with graphene are also very important because graphene provides a suitable platform on which to anchor such nanoparticles for catalytic, photocatalytic and sensor applications.[219–223] Moreover, graphene is being considered as a potential replacement for the widely used graphite anodes of lithium (and more generally, alkali metal) ion batteries, because it is suggested to offer a higher lithium ion storage capacity and to reduce charging times.[224,225] Numerous theoretical studies dealing with the adsorption and diffusion of alkali metal ions on pristine and functionalized graphene[226–229] as well as the positive influence of graphene defects on storage capacity[225,230] can be found in the literature. Current progress in the use of graphene in energy applications and challenges for the field have been nicely summarized in recent reviews.[231,232] Both individual metal atoms and small clusters may bond to graphene, altering its electronic and magnetic properties.[227,233,234] It was suggested that graphene decorated with heavy adatoms could turn into a giant topological insulator,[235] which might be used in magnetic storage devices.[236,237] However, the correct description of magnetocrystalline anisotropy requires the usage of hybrid functionals[238,239] and the inclusion of spin–orbit coupling.[233] The nature of the metal–graphene interaction may be anywhere between non-covalent and partially covalent,[240–242] indicating that any computational method used to study these interactions must reliably describe both London dispersive forces and chemical bonding.[243,244] For catalytic applications involving bond-breaking and bond formation, it is also necessary to use methods that do not suffer from the electron self-interaction error, which leads to an underestimation of reaction barriers. Explicit relativistic effects[245] should also be taken into account, especially when considering the interactions of heavy metals with graphene. Finally, when considering the interactions between metal adatoms and graphene, it is important to account for the spin-states of the metal and to be aware that these may change on binding.[85]

6.5 Hybrid carbon systems

The combination of graphene with other carbon allotropes such as nanotubes and fullerenes has opened up a new set of nanomaterials with many potential applications in areas such as printed electronics, conductive inks, reinforcement of polymers, *etc.* Computational modelling is playing an increasingly central role in studies on nanostructures because it enables the straightforward study of precisely defined structural motifs (joints) and because its atomistic resolution can help to elucidate unknown mechanisms and properties (Fig. 12). Interactions with fullerenes (mostly C_{60}) are of particular interest. MD simulations have shown that fullerenes could potentially be used to detect defects on graphene. He *et al.*[246] used C_{60} molecules to induce controlled ripples on the graphene sheet whose diffraction and interference can reveal cracks and defects on the surface. Several simulations of the diffusion of C_{60} molecules on graphene were performed at a constant temperature and with a temperature gradient.[247,248] Moreover, Peng *et al.*[249] suggested that C_{60}/graphene composites could be used for gas purification especially for some binary mixtures. Numerous computational studies on graphene-hybrid systems among other things are discussed in the recent review published by Zhang *et al.*, which focuses primarily on the computational characterization and simulation of graphene-based materials.[250] It was recently demonstrated that it may be possible to combine graphene and carbon nanotubes in novel composite materials in which the graphene spontaneously rolls up around the nanotube or enters its interior.[251–254] Graphene

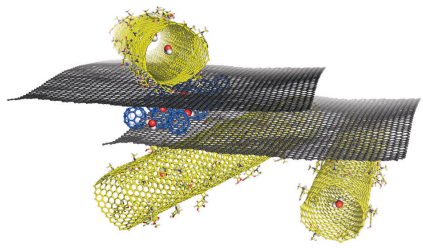

Fig. 12 Molecular modelling may provide unique molecular insight into the structures of graphene hybrid materials, which in turn may help us to design new functional nanosystems.

can also interact with carbon nanotubes to form 3D pillared structures where individual graphene sheets are separated by perpendicularly oriented carbon nanotubes. MD techniques were used to study the mechanical and thermal properties of these nano-networks,[255,256] and there is computational evidence that such pillared graphene structures could be used in gas separation[257] or hydrogen storage.[258] Finally, Georgakilas *et al.*[259] dispersed graphene sheets in aquatic media using hydrophilic functionalized carbon nanotubes and produced highly conductive graphene ink. MD simulations suggested that the formation of aggregates from graphene and hydroxyphenyl-functionalized carbon nanotubes was kinetically controlled and led to a stable colloid dispersion.

6.6 Graphene derivatives

While the properties of pristine graphene have attracted great interest, modified graphene derivatives may be even more interesting, at least in certain applications. The derivative that has attracted most attention is graphene oxide (GO). One obstacle to the modelling of GO stems from its complex structure, which contains epoxy, hydroxyl and carboxy groups. Even the composition of GO is quite uncertain and may depend on the conditions applied in its preparation.[260] Some models have been developed for studying the structure of GO, the most well-known and widely used of which is that of Lerf and Klinowski.[261,262] This model suggests that alcohol and epoxy groups are distributed randomly on the basal plane while the carboxyl groups are located on the edges. The interactions of nucleobases and several amino acids with GO were studied computationally by Vovusha *et al.*[263] It has been shown that complexes with GO are mainly stabilized by hydrogen bonding, in contrast with graphene complexes, which are stabilized mainly through dispersion interactions. Recently, Shih *et al.* used both experiments and molecular dynamics to study GO in solution[264] and to analyse its aggregation as a function of the pH and the protonation of its functional groups. They observed that at low pH values, GO became less hydrophilic due to protonation and formed sandwich-like aggregates in which individual sheets were separated by a confined water layer. However, separate sheets were preferred at higher pH values. Other articles have examined the electrical, structural and chemical changes accompanying GO reduction,[265,266] and a few recent atomistic works have investigated the effect of different reducing atmospheres on the reduction of GO, producing the results that complemented experimental investigations.[267,268] In addition, two molecular dynamics studies investigated this material's unusual mechanical properties.[194,269] Another interesting class of GO-based materials with diverse potential applications are the graphene oxide framework (GOF) materials. GOF is a porous material first synthesized in 2011 that consists of GO sheets connected by linkers. Nicolaï *et al.* developed molecular mechanics parameters for this material and used them to investigate its dynamic properties.[270] They suggested that the density of linkers connecting the GO layers can be used to tune the diffusion properties of GOF materials.

Other graphene derivatives such as graphane and fluorographene have also been studied extensively by computational means.

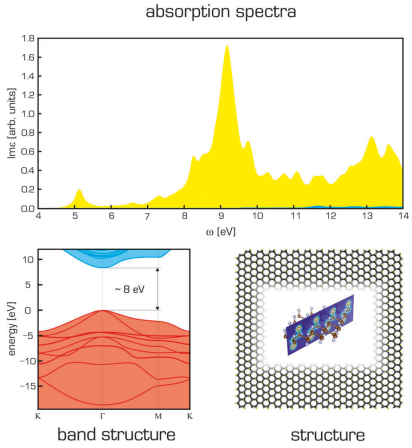

Fig. 13 Structure of fluorographene is shown together with its electronic band structure (calculated using GW(PBE)) and BSE@GW(PBE) adsorption spectra for light polarization parallel (yellow) and perpendicular (blue) to the surface plane.[276]

Graphane was predicted as a graphene derivative on the basis of DFT calculations.[271] Fluorographene and other graphene halides have been studied in some detail:[272] different investigations have focused on their band gaps and optical transitions,[273] the insulating properties of fluorographene[167,274] and the broad UV/VIS photoluminescence band observed experimentally (Fig. 13).[275] It should however be noted that despite the use of computational methods that account for electron–electron and electron–hole correlation effects[276,277] as well as the potential role of defects,[98] it has not been possible to achieve satisfactory agreement between the computational results obtained to date and all of the available experimental data for fluorographene. Graphene-based materials have also been suggested for energy storage, fuel cells, and photovoltaic applications. The current state of computational chemistry methods for studying graphene-based energy materials is summarized in a review by Hughes *et al.*[231] Furthermore, there is an intense effort led by the U.S. Department of Energy (DOE) to design novel materials for molecular storage (mainly molecular hydrogen) using graphene derivatives. Numerous computational studies have investigated the molecular interactions of hydrogen with pristine graphene and doped and substituted graphene materials with the aim of enhancing the physisorption of molecular hydrogen and increasing the adsorption capacity of these materials.[72,278–281]

6.7 Reactivity of graphene and graphene derivatives

Computational studies can also provide unique insights into the mechanisms underpinning the chemical modification, *i.e.*, reactivity, of graphene and its derivatives. For example, a study on cycloaddition reactions involving graphene predicted them

to be thermodynamically favoured at edges whereas the surface was predicted to be unreactive.[282,283] Very recently, fluorographene, which was once considered a nonreactive counterpart of Teflon, has been identified as a reactive material[187,284] and a potential source of new graphene derivatives.[189,285] Analyses of its mechanisms of reaction suggested that fully fluorinated graphene preferentially undergoes S_N2-type substitutions.[187] This finding poses new questions about the nature of the C–F bonds in fluorographene and fluorinated graphenes.[188] DFT calculations suggested that two fluorine atoms were inserted into graphene simultaneously during its reaction with XeF_2. It was also shown that fluorination on one side facilitated the addition of another fluorine atom on the opposite side.[286] Computations can also help to clarify the stability of graphene derivatives such as graphane,[271] graphene halides[273] and graphene oxide.[287] For example, although the structures and distributions of oxidized and unoxidized regions of GO are currently unclear, DFT studies conducted by Yang *et al.*[288] suggest that oxidation loci in GO are highly correlated, which is inconsistent with some previously proposed models that assume a random distribution of oxidized groups on GO.

6.8 Graphene and quantum systems

Finally, we comment on the delicate problems of very light and strongly quantum systems interacting with graphene and graphite. For such specific systems as H, H_2, and He as well as clusters, nanodroplets, films and layers of these substances, a full quantum treatment of both electrons and nuclei is often unavoidable. Tunnelling effects noticeably alter adsorption and diffusion barriers[289] while nuclear delocalization effects change classical optimal geometrical structures and prohibit traditional approaches to computing the quantum zero-point energy.[290,291]

Most research efforts in this area have focused on the adsorption of hydrogen on graphene and graphite. A full quantum description of hydrogen and deuterium physisorption on graphite using an MP2 potential energy surface yielded sticking probabilities of the order of a few percent for collision energies of 0–25 meV.[139,292,293] Sticking increased for collision energies close to those of the relevant diffraction resonances and was also enhanced by raising the surface temperature. Desorption time constants were in the range of 20–50 ps for a surface temperature of 300 K. In contrast, graphene supported on a silicone oxide substrate or suspended over a hole in the substrate exhibited different physisorption properties.[294] The sticking probabilities of hydrogen on these stabilized membranes at 10 K were high ($\sim$50%) at low collision energies ($\lesssim$10 meV), *i.e.* significantly larger than those for graphite. This was attributed to the different nature of the lattice vibrations in the two cases. More recently, the adsorption of hydrogen on graphene and graphite,[140] and on graphene and coronene[142] was studied by the wavepacket propagation method and path integral molecular dynamics. As both physisorption and chemisorption minima are present on the adsorption curve of hydrogen on graphene (Fig. 10), the barrier height between both minima contributes to the chemisorption probability. The barrier, which includes van der Waals, zero-point energy, quantum tunnelling and finite temperature effects, is approximately half or quarter of the height of the barrier predicted by DFT-GGA methods ($\sim$0.2 eV) for graphene. The overall chemisorption probability was about 20%.

The adsorption of molecular hydrogen is often studied because of graphene's potential for hydrogen storage (*cf.* Section 6.6). Kowalczyk *et al.*[295] studied hydrogen in slit-like carbon nanopores at 77 K by grand canonical classical and path-integral Monte Carlo (PIMC) simulations. The volumetric density of stored energy in optimal carbon nanopores exceeded the DOE target for 2010 (45 kg m^{-3}). For the narrow pores (pore width $H \in [0.59–0.7]$ nm), the reduction of the quantum isosteric enthalpy of adsorption at zero coverage was around 50% in comparison to the classical one and quantum confinement-inducing polymer shrinking was observed. Isosteric heats of adsorption for H_2, HD and D_2 as functions of coverage, and adsorption isotherms on graphite were computed by Wang and Johnson[296] using the grand canonical classical PIMC method and shown to agree well with experimental results. The properties of H_2 molecules adsorbed between graphite layers were also analysed by PIMD at temperatures of 300 to 900 K.[297] The storage capacities of carbon foams calculated by Yakobson *et al.*[298] met material-based DOE targets

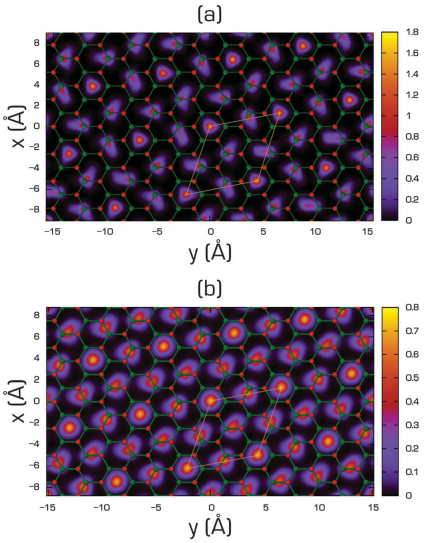

Fig. 14 Helium density (in Å^{-2}) on the x–y plane of the 2/7 phase of ^{4}He on fluorographene (a) and on graphane (b) compared with the geometry of the substrate. Small red balls are centred on the position of fluorine/hydrogen atoms and the small green ones on the carbon atoms. Thin white lines enclose the unit cell of the commensurate 2/7 phase [reprinted with permission from ref. 305. Copyright 2012 by the American Physical Society].

and are comparable to the capacities of a bundle of well-separated open nanotubes of similar diameter. The authors also found that quantum effects appreciably changed the foams' adsorption properties and had to be taken into account. Recently, quantum effects and anharmonicity in the H_2–Li^+–benzene complex, a model for hydrogen storage materials, were studied[299] at zero temperature by DMC and rigid body DMC simulations at DFT PES. H_2 molecules were delocalized above the Li^+–benzene system and H_2 binding enthalpy estimates were between 12.4–16.5 kJ mol^{-1}.

The importance of the substrate in understanding quantum films became evident with the detailed exploration of the phases of He and H_2 on graphite, originating in the late 1960s (superfluidity, Bose–Einstein condensation, and idealized 2D bosonic gas are examples of fundamental phenomena of chemistry and physics). New phenomena occurring on the new 2D substrates have been envisaged opening new fundamental questions to address. While the phase behaviour of ^{4}He and *para*-H_2 films (predicted by the PIMC method) on one side and both sides of graphene[300,301] is expected to be similar to that on graphite,[302–304] the behaviour predicted on fluorographene and graphane is different, due to different symmetry of the interaction potentials, doubled number of adsorption sites and larger corrugation for the adatom.[305–307] For instance, the ground state of the He film on graphite is a 2D crystal commensurate with the substrate (the $\sqrt{3} \times \sqrt{3}\ R30^\circ$ phase), while ^{3}He forms an anisotropic fluid and ^{4}He superfluid on fluorographene and graphane at the low coverage.[305] At higher coverage values both the incommensurate triangular solid and the commensurate state at filling factor 2/7 are found (Fig. 14). An interested reader may find more details on behaviour of monolayer quantum gases on graphene, graphane and fluorographene in the recent review (and references therein) by Reatto *et al.*[308]

7. Conclusions

Computational chemistry provides valuable atomistic insights into the properties of systems that are relevant in biodisciplines and nanoscience. While computational methods are constantly evolving, they have already succeeded in several tasks and are undoubtedly becoming an integral part of the basic research toolkit. Because of the on-going increases in available computing power, the sizes of the systems amenable to modelling and the lengths of the simulation times that can be handled are both increasing, meaning that computational methods will continue to get more powerful and important. We have provided several examples showing how computational methods can be used to obtain insights into the physical and chemical properties of complex molecular systems related to graphene.

8. Perspectives

Despite all the great progress that has been made in modelling noncovalent interactions with graphene, many challenges remain to be addressed. There is still a need for a nonempirical theoretical method that reliably describes London dispersive forces without suffering from the electron-self interaction error and is also computationally affordable and easy to use. The recent progress in methods applying the adiabatic connection fluctuation–dissipation theorem is very promising in this respect. Robust testing of currently available methods is also highly desirable to assess their real performance. This task, is however, partially hampered by the lack of reliable experimental data addressing, *e.g.*, the interaction energies between graphene and adsorbates.

One of the key issues that need to be addressed in today's empirical force fields is the explicit inclusion of polarization. This should be very important especially in describing adsorption processes involving graphene and its derivatives. Another challenge is the correct description of the long-range (asymptotic) dispersive interactions by empirical potentials. Whereas the classical $1/R^6$ London formula results in a $1/R^4$ distance dependence of the interaction energy for a molecule interacting with an infinite graphene sheet, the real distance dependence may be significantly different.[309,310] Because some empirically corrected DFT methods (*e.g.* those based on the DFT-D approach) use this simple dispersion model, they may also describe the asymptotic interactions incorrectly. Unfortunately, the impact of this error is not currently well understood.

Disclosure statement

The authors declare that there is no conflict of interest regarding the publication of this paper.

Acknowledgements

The authors gratefully acknowledge project LO1305 of the Ministry of Education, Youths and Sports. MO acknowledges the Neuron fund to support science. We thank Matúš Dubecký, Piotr Błoński and Petr Lazar for helpful discussions.

References

1 K. S. Novoselov, A. K. Geim, S. V. Morozov, D. Jiang, Y. Zhang, S. V. Dubonos, I. V. Grigorieva and A. A. Firsov, *Science*, 2004, **306**, 666–669.
2 A. K. Geim and K. S. Novoselov, *Nat. Mater.*, 2007, **6**, 183–191.
3 "Ten years in two dimensions." Editorial, *Nat. Nanotechnol.*, 2014, **9**, 725.
4 F. Schedin, A. K. Geim, S. V. Morozov, E. W. Hill, P. Blake, M. I. Katsnelson and K. S. Novoselov, *Nat. Mater.*, 2007, **6**, 652–655.
5 Y. Shao, J. Wang, H. Wu, J. Liu, I. A. Aksay and Y. Lin, *Electroanalysis*, 2010, **22**, 1027–1036.
6 D. Rodrigo, O. Limaj, D. Janner, D. Etezadi, F. J. Garcia de Abajo, V. Pruneri and H. Altug, *Science*, 2015, **349**, 165–168.

7 F. Traversi, C. Raillon, S. M. Benameur, K. Liu, S. Khlybov, M. Tosun, D. Krasnozhon, A. Kis and A. Radenovic, *Nat. Nanotechnol.*, 2013, **8**, 939–945.
8 S. P. Koenig, L. Wang, J. Pellegrino and J. S. Bunch, *Nat. Nanotechnol.*, 2012, **7**, 728–732.
9 V. Georgakilas, M. Otyepka, A. B. Bourlinos, V. Chandra, N. Kim, K. C. Kemp, P. Hobza, R. Zbořil and K. S. Kim, *Chem. Rev.*, 2012, **112**, 6156–6214.
10 D. W. Boukhvalov and M. I. Katsnelson, *J. Phys.: Condens. Matter*, 2009, **21**, 344205.
11 M. Rubeš, P. Nachtigall, J. Vondrášek and O. Bludský, *J. Phys. Chem. C*, 2009, **113**, 8412–8419.
12 P. Lazar, F. Karlický, P. Jurečka, M. Kocman, E. Otyepková, K. Šafářová and M. Otyepka, *J. Am. Chem. Soc.*, 2013, **135**, 6372–6377.
13 R. Podeszwa, *J. Chem. Phys.*, 2010, **132**, 044704.
14 P. V. C. Medeiros, G. K. Gueorguiev and S. Stafström, *Carbon*, 2015, **81**, 620–628.
15 Y. Zhao and D. G. Truhlar, *J. Phys. Chem. C*, 2008, **112**, 4061–4067.
16 G. R. Jenness, O. Karalti and K. D. Jordan, *Phys. Chem. Chem. Phys.*, 2010, **12**, 6375–6381.
17 M. Kocman, M. Pykal and P. Jurečka, *Phys. Chem. Chem. Phys.*, 2014, **16**, 3144–3152.
18 S. Haldar, M. Kolář, R. Sedlák and P. Hobza, *J. Phys. Chem. C*, 2012, **116**, 25328–25336.
19 Y. Hernandez, V. Nicolosi, M. Lotya, F. M. Blighe, Z. Sun, S. De, I. T. McGovern, B. Holland, M. Byrne, Y. K. Gun'Ko, J. J. Boland, P. Niraj, G. Duesberg, S. Krishnamurthy, R. Goodhue, J. Hutchison, V. Scardaci, A. C. Ferrari and J. N. Coleman, *Nat. Nanotechnol.*, 2008, **3**, 563–568.
20 C. Shih and S. Lin, *J. Am. Chem. Soc.*, 2010, **132**, 14638–14648.
21 S. Lin, C.-J. Shih, M. S. Strano and D. Blankschtein, *J. Am. Chem. Soc.*, 2011, **133**, 12810–12823.
22 Z. Qin, M. Taylor, M. Hwang, K. Bertoldi and M. J. Buehler, *Nano Lett.*, 2014, **29**, 7271–7282.
23 V. V. Gobre and A. Tkatchenko, *Nat. Commun.*, 2013, **4**, 2341.
24 M. Pykal, K. Šafářová, K. Machalová Šišková, P. Jurečka, A. B. Bourlinos, R. Zbořil and M. Otyepka, *J. Phys. Chem. C*, 2013, **117**, 11800–11803.
25 F. London, *Trans. Faraday Soc.*, 1937, **33**, 8–26.
26 S. Grimme, *J. Chem. Phys.*, 2003, **118**, 9095.
27 R. A. Distasio Jr. and M. Head-Gordon, *Mol. Phys.*, 2007, **105**, 1073–1083.
28 T. Takatani, E. G. Hohenstein and C. D. Sherrill, *J. Chem. Phys.*, 2008, **128**, 124111.
29 M. Pitoňák, J. Řezáč and P. Hobza, *Phys. Chem. Chem. Phys.*, 2010, **12**, 9611–9614.
30 M. Pitoňák, P. Neogrády, J. Černý, S. Grimme and P. Hobza, *ChemPhysChem*, 2009, **10**, 282–289.
31 C. Riplinger and F. Neese, *J. Chem. Phys.*, 2013, **138**, 034106.
32 C. Riplinger, B. Sandhoefer, A. Hansen and F. Neese, *J. Chem. Phys.*, 2013, **139**, 134101.
33 K. E. Riley, M. Pitonák, P. Jurecka and P. Hobza, *Chem. Rev.*, 2010, **110**, 5023–5063.
34 T. H. Dunning, *J. Chem. Phys.*, 1989, **90**, 1007.
35 C. J. Cramer, *Essentials of Computational Chemistry: Theories and Models*, John Wiley & Sons, New York, 2nd edn, 2004.
36 A. Halkier, T. Helgaker, P. Jørgensen, W. Klopper, H. Koch, J. Olsen and A. K. Wilson, *Chem. Phys. Lett.*, 1998, **286**, 243–252.
37 P. L. Fast, M. L. Sanchez and D. G. Truhlar, *J. Chem. Phys.*, 1999, **111**, 2921–2926.
38 S. K. Min, E. C. Lee, H. M. Lee, D. Y. Kim, D. Y. Kim and K. S. Kim, *J. Comput. Chem.*, 2008, **29**, 1208–1221.
39 P. Jurečka and P. Hobza, *J. Am. Chem. Soc.*, 2003, **125**, 15608–15613.
40 J. Řezáč and P. Hobza, *J. Chem. Theory Comput.*, 2013, **9**, 2151–2155.
41 S. F. Boys and F. Bernardi, *Mol. Phys.*, 1970, **19**, 553–566.
42 M. Mentel and E. J. Baerends, *J. Chem. Theory Comput.*, 2014, **10**, 252–267.
43 I. Shin, M. Park, S. K. Min, E. C. Lee, S. B. Suh and K. S. Kim, *J. Chem. Phys.*, 2006, **125**, 234305.
44 C. Müller and B. Paulus, *Phys. Chem. Chem. Phys.*, 2012, **14**, 7605–7614.
45 A. Erba, S. Casassa, L. Maschio and C. Pisani, *J. Phys. Chem. B*, 2009, **113**, 2347–2354.
46 C. Pisani, M. Busso, G. Capecchi, S. Casassa, R. Dovesi, L. Maschio, C. Zicovich-Wilson and M. Schütz, *J. Chem. Phys.*, 2005, **122**, 094113.
47 M. Marsman, A. Grüneis, J. Paier and G. Kresse, *J. Chem. Phys.*, 2009, **130**, 184103.
48 M. Del Ben, J. VandeVondele and B. Slater, *J. Phys. Chem. Lett.*, 2014, **5**, 4122–4128.
49 G. H. Booth, A. Grüneis, G. Kresse and A. Alavi, *Nature*, 2013, **493**, 365–370.
50 S. Grimme, *Wiley Interdiscip. Rev.: Comput. Mol. Sci.*, 2011, **1**, 211–228.
51 S. Kristyán and P. Pulay, *Chem. Phys. Lett.*, 1994, **229**, 175–180.
52 P. Hobza, J. Šponer and T. Reschel, *J. Comput. Chem.*, 1995, **16**, 1315–1325.
53 P. Jurečka, J. Černý, P. Hobza and D. R. Salahub, *J. Comput. Chem.*, 2007, **28**, 555–569.
54 E. R. Johnson and A. D. Becke, *J. Chem. Phys.*, 2005, **123**, 024101.
55 S. Grimme, *J. Comput. Chem.*, 2004, **25**, 1463–1473.
56 S. Grimme, *J. Comput. Chem.*, 2006, **27**, 1787–1799.
57 S. Grimme, J. Antony, S. Ehrlich and H. Krieg, *J. Chem. Phys.*, 2010, **132**, 154104.
58 A. Tkatchenko and M. Scheffler, *Phys. Rev. Lett.*, 2009, **102**, 073005.
59 A. Tkatchenko, R. A. Distasio, R. Car and M. Scheffler, *Phys. Rev. Lett.*, 2012, **108**, 236402.
60 A. Tkatchenko, *Adv. Funct. Mater.*, 2015, **25**, 2054–2061.
61 S. Grimme, *J. Chem. Phys.*, 2006, **124**, 034108.
62 L. Goerigk and S. Grimme, *J. Chem. Theory Comput.*, 2011, **7**, 291–309.

63 S. Kozuch, D. Gruzman and J. M. L. Martin, *J. Phys. Chem. C*, 2010, **114**, 20801–20808.
64 T. Schwabe and S. Grimme, *Phys. Chem. Chem. Phys.*, 2007, **9**, 3397–3406.
65 M. Dion, H. Rydberg, E. Schröder, D. C. Langreth and B. I. Lundqvist, *Phys. Rev. Lett.*, 2004, **92**, 246401.
66 K. Lee, É. D. Murray, L. Kong, B. I. Lundqvist and D. C. Langreth, *Phys. Rev. B: Condens. Matter Mater. Phys.*, 2010, **82**, 081101.
67 J. Klimeš, D. R. Bowler and A. Michaelides, *J. Phys.: Condens. Matter*, 2010, **22**, 022201.
68 O. A. Vydrov and T. van Voorhis, *J. Chem. Phys.*, 2010, **133**, 244103.
69 D. Langreth and J. Perdew, *Phys. Rev. B: Condens. Matter Mater. Phys.*, 1977, **15**, 2884–2901.
70 A. Tkatchenko, *Adv. Funct. Mater.*, 2015, **25**, 2054–2061.
71 Y. Zhao and D. G. Truhlar, *Theor. Chem. Acc.*, 2008, **120**, 215–241.
72 M. Kocman, P. Jurečka, M. Dubecký, M. Otyepka, Y. Cho and K. S. Kim, *Phys. Chem. Chem. Phys.*, 2015, **17**, 6423–6432.
73 J. Harl, L. Schimka and G. Kresse, *Phys. Rev. B: Condens. Matter Mater. Phys.*, 2010, **81**, 115126.
74 T. Olsen, J. Yan, J. J. Mortensen and K. S. Thygesen, *Phys. Rev. Lett.*, 2011, **107**, 156401.
75 F. Karlický, P. Lazar, M. Dubecký and M. Otyepka, *J. Chem. Theory Comput.*, 2013, **9**, 3670–3676.
76 H. Eshuis, J. E. Bates and F. Furche, *Theor. Chem. Acc.*, 2012, **131**, 1084.
77 X. Ren, P. Rinke, C. Joas and M. Scheffler, *J. Mater. Sci.*, 2012, **47**, 7447–7471.
78 L. Hedin, *Phys. Rev.*, 1965, **139**, A796.
79 A. J. Cohen, P. Mori-Sánchez and W. Yang, *Chem. Rev.*, 2012, **112**, 289–320.
80 A. Heßelmann and A. Görling, *Mol. Phys.*, 2010, **108**, 359–372.
81 A. Heßelmann and A. Görling, *Phys. Rev. Lett.*, 2011, **106**, 093001.
82 M. Dubecký, P. Jurečka, R. Derian, P. Hobza, M. Otyepka and L. Mitas, *J. Chem. Theory Comput.*, 2013, **9**, 4287–4292.
83 J. Ma, D. Alf, A. Michaelides and E. Wang, *J. Chem. Phys.*, 2009, **130**, 154303.
84 J. Ma, A. Michaelides and D. Alfè, *J. Chem. Phys.*, 2011, **134**, 134701.
85 J. Granatier, M. Dubecký, P. Lazar, M. Otyepka and P. Hobza, *J. Chem. Theory Comput.*, 2013, **9**, 1461–1468.
86 L. Horváthová, M. Dubecký, L. Mitas and I. Štich, *Phys. Rev. Lett.*, 2012, **109**, 053001.
87 P. Ganesh, J. Kim, C. Park, M. Yoon, F. A. Reboredo and P. R. C. Kent, *J. Chem. Theory Comput.*, 2014, **10**, 5318–5323.
88 H. Shin, S. Kang, J. Koo, H. Lee, J. Kim and Y. Kwon, *J. Chem. Phys.*, 2014, **140**, 114702.
89 W. M. C. Foulkes, L. Mitas, R. J. Needs and G. Rajagopal, *Rev. Mod. Phys.*, 2001, **73**, 33–83.
90 M. Dubecký, *Acta Phys. Slovaca*, 2014, **64**, 501–574.
91 M. J. S. Dewar, E. G. Zoebisch, E. F. Healy and J. J. P. Stewart, *J. Am. Chem. Soc.*, 1985, **107**, 3902–3909.
92 J. J. P. Stewart, *J. Comput. Chem.*, 1989, **10**, 209–220.
93 J. J. P. Stewart, *J. Mol. Model.*, 2007, **13**, 1173–1213.
94 F. Bloch, *Z. Phys. Chem.*, 1928, **52**, 555–600.
95 J. C. Slater and G. F. Koster, *Phys. Rev.*, 1954, **94**, 1498–1524.
96 M. I. Katsnelson, *Graphene: Carbon in Two Dimensions*, Cambridge University Press, 1st edn, 2012.
97 G. Fiori, S. Lebègue, A. Betti, P. Michetti, M. Klintenberg, O. Eriksson and G. Iannaccone, *Phys. Rev. B: Condens. Matter Mater. Phys.*, 2010, **82**, 153404.
98 S. Yuan, M. Rösner, A. Schulz, T. O. Wehling and M. I. Katsnelson, *Phys. Rev. Lett.*, 2015, **114**, 047403.
99 D. Porezag, T. Frauenheim, T. Köhler, G. Seifert and R. Kaschner, *Phys. Rev. B: Condens. Matter Mater. Phys.*, 1995, **51**, 12947.
100 M. Elstner, D. Porezag, G. Jungnickel, J. Elsner, M. Haugk, T. Frauenheim, S. Suhai and G. Seifert, *Phys. Rev. B: Condens. Matter Mater. Phys.*, 1998, **58**, 7260.
101 M. Elstner, P. Hobza, T. Frauenheim, S. Suhai and E. Kaxiras, *J. Chem. Phys.*, 2001, **114**, 5149–5155.
102 R. Balog, B. Jørgensen, L. Nilsson, M. Andersen, E. Rienks, M. Bianchi, M. Fanetti, E. Laegsgaard, A. Baraldi, S. Lizzit, Z. Sljivancanin, F. Besenbacher, B. Hammer, T. G. Pedersen, P. Hofmann and L. Hornekaer, *Nat. Mater.*, 2010, **9**, 315–319.
103 M. A. Ribas, A. K. Singh, P. B. Sorokin and B. I. Yakobson, *Nano Res.*, 2011, **4**, 143–152.
104 J. P. McNamara and I. H. Hillier, *Phys. Chem. Chem. Phys.*, 2007, **9**, 2362–2370.
105 R. Sharma, J. P. McNamara, R. K. Raju, M. A. Vincent, I. H. Hillier and C. A. Morgado, *Phys. Chem. Chem. Phys.*, 2008, **10**, 2767–2774.
106 A. Ramraj and I. H. Hillier, *J. Chem. Inf. Model.*, 2010, **50**, 585–588.
107 J. Řezáč, J. Fanfrlík, D. Salahub and P. Hobza, *J. Chem. Theory Comput.*, 2009, **5**, 1749–1760.
108 M. Korth, *J. Chem. Theory Comput.*, 2010, **6**, 3808–3816.
109 M. Korth, M. Pitoňák, J. Řezáč and P. Hobza, *J. Chem. Theory Comput.*, 2010, **6**, 344–352.
110 E. G. Gordeev, M. V. Polynski and V. P. Ananikov, *Phys. Chem. Chem. Phys.*, 2013, **15**, 18815–18821.
111 M. A. Vincent and I. H. Hillier, *J. Chem. Inf. Model.*, 2014, **54**, 2255–2260.
112 S. Conti and M. Cecchini, *J. Phys. Chem. C*, 2015, **119**, 1867–1879.
113 L. Zhechkov, T. Heine, S. Patchkovskii, G. Seifert and H. A. Duarte, *J. Chem. Theory Comput.*, 2005, **1**, 841–847.
114 Y. Levy and J. N. Onuchic, *Annu. Rev. Biophys. Biomol. Struct.*, 2006, **35**, 389–415.
115 J. N. Coleman, *Adv. Funct. Mater.*, 2009, **19**, 3680–3695.
116 J. Wang, P. Cieplak and P. A. Kollman, *J. Comput. Chem.*, 2000, **21**, 1049–1074.
117 W. L. Jorgensen, D. S. Maxwell and J. Tirado-Rives, *J. Am. Chem. Soc.*, 1996, **118**, 11225–11236.

118 N. Foloppe and A. D. MacKerell, Jr., *J. Comput. Chem.*, 2000, **21**, 86–104.
119 C. Oostenbrink, A. Villa, A. E. Mark and W. F. van Gunsteren, *J. Comput. Chem.*, 2004, **25**, 1656–1676.
120 H. Ulbricht, G. Moos and T. Hertel, *Phys. Rev. Lett.*, 2003, **90**, 095501.
121 L. Girifalco, M. Hodak and R. Lee, *Phys. Rev. B: Condens. Matter Mater. Phys.*, 2000, **62**, 13104–13110.
122 A. Cheng and W. A. Steele, *J. Chem. Phys.*, 1990, **92**, 3867–3873.
123 H. Sun, *J. Phys. Chem.*, 1998, **5647**, 7338–7364.
124 V. M. Anisimov, I. V. Vorobyov, B. Roux and A. D. MacKerell, *J. Chem. Theory Comput.*, 2007, **3**, 1927–1946.
125 T. a. Ho and A. Striolo, *J. Chem. Phys.*, 2013, **138**, 054117.
126 F. Iori and S. Corni, *J. Comput. Chem.*, 2008, **29**, 1656–1666.
127 Z. E. Hughes, S. M. Tomásio and T. R. Walsh, *Nanoscale*, 2014, **6**, 5438.
128 P. Schyman, W. L. Jorgensen and P. F. Field, *J. Phys. Chem. Lett.*, 2013, **4**, 468–474.
129 R. A. Distasio Jr., O. A. von Lilienfeld and A. Tkatchenko, *Proc. Natl. Acad. Sci. U. S. A.*, 2012, **109**, 14791–14795.
130 S. Stuart, A. Tutein and J. Harrison, *J. Chem. Phys.*, 2000, **112**, 6472–6486.
131 D. W. Brenner, O. A. Shenderova, J. A. Harrison, S. J. Stuart, B. Ni and S. B. Sinnott, *J. Phys.: Condens. Matter*, 2002, **14**, 783–802.
132 A. C. T. van Duin, S. Dasgupta, F. Lorant and W. A. Goddard, *J. Phys. Chem. A*, 2001, **105**, 9396–9409.
133 T. Liang, Y. K. Shin, Y.-T. Cheng, D. E. Yilmaz, K. G. Vishnu, O. Verners, C. Zou, S. R. Phillpot, S. B. Sinnott and A. C. T. van Duin, *Annu. Rev. Mater. Res.*, 2013, **43**, 109–129.
134 M. Z. S. Flores, P. A. S. Autreto, S. B. Legoas and D. S. Galvao, *Nanotechnology*, 2009, **20**, 465704.
135 D. Frenkel and B. Smit, *Understanding Molecular Simulation: From Algorithms to Applications*, Elsevier, 2nd edn, 2001.
136 D. Marx and J. Hutter, *NIC Series: Modern Methods and Algorithms of Quantum Chemistry*, 2000, vol. 1, pp. 301–449.
137 W. F. van Gunsteren, X. Daura and A. E. Mark, *Helv. Chim. Acta*, 2002, **85**, 3113–3129.
138 B. M. Garraway and K.-A. Suominen, *Rep. Prog. Phys.*, 1995, **58**, 365–419.
139 B. Lepetit, D. Lemoine, Z. Medina and B. Jackson, *J. Chem. Phys.*, 2011, **134**, 114705.
140 F. Karlický, B. Lepetit and D. Lemoine, *J. Chem. Phys.*, 2014, **140**, 124702.
141 M. E. Tuckerman, *NIC Series: Quantum Simulations of Complex Many-Body Systems: From Theory to Algorithms*, 2002, vol. 10, pp. 269–298.
142 E. R. M. Davidson, J. Klimeš, D. Alfè and A. Michaelides, *ACS Nano*, 2014, **8**, 9905–9913.
143 M. Lewerenz, *NIC Series: Quantum Simulations of Complex Many-Body Systems: From Theory to Algorithms*, 2002, vol. 10, pp. 1–24.
144 B. Bernu and D. M. Ceperley, *NIC Series: Quantum Simulations of Complex Many-Body Systems: From Theory to Algorithms*, 2002, **vol. 10**, pp. 51–61.
145 L. A. Girifalco and R. A. Lad, *J. Chem. Phys.*, 1956, **25**, 693–697.
146 L. Benedict, N. Chopra and M. Cohen, *Chem. Phys. Lett.*, 1998, **2614**, 490–496.
147 N. L. Allinger, *J. Am. Chem. Soc.*, 1977, **99**, 8127–8134.
148 M. C. Schabel and J. L. Martins, *Phys. Rev. B: Condens. Matter Mater. Phys.*, 1992, **46**, 7185–7188.
149 J.-C. Charlier, X. Gonze and J.-P. Michenaud, *Europhys. Lett.*, 1994, **28**, 403–408.
150 R. Zacharia, H. Ulbricht and T. Hertel, *Phys. Rev. B: Condens. Matter Mater. Phys.*, 2004, **69**, 155406.
151 S. D. Chakarova-Käck, E. Schröder, B. I. Lundqvist and D. C. Langreth, *Phys. Rev. Lett.*, 2006, **96**, 146107.
152 S. Grimme, *J. Phys. Chem. C*, 2007, **111**, 11199–11207.
153 L. Spanu, S. Sorella and G. Galli, *Phys. Rev. Lett.*, 2009, **103**, 196401.
154 S. Lebègue, J. Harl, T. Gould, J. G. Ángyán, G. Kresse and J. F. Dobson, *Phys. Rev. Lett.*, 2010, **105**, 196401.
155 X. Chen, F. Tian, C. Persson, W. Duan and N. Chen, *Sci. Rep.*, 2013, **3**, 3046.
156 J. B. Oostinga, H. B. Heersche, X. Liu, A. F. Morpurgo and L. M. K. Vandersypen, *Nat. Mater.*, 2008, **7**, 151–157.
157 Z. H. Ni, T. Yu, Y. H. Lu, Y. Y. Wang, Y. P. Feng and Z. X. Shen, *ACS Nano*, 2008, **2**, 2301–2305.
158 G. Gui, J. Li and J. Zhong, *Phys. Rev. B: Condens. Matter Mater. Phys.*, 2008, **78**, 075435.
159 J. Berashevich and T. Chakraborty, *Phys. Rev. B: Condens. Matter Mater. Phys.*, 2009, **80**, 033404.
160 X. Fan, L. Liu, J. L. Kuo and Z. Shen, *J. Phys. Chem. C*, 2010, **114**, 14939–14945.
161 X. Fan, Z. Shen, A. Q. Liu and J.-L. Kuo, *Nanoscale*, 2012, **4**, 2157–2165.
162 P. Lazar, R. Zbořil, M. Pumera and M. Otyepka, *Phys. Chem. Chem. Phys.*, 2014, **16**, 14231–14235.
163 D. C. Elias, R. R. Nair, T. M. G. Mohiuddin, S. V. Morozov, P. Blake, M. P. Halsall, A. C. Ferrari, D. W. Boukhvalov, M. I. Katsnelson, A. K. Geim and K. S. Novoselov, *Science*, 2009, **323**, 610–613.
164 A. K. Singh, E. S. Penev and B. I. Yakobson, *ACS Nano*, 2010, **4**, 3510–3514.
165 L. Yang, C. H. Park, Y. W. Son, M. L. Cohen and S. G. Louie, *Phys. Rev. Lett.*, 2007, **99**, 186801.
166 M. Y. Han, B. Özyilmaz, Y. Zhang and P. Kim, *Phys. Rev. Lett.*, 2007, **98**, 206805.
167 R. Zbořil, F. Karlický, A. B. Bourlinos, T. A. Steriotis, A. K. Stubos, V. Georgakilas, K. Šafářová, D. Jančík, C. Trapalis and M. Otyepka, *Small*, 2010, **6**, 2885–2891.
168 D. K. Samarakoon, Z. Chen, C. Nicolas and X.-Q. Wang, *Small*, 2011, **7**, 965–969.
169 J. T. Robinson, J. S. Burgess, C. E. Junkermeier, S. C. Badescu, T. L. Reinecke, F. K. Perkins, M. K. Zalalutdniov, J. W. Baldwin, J. C. Culbertson, P. E. Sheehan and E. S. Snow, *Nano Lett.*, 2010, **10**, 3001–3005.
170 Z. Wang, J. Wang, Z. Li, P. Gong, X. Liu, L. Zhang, J. Ren, H. Wang and S. Yang, *Carbon*, 2012, **50**, 5403–5410.

171 F. Karlický, R. Zbořil and M. Otyepka, *J. Chem. Phys.*, 2012, **137**, 034709.
172 J. Wang, Z. Chen and B. Chen, *Environ. Sci. Technol.*, 2014, **48**, 4817–4825.
173 Y. Liu, X. Dong and P. Chen, *Chem. Soc. Rev.*, 2012, **41**, 2283–2307.
174 K. Szalewicz, *Wiley Interdiscip. Rev.: Comput. Mol. Sci.*, 2012, **2**, 254–272.
175 G. R. Jenness and K. D. Jordan, *J. Phys. Chem. C*, 2009, **113**, 10242–10248.
176 L. Kong, A. Enders, T. S. Rahman and P. A. Dowben, *J. Phys.: Condens. Matter*, 2014, **26**, 443001.
177 P.-P. Zhou and R.-Q. Zhang, *Phys. Chem. Chem. Phys.*, 2015, **17**, 12185–12193.
178 S. K. Mali, J. Greenwood, J. Adisoejoso, R. Phillipson and S. De Feyter, *Nanoscale*, 2015, **7**, 1566–1585.
179 T. Hu and I. C. Gerber, *J. Phys. Chem. C*, 2013, **117**, 2411–2420.
180 F. Schwierz, *Nat. Nanotechnol.*, 2010, **5**, 487–496.
181 T. Ohta, A. Bostwick, T. Seyller, K. Horn and E. Rotenberg, *Science*, 2006, **313**, 951–954.
182 J. W. Yang, G. Lee, J. S. Kim and K. S. Kim, *J. Phys. Chem. Lett.*, 2011, **2**, 2577–2581.
183 H. Ulbricht, R. Zacharia, N. Cindir and T. Hertel, *Carbon*, 2006, **44**, 2931–2942.
184 P. Lazar, E. Otyepková, P. Banáš, A. Fargašová, K. Šafářová, L. Lapčík, J. Pechoušek, R. Zbořil and M. Otyepka, *Carbon*, 2014, **73**, 448–453.
185 Y. H. Lu, W. Chen, Y. P. Feng and P. M. He, *J. Phys. Chem. B*, 2009, **113**, 2–5.
186 Q. Li, X.-Z. Liu, S.-P. Kim, V. B. Shenoy, P. E. Sheehan, J. T. Robinson and R. W. Carpick, *Nano Lett.*, 2014, **14**, 5212–5217.
187 M. Dubecký, E. Otyepková, P. Lazar, F. Karlický, M. Petr, K. Čépe, P. Banáš, R. Zbořil and M. Otyepka, *J. Phys. Chem. Lett.*, 2015, **6**, 1430–1434.
188 S. Zhou, S. D. Sherpa, D. W. Hess and A. Bongiorno, *J. Phys. Chem. C*, 2014, **118**, 26402–26408.
189 P. Lazar, C. K. Chua, K. Holá, R. Zbořil, M. Otyepka and M. Pumera, *Small*, 2015, **11**, 3790–3796.
190 W. Qin, X. Li, W.-W. Bian, X.-J. Fan and J.-Y. Qi, *Biomaterials*, 2010, **31**, 1007–1016.
191 A. N. Camden, S. a. Barr and R. J. Berry, *J. Phys. Chem. B*, 2013, **117**, 10691–10697.
192 S. O'Mahony, C. O'Dwyer, C. A. Nijhuis, J. C. Greer, A. J. Quinn and D. Thompson, *Langmuir*, 2013, **29**, 7271–7282.
193 H. Zhou, P. Ganesh, V. Presser, M. C. F. Wander, P. Fenter, P. R. C. Kent, D. E. Jiang, A. A. Chialvo, J. McDonough, K. L. Shuford and Y. Gogotsi, *Phys. Rev. B: Condens. Matter Mater. Phys.*, 2012, **85**, 035406.
194 N. Wei, C. Lv and Z. Xu, *Langmuir*, 2014, **30**, 3572–3578.
195 K. Xu and J. R. Heath, *Nat. Mater.*, 2013, **12**, 872–873.
196 F. Taherian, V. Marcon, N. F. A. van der Vegt and F. Leroy, *Langmuir*, 2013, **29**, 1457–1465.
197 R. Raj, S. C. Maroo and E. N. Wang, *Nano Lett.*, 2013, **13**, 1509–1515.
198 C.-J. Shih, M. S. Strano and D. Blankschtein, *Nat. Mater.*, 2013, **12**, 866–869.
199 J. Rafiee, X. Mi, H. Gullapalli, A. V. Thomas, F. Yavari, Y. Shi, P. M. Ajayan and N. A. Koratkar, *Nat. Mater.*, 2012, **11**, 217–222.
200 C.-J. J. Shih, Q. H. Wang, S. Lin, K.-C. C. Park, Z. Jin, M. S. Strano and D. Blankschtein, *Phys. Rev. Lett.*, 2012, **109**, 176101.
201 Z. Li, Y. Wang, A. Kozbial, G. Shenoy, F. Zhou, R. McGinley, P. Ireland, B. Morganstein, A. Kunkel, S. P. Surwade, L. Li and H. Liu, *Nat. Mater.*, 2013, **12**, 925–931.
202 N. Patra, B. Wang and P. Král, *Nano Lett.*, 2009, **9**, 3766–3771.
203 X. Sun, Z. Feng, T. Hou and Y. Li, *ACS Appl. Mater. Interfaces*, 2014, **6**, 7153–7163.
204 J. Li, Y. Zhang, J. Yang, K. Bi, Z. Ni, D. Li and Y. Chen, *Phys. Rev. E: Stat., Nonlinear, Soft Matter Phys.*, 2013, **87**, 062707.
205 S. K. Min, W. Y. Kim, Y. Cho and K. S. Kim, *Nat. Nanotechnol.*, 2011, **6**, 162–165.
206 V. Spiwok, P. Hobza and J. Řezáč, *J. Phys. Chem. C*, 2011, **115**, 19455–19462.
207 X. Zhao, *J. Phys. Chem. C*, 2011, **115**, 6181–6189.
208 M. Kabeláč, O. Kroutil, M. Předota, F. Lankaš and M. Šíp, *Phys. Chem. Chem. Phys.*, 2012, **14**, 4217–4229.
209 Y. Cho, S. K. Min, J. Yun, W. Y. Kim, A. Tkatchenko and K. S. Kim, *J. Chem. Theory Comput.*, 2013, **9**, 2090–2096.
210 S. Mogurampelly, S. Panigrahi, D. Bhattacharyya, A. K. Sood and P. K. Maiti, *J. Chem. Phys.*, 2012, **137**, 054903.
211 J. Wintterlin and M. L. Bocquet, *Surf. Sci.*, 2009, **603**, 1841–1852.
212 G. Giovannetti, P. A. Khomyakov, G. Brocks, V. M. Karpan, J. van Den Brink and P. J. Kelly, *Phys. Rev. Lett.*, 2008, **101**, 026803.
213 L. Hu, H. S. Kim, J. Y. Lee, P. Peumans and Y. Cui, *ACS Nano*, 2010, **4**, 2955–2963.
214 P. W. Sutter, J.-I. Flege and E. A. Sutter, *Nat. Mater.*, 2008, **7**, 406–411.
215 X. Li, W. Cai, L. Colombo and R. S. Ruoff, *Nano Lett.*, 2009, **9**, 4268–4272.
216 Z. Sun, Z. Yan, J. Yao, E. Beitler, Y. Zhu and J. M. Tour, *Nature*, 2010, **468**, 549–552.
217 Y. Zhang, L. Zhang and C. Zhou, *Acc. Chem. Res.*, 2013, **46**, 2329–2339.
218 P. Lacovig, M. Pozzo, D. Alfè, P. Vilmercati, A. Baraldi and S. Lizzit, *Phys. Rev. Lett.*, 2009, **103**, 166101.
219 R. Kou, Y. Shao, D. Mei, Z. Nie, D. Wang, C. Wang, V. V. Viswanathan, S. Park, I. A. Aksay, Y. Lin, Y. Wang and J. Liu, *J. Am. Chem. Soc.*, 2011, **133**, 2541–2547.
220 C. Xu, X. Wang and J. Zhu, *J. Phys. Chem. C*, 2008, **112**, 19841–19845.
221 R. Muszynski, B. Seger and P. V. Kamat, *J. Phys. Chem. C*, 2008, **112**, 5263–5266.
222 P. V. Kamat, *J. Phys. Chem. Lett.*, 2010, **1**, 520–527.
223 S. Guo, D. Wen, Y. Zhai, S. Dong and E. Wang, *ACS Nano*, 2010, **4**, 3959–3968.

224 J. Liu, Y. H. Xue, M. Zhang and L. M. Dai, *MRS Bull.*, 2012, **37**, 1265–1272.
225 X. Fan, W. T. Zheng and J. L. Kuo, *ACS Appl. Mater. Interfaces*, 2012, **4**, 2432–2438.
226 M. Khantha, N. A. Cordero, L. M. Molina, J. A. Alonso and L. A. Girifalco, *Phys. Rev. B: Condens. Matter Mater. Phys.*, 2004, **70**, 1–8.
227 K. T. Chan, J. B. Neaton and M. L. Cohen, *Phys. Rev. B: Condens. Matter Mater. Phys.*, 2008, **77**, 235430.
228 E. Lee and K. A. Persson, *Nano Lett.*, 2012, **12**, 4624–4628.
229 R. P. Hardikar, D. Das, S. S. Han, K. Lee and A. K. Singh, *Phys. Chem. Chem. Phys.*, 2014, **16**, 16502–16508.
230 L.-J. Zhou, Z. F. Hou and L.-M. Wu, *J. Phys. Chem. C*, 2012, **116**, 21780–21787.
231 Z. E. Hughes and T. R. Walsh, *Nanoscale*, 2015, **7**, 6883–6908.
232 R. Raccichini, A. Varzi, S. Passerini and B. Scrosati, *Nat. Mater.*, 2014, **14**, 271–279.
233 P. Lazar, J. Granatier, J. Klimeš, P. Hobza and M. Otyepka, *Phys. Chem. Chem. Phys.*, 2014, **16**, 20818–20827.
234 P. V. C. Medeiros, G. K. Gueorguiev and S. Stafström, *Phys. Rev. B: Condens. Matter Mater. Phys.*, 2012, **85**, 205423.
235 J. Hu, J. Alicea, R. Wu and M. Franz, *Phys. Rev. Lett.*, 2012, **109**, 266801.
236 A. Ehrlicher and J. H. Hartwig, *Nat. Mater.*, 2011, **10**, 12–13.
237 I. G. Rau, S. Baumann, S. Rusponi, F. Donati, S. Stepanow, L. Gragnaniello, J. Dreiser, C. Piamonteze, F. Nolting, S. Gangopadhyay, O. R. Albertini, R. M. Macfarlane, C. P. Lutz, B. A. Jones, P. Gambardella, A. J. Heinrich and H. Brune, *Science*, 2014, **344**, 988–992.
238 P. Błoński and J. Hafner, *Phys. Rev. B: Condens. Matter Mater. Phys.*, 2009, **79**, 224418.
239 I. Beljakov, V. Meded, F. Symalla, K. Fink, S. Shallcross, M. Ruben and W. Wenzel, *Nano Lett.*, 2014, **14**, 3364–3368.
240 P. A. Khomyakov, G. Giovannetti, P. C. Rusu, G. Brocks, J. van Den Brink and P. J. Kelly, *Phys. Rev. B: Condens. Matter Mater. Phys.*, 2009, **79**, 195425.
241 J. Granatier, P. Lazar, M. Otyepka and P. Hobza, *J. Chem. Theory Comput.*, 2011, **7**, 3743–3755.
242 M. Stella, S. J. Bennie and F. R. Manby, *Mol. Phys.*, 2015, 1–7.
243 T. P. Hardcastle, C. R. Seabourne, R. Zan, R. M. D. Brydson, U. Bangert, Q. M. Ramasse, K. S. Novoselov and A. J. Scott, *Phys. Rev. B: Condens. Matter Mater. Phys.*, 2013, **87**, 195430.
244 T. Olsen and K. S. Thygesen, *Phys. Rev. B: Condens. Matter Mater. Phys.*, 2013, **87**, 075111.
245 M. Iliaš, V. Kellö and M. Urban, *Acta Phys. Slovaca*, 2010, **60**, 259–391.
246 Y. Z. He, H. Li, P. C. Si, Y. F. Li, H. Q. Yu, X. Q. Zhang, F. Ding, K. M. Liew and X. F. Liu, *Appl. Phys. Lett.*, 2011, **98**, 2012–2015.
247 M. Neek-Amal, N. Abedpour, S. N. Rasuli, A. Naji and M. R. Ejtehadi, *Phys. Rev. E: Stat., Nonlinear, Soft Matter Phys.*, 2010, **82**, 051605.
248 a. Lohrasebi, M. Neek-Amal and M. R. Ejtehadi, *Phys. Rev. E: Stat., Nonlinear, Soft Matter Phys.*, 2011, **83**, 042601.
249 X. Peng, D. Cao and W. Wang, *Ind. Eng. Chem. Res.*, 2010, **49**, 8787–8796.
250 T. Zhang, Q. Xue, S. Zhang and M. Dong, *Nano Today*, 2012, **7**, 180–200.
251 D. Xia, J. Xie, H. Chen, C. Lv, F. Besenbacher, Q. Xue and M. Dong, *Small*, 2010, **6**, 2010–2019.
252 Z. Zhang and T. Li, *Appl. Phys. Lett.*, 2010, **97**, 2012–2015.
253 Y. Jiang, H. Li, Y. Li, H. Yu, K. M. Liew, Y. He and X. Liu, *ACS Nano*, 2011, **5**, 2126–2133.
254 N. Patra, Y. Song and P. Král, *ACS Nano*, 2011, **5**, 1798–1804.
255 V. Varshney, S. S. Patnaik, A. K. Roy, G. Froudakis and B. L. Farmer, *ACS Nano*, 2010, **4**, 1153–1161.
256 L. Xu, N. Wei, Y. Zheng, Z. Fan, H.-Q. Wang and J.-C. Zheng, *J. Mater. Chem.*, 2012, **22**, 1435–1444.
257 R. P. Wesołowski and A. P. Terzyk, *Phys. Chem. Chem. Phys.*, 2011, **13**, 17027–17029.
258 G. K. Dimitrakakis, E. Tylianakis and G. E. Froudakis, *Nano Lett.*, 2008, **8**, 3166–3170.
259 V. Georgakilas, A. Demeslis, E. Ntararas, A. Kouloumpis, K. Dimos, D. Gournis, M. Kocman, M. Otyepka and R. Zbořil, *Adv. Funct. Mater.*, 2015, **25**, 1481–1487.
260 J. G. S. Moo, B. Khezri, R. D. Webster and M. Pumera, *ChemPhysChem*, 2014, **15**, 2922–2929.
261 H. He, J. Klinowski, M. Forster and A. Lerf, *Chem. Phys. Lett.*, 1998, **287**, 53–56.
262 A. Lerf, H. He, M. Forster and J. Klinowski, *J. Phys. Chem. B*, 1998, **102**, 4477–4482.
263 H. Vovusha, S. Sanyal and B. Sanyal, *J. Phys. Chem. Lett.*, 2013, **4**, 3710–3718.
264 C.-J. Shih, S. Lin, R. Sharma, M. S. Strano and D. Blankschtein, *Langmuir*, 2012, **28**, 235–241.
265 C. Mattevi, G. Eda, S. Agnoli, S. Miller, K. A. Mkhoyan, O. Celik, D. Mastrogiovanni, C. Cranozzi, E. Carfunkel and M. Chhowalla, *Adv. Funct. Mater.*, 2009, **19**, 2577–2583.
266 A. Bagri, C. Mattevi, M. Acik, Y. J. Chabal, M. Chhowalla and V. B. Shenoy, *Nat. Chem.*, 2010, **2**, 581–587.
267 R. M. Abolfath and K. Cho, *J. Phys. Chem. A*, 2012, **116**, 1820–1827.
268 B. Narayanan, S. L. Weeks, B. N. Jariwala, B. Macco, J.-W. Weber, S. J. Rathi, M. C. M. van de Sanden, P. Sutter, S. Agarwal and C. V. Ciobanu, *J. Vac. Sci. Technol., A*, 2013, **31**, 040601.
269 J. Zhang and D. Jiang, *Carbon*, 2014, **67**, 784–791.
270 A. Nicolaï, P. Zhu, B. G. Sumpter and V. Meunier, *J. Chem. Theory Comput.*, 2013, **9**, 4890–4900.
271 J. O. Sofo, A. S. Chaudhari and G. D. Barber, *Phys. Rev. B: Condens. Matter Mater. Phys.*, 2007, **75**, 153401.
272 F. Karlický, K. Kumara Ramanatha Datta, M. Otyepka and R. Zbořil, *ACS Nano*, 2013, **7**, 6434–6464.
273 F. Karlický, R. Zbořil and M. Otyepka, *J. Chem. Phys.*, 2012, **137**, 034709.
274 R. R. Nair, W. Ren, R. Jalil, I. Riaz, V. G. Kravets, L. Britnell, P. Blake, F. Schedin, A. S. Mayorov, S. Yuan, M. I. Katsnelson, H. M. Cheng, W. Strupinski, L. G. Bulusheva, A. V. Okotrub, I. V. Grigorieva,

A. N. Grigorenko, K. S. Novoselov and A. K. Geim, *Small*, 2010, **6**, 2877–2884.
275 K. J. Jeon, Z. Lee, E. Pollak, L. Moreschini, A. Bostwick, C. M. Park, R. Mendelsberg, V. Radmilovic, R. Kostecki, T. J. Richardson and E. Rotenberg, *ACS Nano*, 2011, **5**, 1042–1046.
276 F. Karlický and M. Otyepka, *J. Chem. Theory Comput.*, 2013, **9**, 4155–4164.
277 F. Karlický and M. Otyepka, *Ann. Phys.*, 2014, **526**, 408–414.
278 S. Patchkovskii, J. S. Tse, S. N. Yurchenko, L. Zhechkov, T. Heine and G. Seifert, *Proc. Natl. Acad. Sci. U. S. A.*, 2005, **102**, 10439–10444.
279 A. Du, Z. Zhu and S. C. Smith, *J. Am. Chem. Soc.*, 2010, **132**, 2876–2877.
280 K. C. Kemp, H. Seema, M. Saleh, N. H. Le, K. Mahesh, V. Chandra and K. S. Kim, *Nanoscale*, 2013, **5**, 3149–3171.
281 M. Seydou, K. Lassoued, F. Tielens, F. Maurel, F. Raouafi and B. Diawara, *RSC Adv.*, 2015, **5**, 14400–14406.
282 Y. Cao, S. Osuna, Y. Liang, R. C. Haddon and K. N. Houk, *J. Am. Chem. Soc.*, 2013, **135**, 17643–17649.
283 I. K. Petrushenko, *Monatsh. Chem.*, 2014, **145**, 891–896.
284 K. E. Whitener, R. Stine, J. T. Robinson and P. E. Sheehan, *J. Phys. Chem. C*, 2015, **119**, 10507–10512.
285 V. Urbanová, K. Holá, A. B. Bourlinos, K. Čépe, A. Ambrosi, A. H. Loo, M. Pumera, F. Karlický, M. Otyepka and R. Zbořil, *Adv. Mater.*, 2015, **27**, 2305–2310.
286 S. S. Lee, S. W. Jang, K. Park, E. C. Jang, J. Y. Kim, D. Neuhauser and S. Lee, *J. Phys. Chem. C*, 2013, **117**, 5407–5415.
287 S. Zhou and A. Bongiorno, *Sci. Rep.*, 2013, **3**, 2484.
288 J. Yang, G. Shi, Y. Tu and H. Fang, *Angew. Chem., Int. Ed.*, 2014, **53**, 10190–10194.
289 E. M. McIntosh, K. T. Wikfeldt, J. Ellis, A. Michaelides and W. Allison, *J. Phys. Chem. Lett.*, 2013, **4**, 1565–1569.
290 P. Svrčková, A. Vítek, F. Karlický, I. Paidarová and R. Kalus, *J. Chem. Phys.*, 2011, **134**, 224310.
291 F. Calvo, F. Y. Naumkin and D. J. Wales, *J. Chem. Phys.*, 2011, **135**, 124308.
292 Z. Medina and B. Jackson, *J. Chem. Phys.*, 2008, **128**, 114704.
293 V. Buch, *J. Chem. Phys.*, 1989, **91**, 4974.
294 B. Lepetit and B. Jackson, *Phys. Rev. Lett.*, 2011, **107**, 236102.
295 P. Kowalczyk, P. A. Gauden, A. P. Terzyk and S. K. Bhatia, *Langmuir*, 2007, **23**, 3666–3672.
296 Q. Wang and J. K. Johnson, *Mol. Phys.*, 1998, **95**, 299–309.
297 C. P. Herrero and R. Ramírez, *Phys. Rev. B: Condens. Matter Mater. Phys.*, 2010, **82**, 174117.
298 A. K. Singh, J. Lu, R. S. Aga and B. I. Yakobson, *J. Phys. Chem. C*, 2011, **115**, 2476–2482.
299 S. J. Kolmann, J. H. D'Arcy and M. J. T. Jordan, *J. Chem. Phys.*, 2013, **139**, 234305.
300 Y. Kwon and D. M. Ceperley, *Phys. Rev. B: Condens. Matter Mater. Phys.*, 2012, **85**, 224501.
301 M. C. Gordillo, *Phys. Rev. B: Condens. Matter Mater. Phys.*, 2013, **88**, 10–13.
302 F. F. Abraham and J. Q. Broughton, *Phys. Rev. Lett.*, 1987, **59**, 64–67.
303 M. Pierce and E. Manousakis, *Phys. Rev. B: Condens. Matter Mater. Phys.*, 1999, **59**, 3802–3814.
304 D. Sato, K. Naruse, T. Matsui and H. Fukuyama, *Phys. Rev. Lett.*, 2012, **109**, 235306.
305 M. Nava, D. E. Galli, M. W. Cole and L. Reatto, *Phys. Rev. B: Condens. Matter Mater. Phys.*, 2012, **86**, 174509.
306 L. Reatto, M. Nava, D. E. Galli, C. Billman, J. O. Sofo and M. V. Cole, *J. Phys.: Conf. Ser.*, 2012, **400**, 012010.
307 M. Nava, D. E. Galli, M. W. Cole and L. Reatto, *J. Low Temp. Phys.*, 2013, **171**, 699–710.
308 L. Reatto, D. E. Galli, M. Nava and M. W. Cole, *J. Phys.: Condens. Matter*, 2013, **25**, 443001.
309 J. F. Dobson, A. White and A. Rubio, *Phys. Rev. Lett.*, 2006, **96**, 073201.
310 T. Gould, E. Gray and J. F. Dobson, *Phys. Rev. B: Condens. Matter Mater. Phys.*, 2009, **79**, 113402.

D Fluorographene—The Youngest Member of Graphene Family

Chem. Listy *110*, 335–343 (2016) Referát

FLUOROGRAFEN – BENJAMÍNEK V RODINĚ GRAFENOVÝCH DERIVÁTŮ

Věnováno RNDr. Zdeňku Havlasovi, DrSc., k jeho 65. narozeninám.

MARTIN PYKAL, RADEK ZBOŘIL a MICHAL OTYEPKA

Regionální centrum pokročilých technologií a materiálů, Katedra fyzikální chemie, Přírodovědecká fakulta Univerzity Palackého v Olomouci, tř. 17. listopadu 12, 771 46 Olomouc, Česká republika
michal.otyepka@upol.cz

Došlo 25.11.15, přijato 15.2.16.

Klíčová slova: funkcionalizace, grafen, fluorografen, fluorovaný grafen, grafen fluorid, reaktivita, vlastnosti

Obsah

1. Úvod

Grafen je uhlíkový alotrop[1] rozprostírající se ve dvou dimenzích (2D), kde jednotlivé atomy uhlíku jsou uspořádány v pravidelných šestiúhelnících připomínajících včelí plástve. Neobvyklé vlastnosti grafenu přitahovaly vědce již od 60. let 20. století[2], tedy dávno předtím, než se ho podařilo úspěšně izolovat. 2D krystaly byly považovány za termodynamicky nestabilní[3,4], a proto i grafen byl vnímán jen jako základní strukturní jednotka grafitu, která napomáhá osvětlení vlastností tohoto známého 3D materiálu. Nakonec byl v roce 2004 grafen izolován[5], což způsobilo doslova revoluci v nanomateriálovém výzkumu[6]. Obzvláště některé fyzikální i chemické vlastnosti jako transparentnost (~97,4 %), mimořádná mechanická pevnost v tahu (~1100 GPa), chemická odolnost, vynikající tepelná (~5000 W $m^{-1} K^{-1}$) a elektrická vodivost (až ~200 000 $cm^2 V^{-1} s^{-1}$) dávaly a stále dávají velký příslib pro aplikace a technologické využití zahrnující například biosenzory, levné sekvenování DNA, povrchové úpravy materiálů, separační technologie a řadu dalších[7–10]. Díky svým unikátním vlastnostem a obrovskému aplikačnímu potenciálu se grafen stal bezpochyby ikonickým materiálem posledního desetiletí.

Nicméně určité vlastnosti grafenu nejsou výhodné pro všechny aplikace. Pokud bychom uměli řídit šířku zakázaného pásu, mohli bychom připravit dvojrozměrné polovodiče a rozšířit aplikační možnosti grafenu v elektronice[11]. Také velká hydrofobicita grafenu omezuje jeho uplatnění např. v senzorických aplikacích ve vodném prostředí. Vnesení magnetického uspořádání do grafenu by zase otevřelo jeho cestu ke spintronice. Vlastnosti grafenu lze změnit jeho derivatizací[12,13], tj. kovalentní funkcionalizací. Přímá funkcionalizace naráží na nízkou ochotu grafenu reagovat, a proto se pro funkcionalizace hojně využívá grafen oxid[14]. Zde však narážíme na omezení pramenící z nejasně definované struktury grafen oxidu, která obsahuje řadu kyslíkových funkčních skupin a závisí na metodě přípravy[15]. Nalezení vhodného a strukturně dobře definovaného prekurzoru pro přípravu grafenových derivátů by otevřelo nové cesty pro syntézu dalších derivátů s možností řídit jejich chemické složení a fyzikálně-chemické vlastnosti.

V roce 2010 byl připraven fluorografen (FG)[16], také zavedený jako grafen fluorid[17], který stejně jako jeho „starší sourozenec“ grafen vykazuje řadu zajímavých vlastností. Opět se jedná o 2D strukturu (jejíž sumární vzorec lze formálně zapsat jako $(CF)_n$) hexagonálních uhlíkových kruhů s tím rozdílem, že na každý uhlík je kovalentně navázán atom fluoru. Tím se změní výsledná hybridizace grafenového uhlíku z sp^2 na sp^3, což má za následek zánik volných π-elektronů, lokální zprohýbání struktury a nakonec i změnu základních charakteristik materiálu (obr. 1). Z pohledu elektronických vlastností jde o izolant, který získal statut nejtenčího známého izolantu[16]. Postupně se však ukazuje, že daleko nejzajímavější je chemie tohoto grafenového derivátu a s ní související překvapivá reaktivita. Původně se totiž předpokládalo, že podobně jako poly(tetrafluoroethylen) a další příbuzné perfluorované uhlovodíky bude i fluorografen poměrně inertní materiál, nepříliš ochotný k chemickým přeměnám[16]. Tuto domněnku navíc podpořil další společný rys perfluorovaných uhlovodíků, a to poměrně vysoká teplotní stabilita fluorografenu[16]. Poslední studie však naznačují[18–20], že fluorografen může být prekurzorem v mnoha substitučních reakcích a vést tak k celé škále nových grafenových derivátů[21].

2. Příprava fluorografenu

Podobně jako u většiny nových materiálů také u fluorografenu je nalezení levného a jednoduchého způsobu přípravy výchozím bodem pro další výzkum. Do dnešní doby bylo úspěšně vyvinuto několik technik přípravy fluorografenu (obr. 2), jež těží také ze zkušeností získaných při přípravě grafenu. Nejběžněji se dnes fluorografen při-

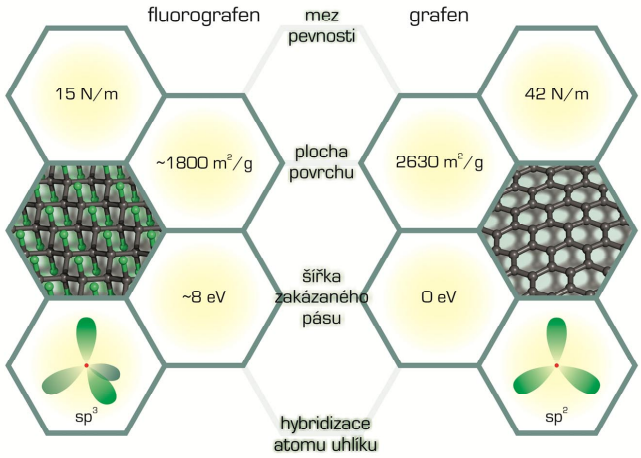

Obr. 1. **Porovnání některých základních charakteristik fluorografenu (vlevo) a grafenu (vpravo)**

pravuje třemi hlavními způsoby. Zajímavé je, že jednotlivé stěžejní metody byly publikovány téměř ve stejnou dobu v roce 2010. Prvním přístupem, který zde zmíníme, je reakce grafenu s XeF_2 nebo F_2, kdy je pomocí různých experimentálních podmínek možné připravit jak fluorografen, tak také částečně fluorovaný grafen[16,22–24]. Jelikož je grafen v atmosféře F_2 za pokojové teploty stabilní, je nutné jej vystavit buď vyšším teplotám, nebo reakci s atomárním fluorem, který se produkuje rozkladem XeF_2 studenou plazmou. Reakce s XeF_2 skýtá navíc výhodu v relativně jednoduché a nenáročné experimentální instrumentaci, neboť se provádí i při běžné laboratorní teplotě. Publikované fluorační postupy se liší v řadě nastavení, např. způsobu přípravy grafenu pro následnou fluoraci, uchycení grafenu v komoře či době vystavení fluračnímu médiu, které ovlivňují poměr F : C v konečných produktech[16]. Struktura některých čerstvě připravených částečně fluorovaných grafenů není stabilní, neboť byla pozorována samovolná defluorizace a pomalý pokles obsahu fluoru, než bylo dosaženo stabilní stechiometrie[25]. Nevýhodou zmiňovaných postupů jsou vysoké ekonomické nároky, které jsou potřebné pro přípravu velkých objemů ve vysoké kvalitě.

Další skupina syntetických přístupů k fluorografenu zahrnuje exfoliaci fluorografitu. Pod pojmem exfoliace se rozumí proces, kdy dochází k odlupování pokud možno jednotlivých monovrstev z mateřského vrstevnatého materiálu, a to buď mechanickou[26], anebo chemickou cestou[17]. I když je výsledkem většinou produkt s vysokou kvalitou, mechanická fyzikální cesta není vzhledem k náročnosti celého procesu a nízkým výtěžkům příliš vhodná pro masovou produkci. Chemická exfoliace v kapalné fázi s různými rozpouštědly, jako jsou sulfolan, dimethylformamid, tetrahydrofuran nebo *N*-methyl-2-pyrrolidon, se tak jeví jako schůdná cesta pro přípravu většího množství

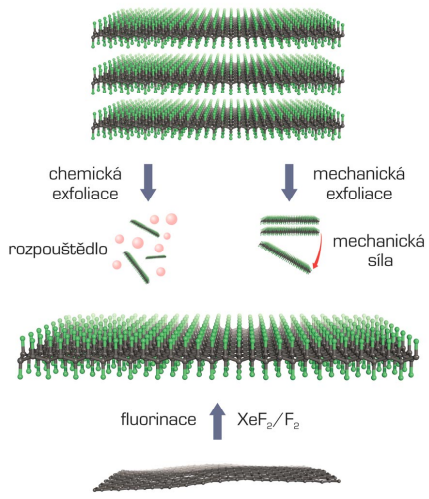

Obr. 2. **Schéma možných metod přípravy fluorografenu (ve středu) z fluorografitu (nahoře) a grafenu (dole)**

koloidů fluorografenu[17,27,28]. Jak ale ukázala nedávná studie, dipolární rozpouštědla mohou přímo způsobovat změny ve struktuře fluorografenu[29], což je třeba vzít v úvahu při přípravě stabilních koloidů fluorografenu. Fluorografen lze také exfoliovat v dalších běžných organických rozpouštědlech (např. acetonu, ethanolu či *n*-oktanu), avšak stabilita získaných koloidů je nízká[28]. Známy jsou také příklady exfoliace v iontových kapalinách[30], nicméně odstranění reziduálních zbytků iontových kapalin je problematické.

Poslední z běžných metod využívaných k přípravě fluorografenu je fluorace grafen oxidu (GO) za pomocí HF nebo F_2 (cit.[31]). Nevýhodou tohoto přístupu je, stejně jako u samotného prekurzoru GO, nepříliš dobře charakterizovaná struktura vzniklého produktu, kdy mluvíme spíše o vysoce fluorovaném grafen oxidu. Nicméně nedávno se pomocí tohoto prekurzoru podařilo připravit fluorografan[32] i fluorografen s dobře definovaným složením[33]. Společným rysem exfoliačních technik jsou pak velikosti získaných fluorografenových vloček, které se většinou pohybují v rozměrech od 200 nm do 2 μm.

3. Vlastnosti fluorografenu

V dalším textu se budeme věnovat vlastnostem příslušejícím stechiometrickému fluorografenu $(C_1F_1)_n$, pokud nebude výslovně uvedeno jinak.

3.1. Strukturní vlastnosti

V porovnání s chemickou strukturou grafenu dochází u fluorografenu ke ztrátě aromaticity způsobenou změnou hybridizace uhlíkového atomu z sp^2 na sp^3. Přesto si tento derivát zachovává řadu zajímavých optických, elektronických a jiných vlastností. Z původně plochého grafenu s nulovým zakázaným pásem a delokalizovanými oblaky elektronů nad a pod rovinou vzniká lokálně zprohýbaný izolant bez volných elektronů. Nedávné kvantově chemické výpočty explicitně zahrnující elektron-elektronové korelace z prvních principů (na úrovni GW@HSE06) udávají hodnotu zakázaného pásu až 8,3 eV (cit.[34]).

Struktura fluorografenu může být také odvozena, analogicky jako u grafenu, od 3D krystalu fluorografitu $(CF)_n$, kdy v jeho nejstabilnější předpovězené formě pro monokrystal jsou jednotlivé vrstvy – fluorografeny – v židličkové konformaci a vzájemném AB uspořádání. Polovina atomů uhlíku v jedné vrstvě tedy leží nad středy hexagonálních kruhů druhé vrstvy (obr. 3), přičemž jednotlivé vrstvy k sobě poutají slabé nevazebné interakce. Pomocí experimentálních technik jako rentgenová difrakční analýza (XRD) nebo nukleární magnetická rezonance (NMR) byly navrženy další struktury vzájemného uspořádání. První teoretické výpočty naznačily, že jednotlivé formy se mezi sebou energeticky liší jen velmi málo a že efekt způsobený jednotlivými motivy vrstvení není příliš významný[35]. To bylo následně potvrzeno i za použití mnohem náročnější výpočetní metody RPA (z angl. random

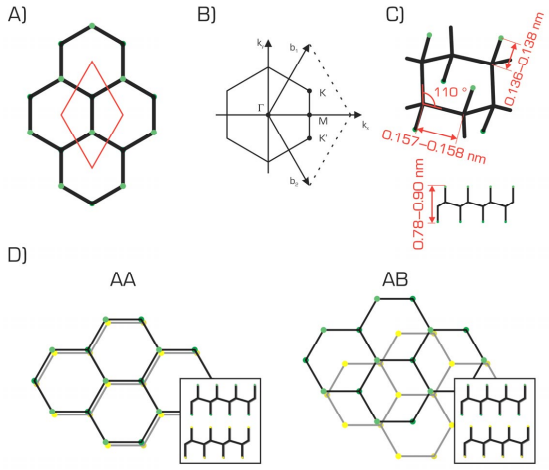

Obr. 3. **A) Schematický obrázek hexagonální mřížky fluorografenu** (atomy fluoru jsou označeny zelenou barvou, uhlíkové atomy a vazby mezi nimi černou) s vyznačenou elementární buňkou (červeně)**, B) první Brillouinova zóna reciproké mřížky s vyznačenými vysoce symetrickými Γ, M a K body, C) základní geometrické parametry fluorografenu, D) AA a AB motivy vrstvení fluorografenů**

phase approximation), která zahrnuje nelokální elektronovou korelaci z prvních principů. Řádné zahrnutí nelokálních elektronových korelačních efektů je v tomto případě nutné, abychom dokázali korektně popsat van der Waalsovy (vdW) interakce. Ty jsou dominantně působící silou mezi jednotlivými vrstvami fluorografenu, které se mezi sebou vážou energií 0,19 J m^{-2} (cit.[36]).

Z dat elektronové difrakční analýzy, mikroskopie atomárních sil (AFM), skenovací elektronové (SEM) a transmisní elektronové (TEM) mikroskopie (obr. 4), rentgenové fotoelektronové spektroskopie (XPS) a Ramanovy spektroskopie (která však může poskytnout informace jen o částečně fluorovaných systémech, jelikož fluorografen je Ramanovsky neaktivní materiál pro běžně používané lasery (obr. 5)) byly získány další poznatky ohledně struktury, vaznosti a složení fluorografenu. V porovnání s elementární buňkou grafenu dochází u fluorografenu ke zvětšení mřížkové konstanty v rovině uhlíkové sítě o 1 % (z 246 pm na 248 pm). To je způsobeno změnou hybridizace atomu uhlíku doprovázenou prodloužením vazby C–C (jejíž délka činí 142 pm v grafenu a 158 pm ve fluorografenu) a lokálním zvrásněním struktury. Tloušťka jedné vrstvy fluorografenu z AFM měření se pohybuje v rozmezí 780–900 pm (cit.[17,37]). Experimentálně byla stanovena také mřížková konstanta *c* fluorografitu, která činí 582–620 pm (cit.[23,38]) a která závisí na poměru F : C ve struktuře[39]. Teoreticky vypočtená mřížková konstanta *c* se pohybuje v rozmezí 566–579 pm (cit.[36,40,41]). Pokud k mřížkové konstantě připočteme van der Waalsův poloměr atomu fluoru (~150 pm), můžeme porovnávat tloušťku fluorografenu s naměřenými hodnotami AFM (další

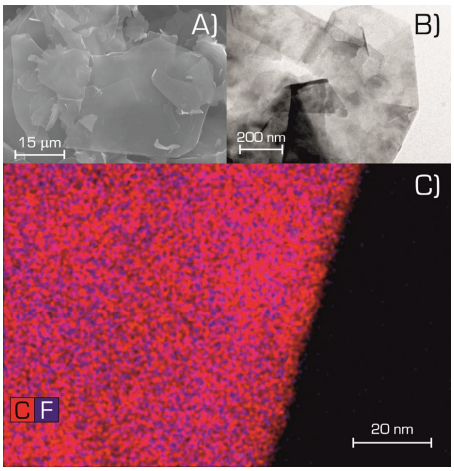

Obr. 4. **SEM (A) a TEM (B) snímek fluorografenu, C) mapování prvkového složení fluorografenu** (uhlík znázorněn červenou a fluor modrou barvou)

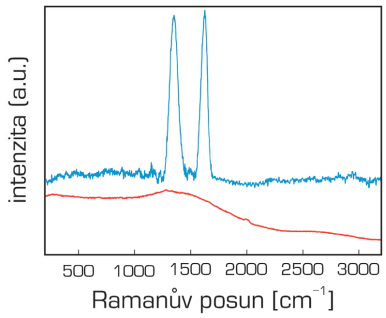

Obr. 5. **Porovnání Ramanových spekter fluorovaného grafenu C_1F_x (x~1,1) (červeně) a grafenových teček (modře) zaznamenaných s excitační vlnovou délkou laseru 633 nm**

geometrické charakteristiky fluorografenu jsou shrnuty na obr. 3). Z AFM měření byl také získán Youngův modul pružnosti s hodnotou 100 ± 30 N m^{-1} (0,3 TPa), což odpovídá přibližně třetině pevnosti grafenu[16]. Nicméně teoreticky předpovězená hodnota 226 N m^{-1} je o polovinu větší[42]. Tato neshoda může pocházet z přítomnosti defektů ve struktuře zkoumaného vzorku. Další teoretická práce pak naznačila, že na rozdíl od grafenu zůstává struktura fluorografenu výrazně nezprohýbaná, a to i při vysokých teplotách[43].

Co se týče vazebných poměrů mezi uhlíkem a fluorem, převažuje motiv jednoduché C–F vazby (s četností ~86 % ze všech vazebných motivů vyskytujících se ve fluorografenu), které je na základě spektroskopických dat připisován tzv. semi-iontový charakter (tj. někde na pomezí kovalentní a iontové vazby)[34,44]. Síla vazby se může měnit s koncentrací fluoru a uspořádáním celé struktury[45] a výpočetní chemie pomohla detailněji porozumět tomuto chování. Bylo zjištěno, že disociační energie vazby C–F v systémech s malou koncentrací fluoru se pohybuje okolo 209 kJ mol^{-1}, kdežto u plně fluorované struktury dosahuje i více než dvojnásobku (až 469 kJ mol^{-1})[21], což odpovídá energiím C–F vazeb v běžných organických sloučeninách[46]. Další minoritně zastoupené vazebné motivy jako CF_2 nebo CF_3, kdy jsou jednotlivé uhlíky vázány se dvěma či třemi atomy fluoru, mohou být nalezeny primárně na defektech a na volných hranách[22]. Tyto motivy jsou také zodpovědné za nestechiometrii a vyšší poměr fluoru (F : C > 1) ve struktuře fluorografenu.

3.2. Elektronické vlastnosti

Fluorografen je považován za izolant se širokým zakázaným pásem nejenom proto, že voltampérová charakte-

Tabulka I
Shrnutí vypočtených hodnot pro šířku zakázaného pásu E_g s použitím rozdílných metod

Použitá metoda	E_g [eV]	Lit.
LDA	3,0–3,5	40, 51
GGA	3,0–4,2	26, 52
GGA(PBE)	3,1	50
Hybridní DFT (HSE06)	5,1	50
GW_0, G_0W_0	7,3–7,5	42,48
GW@HSE06	8,3	34

ristika u stechiometrického fluorografenu je silně nelineární s rezistivitou větší než 1 GΩ, ale je navíc téměř nezávislá na napětí na hradle. Šířka zakázaného pásu fluorografenu se odhaduje zejména z optických spekter[16] či měření NEXAFS (z angl. near edge X-ray absorption fine structure)[24] a předpokládá se, že je vyšší než 3,0 eV, resp. 3,8 eV (viz následující část o optických vlastnostech fluorografenu). Navíc bylo prokázáno, že fluorace grafenu způsobuje nárůst hodnoty zakázaného pásu už při nízkých poměrech F : C ve struktuře[22]. Přímá dI/dV měření na parciálně fluorovaném grafenu $CF_{0,25}$ ukázala na zakázaný pás[47] o šířce 2,9 eV.

Kvůli nejasnostem, které se týkají elektronové struktury fluorografenu, je tato oblast intenzivně studována teoreticky. Obecně se výpočetní metody shodují ve tvaru pásové struktury a ukazují, že fluorografen má nejužší vzdálenost mezi vodivostním a valenčním pásem v Γ bodě (obr. 6). V odhadech šířky zakázaného pásu se však metody diametrálně odlišují (tab. I). Minimální hodnota zakázaného pásu pro fluorografen (3,0 eV)[26] byla získána při použití metody funkcionálu hustoty (DFT) s aproximací lokální hustoty (LDA) nebo se standardní zobecněnou gradientovou aproximací (GGA), přičemž byly prozkoumány i jiné konformace, které ve výsledku vykazovaly jen malé rozdíly od nejstabilnějšího uspořádání[48]. Je známo, že LDA i GGA funkcionály tuto hodnotu systematicky podceňují[41], proto je jejich na první pohled dobrá shoda s experimentálními hodnotami pouze náhodná. Na druhou stranu Hartreeova-Fockova (HF) metoda zase danou hodnotu přeceňuje[49]. Zde se proto nabízí příležitost využít tzv. hybridních funkcionálů, které mají výměnný funkcionál konstruovaný jako směs HF a DFT výměny. Tyto hybridní funkcionály často dobře popisují šířky zakázaných pásů jak u pevných látek, tak i u některých uhlíkových materiálů. V případě fluorografenu hybridní funkcionál HSE06 predikuje hodnotu zakázaného pásu 5,1 eV (cit.[50]). Při použití ještě náročnější vícečásticové GW aproximace byla odhadnuta šířka zakázaného pásu 8,3 eV (cit.[50]). Nicméně takto vypočtené hodnoty z GW elektronické struktury fluorografenu není možné přímo srovnávat s experimentálně pozorovanými přechody z optických spekter, které navíc zahrnují tvorbu excitonu. Tento zásadní rozdíl mezi velmi přesnými výpočty a experimenty si jistě zaslouží detailní rozbor.

3.3. Optické vlastnosti

Fluorografen je takřka transparentní pro viditelné spektrum světla a začíná lehce absorbovat až v modré oblasti spektra. Šířka optického zakázaného pásu u fluorografenu byla stanovena z fotoluminiscenčních měření disperze fluorografenu v acetonu. Byly pozorovány dva zřetelné emisní píky při 3,8 a 3,65 eV, které jen potvrzovaly, že fluorografen je materiál s širokým optickým zakázaným pásem[24]. První pík při 3,8 eV měl stejnou ener-

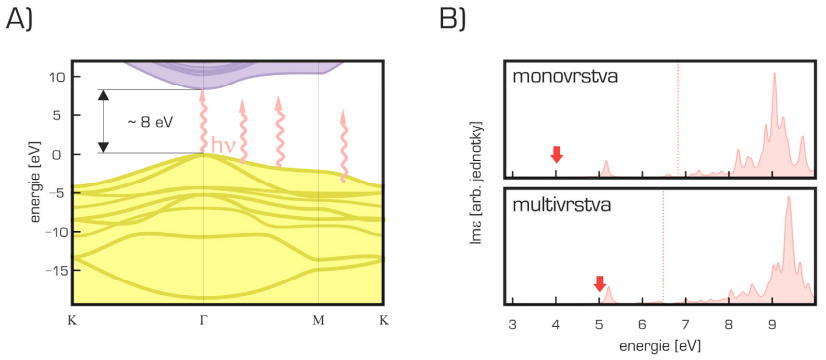

Obr. 6. **A) Vypočtená elektronická struktura fluorografenu na úrovni GW@PBE s vyznačenou šířkou zakázaného pásu, B) optická spektra monovrstvy a multivrstevnatého fluorografenu získaná pomocí BSE+G_1W_0@PBE,** experimentální hodnoty pro optické zakázané pásy jsou znázorněny šipkami

gii, jaká byla již pozorována rentgenovou absorpční spektroskopií (NEXAFS), a proto byl tento pík přiřazen zářivé rekombinaci volných elektronů s volnými dírami. Druhý pík s nižší energií o 156 meV odpovídal fononem asistované rekombinaci, na které se podílí vibrační mód vazby C–F. Tyto výsledky jsou navíc konzistentní s infračervenou spektroskopií s Fourierovou transformací, která pozoruje C–F vibraci při 1211 cm^{-1} (což v harmonické aproximaci odpovídá energii 150 meV)[53]. V případě menšího stupně fluorace se ve spektru objevil ještě jeden pík při 2,88 eV doprovázený píkem, který měl o 157 meV menší energii.

Teoretické výpočty absorpčních a emisních vlastností materiálů patří k náročným úlohám teoretické chemie. Pro jejich kvalitní popis je nezbytné zahrnout řádně nejen elektron-elektronové korelace, ale také korelace elektron-díra, což dovolují výpočty vycházející s Betheho-Salpeterovy rovnice (BSE). Kvalitu výpočtů ovlivňuje také řada parametrů, které nastavují výpočty, např. hustotou vzorkování k-prostoru, energetickým omezením použitých rovinných vln a použitou elektronovou hustotou[41]. Optická spektra grafit fluoridu, vrstevnatého materiálu sestávajícího z vrstev fluorografenu, jež jsou vzájemně poutány slabými nekovalentními interakcemi, zejména disperzními silami[36], pak ukazují, že významná absorpce elektromagnetického záření nastává při ~5 eV (cit.[38]). Velmi přesné teoretické výpočty na úrovni G_0W_0@PBE ukazují, že v uvedené oblasti se nachází významný excitonový pík grafit fluoridu, a jsou tedy ve výborném souladu s experimentem[41]. Výpočty naznačují, že pozice excitonového píku se jen málo mění s počtem vrstev v materiálu, a to z hodnoty 5,14 eV pro jedinou vrstvu na 5,20 eV v případě mnohovrstevnatého systému[41] (obr. 6). Naopak, jak již bylo zmíněno výše, experimentální měření na fluorografenu ukazují významnou změnu, tj. posun prvního absorpčního píku z ~5 eV u grafit fluoridu na ~3 eV u fluorografenu. Vzhledem k tomu, že grafit fluorid je materiál vázaný slabými nekovalentními silami, nelze hledat oporu pro takto významný posun např. v elektrostatické či polarizační interakci mezi vrstvami. Možné vysvětlení může nabízet přítomnost defektů ve struktuře fluorografenu, ale jejich úloha se zdá být nevýznamná[54]. Zmíněná neshoda šířky optického i elektronického zakázaného pásu fluorografenu predikovaného teoreticky a změřeného experimentálně tak stále zůstává hádankou.

4. Reaktivita fluorografenu

Přestože byl fluorografen považován za inertní, a tedy chemicky nudný materiál, je dnes studium reaktivity fluorografenu dynamicky se rozvíjející oblastí. Fluorografen již od svého počátku byl označen za dvourozměrný analog poly(tetrafluoroethylenu), známého spíše pod komerčním názvem teflon®, což je registrovaná obchodní značka firmy DuPont. Ten se často používá jako inertní a vysoce teplotně stabilní materiál v kuchyňském náčiní či laboratořích místo chemického skla. Podobně jako teflon se také fluorografen začíná rozkládat až při teplotách přesahujících 300 °C (cit.[16]) a následně se nad 500 °C mění na těkavé sloučeniny s malou molekulovou hmotností např. C_2F_4 (cit.[55]). To vše podporuje domněnku, že i chemické chování fluorografenu by mělo kopírovat chování teflonu.

Prvním náznakem, že situace může být odlišná, byla reakce fluorografenu s KI, kdy při teplotě 150 °C vznikl grafen[17]. Během reakce byl spektroskopicky identifikován jako meziprodukt grafen jodid, tj. sloučenina s vazbami C–I. Předpokládá se, že během reakce dochází k postupné substituci atomů fluoru za jód. Teoretické výpočty ukázaly, že vazba C–I, a tedy i jodový analog fluorografenu – jodografen, je nestabilní a za normálních podmínek se samovolně rozpadá zpět na grafen za současného uvolnění molekul I_2. Toto chování není překvapivé, neboť pokud proběhne navázání objemných atomů jódu na sp^3 uhlíkový skelet tvořený kondenzovanými cyklohexany, dojde k významnému překryvu orbitalů atomu jódu a oslabení vazby C–I. Dlužno podotknout, že analýza dalších podobných analogů ukázala, že snad pouze chlorografen by mohl existovat za nízkých teplot[17,56], popř. že lze připravit stabilní vybrané směsné halogeny grafenu. Některé směsné halogengrafeny by pak mohly být zajímavé i z toho hlediska, že jejich odhadovaná šířka zakázaného pásu se pohybuje v oblasti hodnot pro běžné polovodiče (~1–1,5 eV)[50].

I již zmíněná reakce grafenu s fluoračním činidlem XeF_2, využívaná hojně při syntéze fluorografenu, je sama o sobě zajímavá a může také mnohé napovědět o chemii fluorografenu. Reakce s XeF_2 silně závisí na zvolených experimentálních podmínkách. Pokud se např. reakci s XeF_2 vystaví pouze jediná strana prekurzoru (např. ponecháním grafenu na měděné fólii), mohou vzniknout struktury, kdy je fluor přítomný jen na exponované straně grafenu (tzv. Januszovské struktury), navíc v přesně definovaném poměru C_4F (cit.[22]). Při reakcích bez tohoto sterického omezení (např. pokud celý proces probíhá na vzorku umístěném na zlaté mřížce umožňující přístup XeF_2 z obou stran) dochází k postupné adici fluoru na všechny atomy uhlíku. Následné teoretické práce na úrovni DFT přišly s osvětlením molekulárního mechanismu procesu fluorace grafenu. Pokud reakce probíhá pouze na jedné straně grafenu, děje se tak preferenčně na *para* pozicích (1, 4) benzenových kruhů, což odpovídá právě experimentálně pozorovanému 25% pokrytí. Dále bylo vypozorováno, že navázáním atomu fluoru na jedné straně se sníží energetická bariéra pro navázání dalšího fluoru na *ortho* pozici (1, 2) na straně opačné. To vede při řadě následných adicí k úplnému pokrytí povrchu grafenu[57].

Mnohem zajímavější je však řada prací, které nedávno ukázaly, že fluorografen reaguje s celou řadou činidel např. NaSH, NaOH, CCl_2, $NaNH_2$ a N_2H_4 (obr. 7), a to již při pokojové teplotě. Tyto studie potvrzují, že fluorografen může být velmi vhodným prekurzorem pro syntézu řady grafenových derivátů. Výhodou fluorografenu je, že jde o strukturně dobře definovaný materiál, který je dostupný v dostatečném množství, neboť jeho mateřský materiál grafit fluorid se používá jako průmyslový lubrikant. Za zmínku stojí, že chemické modifikace fluorografitů byly předmětem výzkumu v 80. letech minulého století

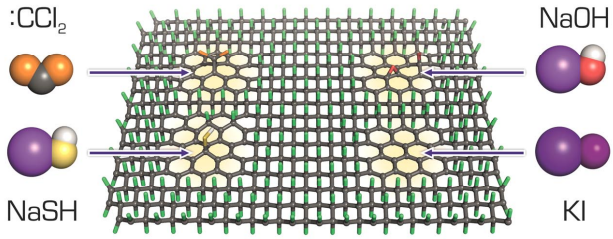

Obr. 7. **Schéma znázorňující reakční produkty reakcí fluorografenu s rozdílnými výchozími látkami**

i v tehdejší ČSSR[58,59]. V současné době se v ČR výzkum fluorografenu soustředí v Regionálním centru pokročilých technologií a materiálů v Olomouci a na Vysoké škole chemicko-technologické v Praze.

Reaktivita fluorografenu a částečně fluorovaných grafenů byla nedávno studována teoreticky a byly prozkoumány různé mechanismy štěpení vazby C–F (cit.[21]). Bylo zjištěno, že energie pro homolytické i heterolytické štěpení je relativně velká (více než 418 kJ mol^{-1}), ale v případě homolytického štěpení vazby dojde k jejímu podstatnému snížení, pokud je atom fluoru obklopen aromatickými uhlíky (až na hodnotu okolo 209 kJ mol^{-1}). To může také částečně vysvětlovat experimentálně pozorovanou samovolnou defluorizaci u málo fluorovaných systémů. Výpočty naznačily, že fluorografen je překvapivě náchylný k S_N2 nukleofilnímu ataku, i když terciální fluory preferují S_N1 mechanismus[46]. Experimentálně pak bylo prokázáno, že např. reakcí s hydroxidy dochází za běžných podmínek současně k substituci a eliminaci fluoru s tím, že eliminace převládá. Soutěž mezi substitucí a eliminací lze odůvodnit tím, že řada nukleofilů je zároveň i redukčními činidly a vedle substituce tak dochází k reduktivní eliminaci. Je třeba podotknout, že stále nebyly důsledně prozkoumány všechny možné reakční cesty fluorografenu a úloha jednotlivých reakčních partnerů a jsme tak stále ještě na začátku pochopení jeho reaktivity. Nicméně řada experimentů jednoznačně vyvrací představy o analogii mezi fluorografenem a teflonem®.

Nový derivát grafenu, thiofluorografen, byl připraven reakcí fluorografenu s NaSH (cit.[19]). Prvkové mapování ve vysoce rozlišené transmisní elektronové spektroskopii odhalilo, že atomy síry a fluoru jsou rovnoměrně rozprostřeny po celém povrchu nově vzniklého derivátu. Následně pomocí DFT výpočtů byl navržen vhodný strukturní model, kdy byly vzaty v úvahu možné vzájemné konfigurace –SH skupiny a atomu fluoru. Právě přítomnost atomů fluoru ve struktuře materiálu stabilizuje jinak spontánně se desorbující thiolové skupiny z grafenu, přičemž nejstabilnější relativní uspořádání –F a –SH skupin odpovídalo *ortho* (1, 2) konfiguraci, následováno *meta* (1, 3) a *para* (1, 4) konfiguracemi se stejnou, resp. s opačnou relativní pozicí skupin. Odhadovaná šířka zakázaného pásu thiofluorografenu se pohybuje v rozmezí 1–2 eV, což je hodnota splňující požadavky pro potencionální využití v polovodičové elektrotechnice. Ukázalo se také, že vzniklý hydrofilní thiofluorografen lze využít jako vhodný impedimetrický senzor k detekci hybridizace DNA[19].

Zajímavá chemie stojí také za reakcí fluorografenu s dichlorkarbenem, který se připravuje známou reakcí chloroformu s NaOH za přítomnosti katalyzátoru fázového přenosu[18]. Pomocí energiově disperzní spektroskopie (EDS) byla zjištěna homogenní distribuce funkčních $=CCl_2$ skupin po celé ploše zkoumané vločky. Mechanismus reakce byl prozkoumán i na úrovni DFT. Modelově byla studována adice dichlorkarbenu na grafen, kde byla nalezena dvě minima: lokální minimum odpovídající fyzisorbovanému stavu a globální minimum chemisorbovaného stavu, přičemž oba stavy se mezi sebou energeticky liší jen o 31,8 kJ mol^{-1}, ale jsou od sebe odděleny relativně velkou energetickou bariérou 133 kJ mol^{-1}. Jelikož dichlorkarben preferuje adici na nenasycené vazby, které se ve fluorografenu z podstaty nenachází, byla pozornost převážně věnována právě mechanismu cykloadice na fluorografen a také na částečně fluorovaný grafen. K funkcionalizaci fluorografenu dichlorkarbenem pravděpodobně dochází ve dvou krocích, kdy v prvním způsobuje fyzisorbovaný dichlorkarben defluorizaci prekurzoru a desorbuje se z povrchu buď jako CCl_2F nebo CCl_2F_2 a následně se ve druhém kroku na nově vzniklé nenasycené vazby aduje další molekula dichlorkarbenu. Nelze ani vyloučit možnost, že v alkalickém prostředí nejprve dochází k eliminaci fluorů[21] a na vznikající nenasycené vazby se dichlorkarben aduje.

Zdá se, že v oblasti chemie fluorografenu je velký potenciál pro přípravu nových grafenových derivátů, ale zůstává zde nezodpovězena řada otázek. Teoretické výpočty mohou poskytnout cenný nástroj pro analýzu chemických reakcí[60], avšak dlužno podotknout, že studium reakcí nanomateriálů představuje nelehký úkol pro teoretickou chemii a bude vyžadovat i další rozvoj neempirických

výpočetních metod[61]. Není vyloučeno, že v dohledné budoucnosti může studium reaktivity fluorografenu těžit z pokroku v oblasti reaktivní molekulové mechaniky (MM), využívající empirické potenciály umožňující zánik a tvorbu vazeb, např. ReaxFF[62]. Silná stránka tohoto přístupu spočívá v možnosti studia reaktivity systémů čítajících až několik tisíc atomů, což je neporovnatelně více ve srovnání s aparátem kvantové chemie, kde jsme většinou řádově limitováni na modely čítající desítky, nejvýše stovky atomů. První práce využívající reaktivní MM věnující se mechanickým a tepelným vlastnostem fluorografenu byla publikována teprve nedávno[43]. Následující práce zabývající se termickým rozkladem fluorografenu[63] narazila na zatím nepříliš zvládnutou parametrizaci C–F vazeb fluorografenu (nutno podotknout, že problematika s ní související není detailně pochopena ani na úrovni kvantové chemie) a v důsledku toho neuspokojivě popisuje některá pozorování z dostupných experimentálních prací. Například při simulaci termického rozkladu fluorografenu nebyly pozorovány nízkomolekulární produkty popsané výše. Nicméně za předpokladu úspěšné reparametrizace se může z reaktivní molekulové mechaniky v budoucnu stát velmi silný nástroj schopný pomoci poodhalit a vysvětlit neobyčejné chemické chování fluorografenu.

5. Závěr

Grafen, jeho deriváty a další 2D struktury jsou mimořádné nanomateriály s velkým příslibem budoucího uplatnění v řadě technologií. Dosud však není dokonale zvládnuta např. cílená příprava grafenových derivátů s požadovanými vlastnostmi. Fluorografen, který do rodiny 2D materiálů vstoupil v roce 2010 jako nejtenčí známý izolant, je neobvykle chemicky zajímavý materiál. Reaguje za běžných podmínek s řadou chemických látek, např. NaSH, NaOH, CCl_2, $NaNH_2$ a N_2H_4, a lze tak připravit řadu grafenových derivátů. Mezi jinými např. thiofluorografen, který lze využít jako vhodný impedimetrický senzor hybridizace DNA. Společné úsilí experimentátorů a teoretiků pomáhá poodhalit pravidla reaktivity fluorografenu. Dosud získané poznatky dávají velký příslib pro to, abychom jednou chemii tohoto systému nejen pochopili, ale byli jsme schopni cíleně řídit přípravu grafenových derivátů. To by otevřelo nové horizonty nanomateriálovému výzkumu a aplikacím nových 2D materiálů.

Děkujeme Kláře Čépe, Ondřeji Tomancovi, Kateřině Holé, Arianě Fargašové a Františku Karlickému za laskavé poskytnutí podkladů pro obrázky. Za finanční podporu patří dík projektu Ministerstva školství, mládeže a tělovýchovy LO1305. Michal Otyepka také děkuje nadačnímu fondu Neuron pro podporu vědy.

LITERATURA

1. Georgakilas V., Perman J. A., Tuček J., Zbořil R.: Chem. Rev. *115*, 4744 (2015).
2. Boehm H. P., Clauss A., Fischer G., Hofmann U.: Proc. Fifth Conf. Carbon *1962*, 73.
3. Peierls R.: Helv. Phys. Acta *7*, 81 (1934).
4. Landau L. D.: Phys. Z. Sowjetunion *11*, 26 (1937).
5. Novoselov K. S., Geim A. K., Morozov S. V, Jiang D., Zhang Y., Dubonos S. V, Grigorieva I. V, Firsov A. A.: Science *306*, 666 (2004).
6. Geim A. K., Novoselov K. S.: Nat. Mater. *6*, 183 (2007).
7. Schedin F., Geim a K., Morozov S. V, Hill E. W., Blake P., Katsnelson M. I., Novoselov K. S.: Nat. Mater. *6*, 652 (2007).
8. Shao Y., Wang J., Wu H., Liu J., Aksay I. A., Lin Y.: Electroanalysis *22*, 1027 (2010).
9. Traversi F., Raillon C., Benameur S. M., Liu K., Khlybov S., Tosun M., Krasnozhon D., Kis A., Radenovic A.: Nat. Nanotechnol. *8*, 939 (2013).
10. Koenig S. P., Wang L., Pellegrino J., Bunch J. S.: Nat. Nanotechnol. *7*, 728 (2012).
11. Schwierz F.: Nat. Nanotechnol. *5*, 487 (2010).
12. Georgakilas V., Otyepka M., Bourlinos A. B., Chandra V., Kim N., Kemp K. C., Hobza P., Zboril R., Kim K. S.: Chem. Rev. *112*, 6156 (2012).
13. Criado A., Melchionna M., Marchesan S., Prato M.: Angew. Chem., Int. Ed. *54*, 10734 (2015).
14. Chen D., Feng H., Li J.: Chem. Rev. *112*, 6027 (2012).
15. Compton O. C., Nguyen S. T.: Small *6*, 711 (2010).
16. Nair R. R., Ren W., Jalil R., Riaz I., Kravets V. G., Britnell L., Blake P., Schedin F., Mayorov A. S., Yuan S., Katsnelson M. I., Cheng H. M., Strupinski W., Bulusheva L. G., Okotrub A. V, Grigorieva I. V, Grigorenko A. N., Novoselov K. S., Geim A. K.: Small *6*, 2877 (2010).
17. Zbořil R., Karlický F., Bourlinos A. B., Steriotis T. a, Stubos A. K., Georgakilas V., Šafářová K., Jančík D., Trapalis C., Otyepka M.: Small *6*, 2885 (2010).
18. Lazar P., Chua C. K., Holá K., Zbořil R., Otyepka M., Pumera M.: Small *11*, 3790 (2015).
19. Urbanová V., Holá K., Bourlinos A. B., Čépe K., Ambrosi A., Loo A. H., Pumera M., Karlický F., Otyepka M., Zbořil R.: Adv. Mater. *27*, 2305 (2015).
20. Whitener K. E., Stine R., Robinson J. T., Sheehan P. E.: J. Phys. Chem. C *119*, 10507 (2015).
21. Dubecký M., Otyepková E., Lazar P., Karlický F., Petr M., Čépe K., Banáš P., Zbořil R., Otyepka M.: J. Phys. Chem. Lett. *6*, 1430 (2015).
22. Robinson J. T., Burgess J. S., Junkermeier C. E., Badescu S. C., Reinecke T. L., Perkins F. K., Zalalutdniov M. K., Baldwin J. W., Culbertson J. C., Sheehan P. E., Snow E. S.: Nano Lett. *10*, 3001 (2010).
23. Cheng S.-H., Zou K., Okino F., Gutierrez H. R., Gupta A., Shen N., Eklund P. C., Sofo J. O., Zhu J.: Phys. Rev. B *81*, 205435 (2010).
24. Jeon K. J., Lee Z., Pollak E., Moreschini L., Bostwick A., Park C. M., Mendelsberg R., Radmilovic V., Kostecki R., Richardson T. J., Rotenberg E.: ACS Nano *5*, 1042 (2011).

25. Stine R., Lee W. K., Whitener K. E., Robinson J. T., Sheehan P. E.: Nano Lett. *13*, 4311 (2013).
26. Withers F., Dubois M., Savchenko A. K.: Phys. Rev. B *82*, 073403 (2010).
27. Bourlinos A. B., Šafářová K., Šišková K., Zbořil R.: Carbon *50*, 1425 (2012).
28. Gong P., Wang Z., Wang J., Wang H., Li Z., Fan Z., Xu Y., Han X., Yang S.: J. Mater. Chem. *22*, 16950 (2012).
29. Wang X., Wang W., Liu Y., Ren M., Xiao H., Liu X.: Phys. Chem. Chem. Phys. 16 (2016) DOI: 10.1039/c5cp06914a.
30. Chang H., Cheng J., Liu X., Gao J., Li M., Li J., Tao X., Ding F., Zheng Z.: Chem. Eur. J. *17*, 8896 (2011).
31. Wang X., Dai Y., Gao J., Huang J., Li B., Fan C., Yang J., Liu X.: ACS Appl. Mater. Interfaces *5*, 8294 (2013).
32. Sofer Z., Šimek P., Mazánek V., Šembera F., Janoušek Z., Pumera M.: Chem. Commun. *51*, 5633 (2015).
33. Mazánek V., Jankovský O., Luxa J., Sedmidubský D., Janoušek Z., Šembera F., Mikulics M., Sofer Z.: Nanoscale *7*, 13646 (2015).
34. Karlický F., Otyepka M.: J. Chem. Theory Comput. *9*, 4155 (2013).
35. Han S. S., Yu T. H., Merinov B. V., van Duin A. C. T., Yazami R., Goddard W. A.: Chem. Mater. *22*, 2142 (2010).
36. Lazar P., Otyepková E., Karlický F., Čépe K., Otyepka M.: Carbon *94*, 804 (2015).
37. Pu L., Ma Y., Zhang W., Hu H., Zhou Y., Wang Q., Pei C.: RSC Adv. *3*, 3881 (2013).
38. Wang B., Sparks J. R., Gutierrez H. R., Okino F., Hao Q., Tang Y., Crespi V. H., Sofo J. O., Zhu J.: Appl. Phys. Lett. *97*, 141915 (2010).
39. Kita Y., Watanabe N., Fujii Y.: J. Am. Chem. Soc. *101*, 3832 (1979).
40. Charlier J.-C., Gonze X., Michenaud J.-P.: Phys. Rev. B *47*, 16162 (1993).
41. Karlický F., Otyepka M.: Ann. Phys. *526*, 408 (2014).
42. Leenaerts O., Peelaers H., Hernández-Nieves A. D., Partoens B., Peeters F. M.: Phys. Rev. B *82*, 195436 (2010).
43. Singh S. K., Srinivasan S. G., Neek-Amal M., Costamagna S., van Duin A. C. T., Peeters F. M.: Phys. Rev. B *87*, 104114 (2013).
44. Sato Y., Itoh K., Hagiwara R., Fukunaga T., Ito Y.: Carbon *42*, 3243 (2004).
45. Zhou S., Sherpa S. D., Hess D. W., Bongiorno A.: J. Phys. Chem. C *118*, 26402 (2014).
46. Sandford G.: Tetrahedron *59*, 437 (2003).
47. Kwon S., Ko J. H., Jeon K. J., Kim Y. H., Park J. Y.: Nano Lett. *12*, 6043 (2012).
48. Samarakoon D. K., Chen Z., Nicolas C., Wang X.-Q.: Small *7*, 965 (2011).
49. Karlický F., Kumara Ramanatha Datta K., Otyepka M., Zbořil R.: ACS Nano *7*, 6434 (2013).
50. Karlický F., Zbořil R., Otyepka M.: J. Chem. Phys. *137*, 034709 (2012).
51. Takagi Y., Kusakabe K.: Phys. Rev. B *65*, 121103 (2002).
52. Boukhvalov D. W., Katsnelson M. I.: J. Phys.: Condens. Matter *21*, 344205 (2009).
53. Wang Y., Lee W. C., Manga K. K., Ang P. K., Lu J., Liu Y. P., Lim C. T., Loh K. P.: Adv. Mater. *24*, 4285 (2012).
54. Yuan S., Rösner M., Schulz A., Wehling T. O., Katsnelson M. I.: Phys. Rev. Lett. *114*, 047403 (2015).
55. Chen G., Shi Z., Yu J., Wang Z., Xu J., Gao B., Hu X.: Thermochim. Acta *589*, 63 (2014).
56. Şahin H., Ciraci S.: J. Phys. Chem. C *116*, 24075 (2012).
57. Lee S. S., Jang S. W., Park K., Jang E. C., Kim J. Y., Neuhauser D., Lee S.: J. Phys. Chem. C *117*, 5407 (2013).
58. Klouda K., Peka I., Moltašová J., Hrabal L., Hejlek L., Dědek V., Pošta A.: CZ 239412 (1987).
59. Klouda K., Peka I., Pošta A., Dědek V.: CZ 237710 (1987).
60. Havlas Z., Zahradník R.: Int. J. Quantum Chem. *26*, 607 (1984).
61. Karlický F., Lazar P., Dubecký M., Otyepka M.: J. Chem. Theory Comput. *9*, 3670 (2013).
62. Van Duin A. C. T., Dasgupta S., Lorant F., Goddard W. A.: J. Phys. Chem. A *105*, 9396 (2001).
63. Paupitz R., Autreto P. A. S., Legoas S. B., Srinivasan S. G., van Duin A. C. T., Galvão D. S.: Nanotechnology *24*, 035706 (2013).

M. Pykal, R. Zbořil, and M. Otyepka *(Regional Centre of Advanced Technologies and Materials, Department of Physical Chemistry, Faculty of Science, Palacký University Olomouc):* **Fluorographene – The Youngest Member of Graphene Family**

Discovery of two-dimensional (2D) materials caused a revolution in nanomaterial science. Nowadays the 2D materials constitute an integral part of material chemistry but they are still in the process of dramatic development. In 2010, fluorographene (graphene fluoride) extended the family of 2D materials and is now considered as the thinnest known insulator with a band gap as large as 8 eV. For a long time, fluorographene was considered as an unreactive 2D counterpart of teflon®. However, recent studies show that fluorographene can react with numerous reagents yielding interesting new graphene derivatives. Intensive experimental and theoretical effort is paid to a comprehension of properties and reactivity of this chemical structure. If we succeed in controlling the chemical behavior of this material, fluorographene may become a rising star of future material research.